



Rijkswaterstaat
Ministerie van Infrastructuur en Waterstaat

UNIVERSITY
OF TWENTE.

Relations for clay erosion by wave overtopping based on the fire hose method

Master thesis

May 18, 2022

I.M.J. (Irma) van Rozendaal

Faculty of Engineering Technology
Civil Engineering and Management
Marine and Fluvial systems

Graduation Committee:

Prof. Dr. S.J.M.H. Hulscher	(University of Twente)
Dr. J.J. Warmink	(University of Twente)
Dr. Ir. M. van Damme	(Rijkswaterstaat)
Dr. V.M. van Bergeijk	(Deltares)

Preface

This thesis report marks the end of my Master in Civil Engineering and Management at the University of Twente. I would like to thank my friends and family, who supported me during my six years in Enschede and made this time wonderful. Even though, my Master went a little different than expected beforehand due to the coronavirus, I have enjoyed my study to the fullest. Furthermore, I would like to thank the people that helped me during my thesis.

First of all, I would like to thank my daily supervisor Myron from Rijkswaterstaat for guiding and helping me during my thesis. Additionally, I want to thank my supervisors from the University of Twente - Vera, Jord, and Suzanne - for their guiding during this study. Without the help of Rens, Jelle, and Ligaya this study would not be possible and I would like to thank you all for helping me improving the setup of the fire hose method experiments and performing the experiments.

I hope you will enjoy reading this thesis report.

Irma van Rozendaal,

Enschede, May 2022

Summary

One of the failure mechanisms for grass-covered dikes is wave overtopping, which occurs during extreme events when waves overtop the crest of the dike and flow over the landward slope. These waves cause high hydraulic loads on the cover of the dike and when these loads exceed the strength of the cover material, the material erodes. Dikes are commonly constructed with a sand or clay core and an erosion resistant clay and grass layer to protect the dike against waves. By performing experiments, the erosive behaviour of the cover materials, such as clay, can be investigated. Due to a lack of knowledge, the erosion resistance of clay is currently not taken into account in the assessment of dikes.

Clay used in dikes in the Netherlands is classified based on its capacity to resist erosion into three categories: Erosion resistant, Moderately erosion resistant, and Little erosion resistant. This categorisation is based on Rotating Cylinder Tests (RCT) performed by Grondmechanica Delft between 1985 and 1987. In 2017, this categorisation was updated based on new insights to optimise the use of clay in dikes.

Next to RCT, other small-scale experiments are used to inspect the erosive behaviour of materials. These tests can be performed in laboratories or in situ and are relatively cheap and logistically easy to perform. The disadvantages of using small-scale experiments is that the hydraulic loads exerted on the soil could differ from the loads occurring during wave overtopping and the heterogeneous character of the material is not taken into account during a single test. Consequently, multiple experiments must be performed to gain enough insight in the erosive behaviour of the clay. Large-scale experiments overcome these problems. However, these experiments are logistically challenging and expensive to perform. Deltares has designed a new test method commissioned by Rijkswaterstaat, which overcomes the aforementioned problems: the fire hose method. Experiments with the fire hose method have previously been performed, however the test on bare clay had to be aborted after only three minutes due to the high erosion rate. The experimental setup has been adjusted in this study, such that it can be used to determine the erosion resistance of clay. The aim of this study is to indicate to what extent the fire hose method can be used to accurately determine the erosion resistance of clay in dikes against wave overtopping.

The adjusted setup is used to perform experiments on clay in the Hedwige-Prosperpolder. During these experiments, the grass cover is removed and the nozzle of the fire hose method setup is placed above the clay. Flow velocities between 1.25 m/s and 5.25 m/s are exerted on the clay. After each interval, the depth of the hole is measured and used to calculate the erosion rate. Using the flow velocity and the erosion profile of the hole, the stresses on the clay are calculated. This information is needed to determine the parameters ‘erodibility coefficient’ (k) and ‘critical stress’ (τ_c), which are commonly used to define the erosion resistance of clay. The results of the fire hose method experiments are analysed to find a relation between the applied normal and shear stresses and the observed erosion rate. This has been done for the ‘erosion rate of the depth’ (E_d), ‘average erosion rate’ (E_{av}), ‘maximum erosion rate’ (E_{max}), and ‘erosion rate of the volume’ (E_V). The analysis indicated that when using the maximum erosion rate and erosion rate of the volume a negative trend is observed between the applied stress and observed erosion rate. This contradicts what is observed during large-scale field experiments and to theory. Using the erosion rate of the depth and average erosion rate, a positive trend is observed. However, the erosion rate of the depth results in a large spread in the outcome. This spread is lowered when using the average erosion rate. However, this significantly reduces the amount of data, which increases the uncertainty in the trend.

Wave overtopping experiments are performed on clay as well in the Hedwige-Prosperpolder. The erosion rate is analysed for 20 waves of 500 L/m, 10 waves of 1500 L/m, and 10 waves of 2000 L/m

and used to calculate the normal and shear stresses. These results have been used to indicate to what extent the results of the fire hose method can be correlated to the results of wave overtopping experiments. Both experiments showed a large spread in the observed erosion rate, which can be caused by the heterogeneous character of the clay. Over the depth of the clay layer and length of the dike, the structure of the clay highly varies, which can result in large variations in the observed erosion rate under similar hydraulic loads. The magnitude of the calculated normal stresses and observed erosion rate are of the same order for both experiments. Since the shear stress cannot be calculated for the fire hose method experiments, this is expressed as the flow velocity of the jet and overtopping wave. The flow velocity of the waves of 1500 L/m and 2000 L/m is larger than the maximum flow velocity used during the fire hose method experiments. However, the flow velocity of the waves of 1500 L/m is close to 5.25 m/s, which was the maximum flow velocity used during the fire hose method. The data show approximately the same range for the erosion rate for both situations. The flow velocity for the waves of 500 L/m lays between 3.25 m/s and 4.42 m/s, which were used during the fire hose method experiments. However, hereby the magnitude of the erosion rate observed during the wave overtopping experiments is larger than those observed during the fire hose method experiments.

Uncertainties arise for both test methods. The biggest uncertainties for the fire hose method experiments arise during the analysis of the data. Multiple assumptions are made to calculate the normal stress, which are shown to be incorrect. Furthermore, the effect of the remaining water in the erosion hole is not taken into account. The main uncertainty during the analysis of the wave overtopping experiments is that using photogrammetry, clay and water cannot be distinguished from each other, which results in an underestimation of the erosion speed. Consequently, it is expected that the actual erosion speed of the wave overtopping experiments is larger after the results are analysed further.

The hydraulic loads exerted on the clay during the fire hose method experiments are representative for the loads occurring during wave overtopping. The current results showed a large spread, which make it not possible to define a value for the parameters erodibility coefficient and critical stress. This makes the current setup still unsuitable to determine the erosive behaviour of clay. It is recommended to recalculate the normal stresses and erosion rates after the complete analysis of the results of the wave overtopping experiments are completed. Secondly, the spread in the outcome of the fire hose method should be minimised, such that it can be used to define the erosion resistance of clay. If this is both possible, it is recommended to perform more fire hose method experiments on clay to verify whether the method can be used to define the erosion resistance of clay.

Samenvatting

Een van de faalmechanismen voor dijken met grasbekleding is golfoverslag. Dit gebeurt tijdens extreme evenementen wanneer golven over de kruin van de dijk slaan en over de helling aan de landzijde stromen. Deze golven veroorzaken hoge hydraulische belastingen op de bekleding van de dijk en wanneer deze belastingen hoger zijn dan de sterkte van de bekleding, zal het materiaal eroderen. Dijken zijn vaak opgebouwd uit een zand- of kleikern met een erosie resistente klei en gras laag om de dijk te beschermen tegen golven. Door experimenten uit te voeren, kan het erosieve gedrag van bekledingsmaterialen, zoals klei, geïnspecteerd worden. Door het gebrek aan kennis over de weerstand die klei kan bieden tegen erosie, wordt deze momenteel buiten beschouwing gelaten bij in de beoordeling van dijken.

Klei gebruikt in dijken in Nederland wordt geclassificeerd op basis van zijn capaciteit om erosie te weerstaan. Er zijn drie categorieën: Erosie resistent, Matig erosie resistent en Weinig erosie resistent. De categorisatie is gebaseerd op Rotatie Cilinder Testen (RCT) uitgevoerd door Grondmechanica Delft tussen 1985 en 1987. In 2017 is deze categorisatie geüpdatet, gebaseerd op nieuwe inzichten om het gebruik van klei in dijken te optimaliseren.

Naast de RCT worden andere kleinschalige proeven uitgevoerd om het erosieve gedrag van materialen te inspecteren. Deze testen worden uitgevoerd in laboratoria of in het veld en zijn relatief goedkoop en logistiek makkelijk uit te voeren. De nadelen van kleinschalige experimenten is dat de hydraulische belastingen, die op de grond worden uitgeoefend, kunnen verschillen van de belastingen die optreden tijdens golfoverslag en het heterogene karakter van het materiaal wordt niet meegenomen met het uitvoeren van één proef. Als gevolg zijn meerdere proeven benodigd om genoeg inzicht te genereren over het erosieve gedrag van klei. Grootschalige proeven komen deze problemen te boven. Echter zijn deze proeven logistiek lastig en duur om uit te voeren. Deltares heeft in opdracht van Rijkswaterstaat een nieuwe testmethode ontwikkeld, waarmee voorgenoemde problemen opgelost worden: de brandslangmethode. Er zijn al proeven uitgevoerd met deze methode, maar de proef op kale klei moest na drie minuten stopgezet worden vanwege de hoge erosiesnelheid. De opstelling van de testmethode is in dit onderzoek aangepast, zodat de weerstand van klei tegen erosie bepaald kan worden. Het doel van dit onderzoek is om aan te geven in welke mate de brandslangmethode gebruikt kan worden om accuraat de weerstand van klei tegen erosie te bepalen.

De aangepaste opstelling is gebruikt om experimenten uit te voeren in de Hedwige-Prosperpolder. Tijdens deze proeven is de grasmat verwijderd en de spuitmond van de testopstelling boven de klei geplaatst. Stroomsnelheden tussen 1.25 m/s en 5.25 m/s zijn toegepast op de klei. Na elke interval is de diepte van de kuil gemeten, waarna de erosiesnelheid is berekend. Met de stroomsnelheid en het erosieprofiel van het gat zijn de spanningen op de klei berekend. Deze informatie is nodig om de parameters ‘erodeerbaarheid’ (k) en ‘kritische stress’ (τ_c) te bepalen. Deze worden doorgaans gebruikt om de weerstand tegen erosie te definiëren. De resultaten van de proeven met de brandslangmethode zijn geanalyseerd, om een relatie te vinden tussen de uitgeoefende normaal- en schuifspanning en de geobserveerde erosiesnelheid. Dit is gedaan voor de ‘erosiesnelheid van de diepte’ (E_d), ‘gemiddelde erosiesnelheid’ (E_{av}), ‘maximale erosiesnelheid’ (E_{max}) en de ‘erosiesnelheid van het volume’ (E_V). De analyse heeft aangetoond dat wanneer de maximale erosiesnelheid of de erosiesnelheid van het volume gebruikt worden, een negatieve trend te zien is. Dit is tegenstrijdig met wat er geobserveerd wordt in het veld en benoemd wordt in de literatuur. Door gebruik te maken van de erosiesnelheid van de diepte of de gemiddelde erosiesnelheid, wordt een positieve trend zichtbaar. Echter, wanneer de erosiesnelheid van de diepte gebruikt wordt, is een grote spreiding in de resultaten zichtbaar. Deze spreiding verminderd wanneer de gemiddelde erosiesnelheid gebruikt wordt, maar hierbij is de

hoeveelheid data significant gereduceerd, waardoor de onzekerheid in de trend toeneemt.

Golfoverslagproeven zijn ook uitgevoerd op klei in de Hedwige-Prosperpolder. De erosiesnelheid is geanalyseerd voor 20 golven van 500 L/m, 10 golven van 1500 L/m en 10 golven van 2000 L/m. Deze zijn gebruikt om de normaal- en schuifspanningen te berekenen. Dit is gebruikt om aan te geven in welke mate de resultaten van de brandslangmethode gecorreleerd kunnen worden aan de resultaten van de golfoverslagproeven. Voor beide proeven was een grote spreiding in de geobserveerde erosiesnelheid te zien. Deze kan veroorzaakt worden door het heterogene karakter van de klei. Over de diepte van de kleilaag en lengte van de dijk varieert de structuur sterk, wat kan leiden tot grote variaties in de geobserveerde erosiesnelheid onder vergelijkbare belastingen voor beide experimenten. Omdat de schuifspanning niet berekend kan worden voor de brandslangmethode wordt deze uitgedrukt met de stroomsnelheid van de waterstraal en de golf. De stroomsnelheid van de golven van 1500 L/m en 2000 L/m is groter dan de maximale stroomsnelheid toegepast tijdens de brandslangmethode. Echter ligt de stroomsnelheid van de golven van 1500 L/m dicht bij de stroomsnelheid van 5.25 m/s, wat de maximale stroomsnelheid was tijdens de brandslangproeven. De data laten ongeveer hetzelfde bereik zien voor de erosiesnelheid voor beide situaties. De stroomsnelheid voor de golven van 500 L/m ligt tussen 3.25 m/s en 4.42 m/s, welke toegepast zijn tijdens de brandslangmethode. Echter is de grootte van de geobserveerde erosiesnelheid tijdens de golfoverslagproeven hoger dan deze geobserveerd tijdens de brandslangproeven.

Onzekerheden treden op bij het uitvoeren van beide experimenten. De grootste onzekerheden voor de brandslangproeven ontstaan bij het analyseren van de data. Voor het berekenen van de normaalspanning zijn verschillende aannames gemaakt, die in de praktijk niet juist blijken te zijn. Verder wordt er ook geen rekening gehouden met het effect dat het resterende water heeft op de normaalspanning in het gat. De grootste onzekerheid in het analyseren van de resultaten van de golfoverslagproeven ontstaat doordat met de huidige analysemethode geen verschil kan worden gemaakt tussen de klei en het resterende water, waardoor de erosiesnelheid onderschat wordt. Hierdoor is verwacht dat in werkelijkheid de verschillen in de geobserveerde erosiesnelheid tussen de brandslangmethode en de golfoverslagproeven groter zullen zijn na een verdere analyse van de resultaten van de golfoverslagproeven.

Met de brandslangmethode worden hydraulische belastingen gegenereerd op de klei die representatief zijn voor de belastingen die optreden tijdens golfoverslag. De huidige resultaten leverden een dusdanig grote spreiding op, waardoor het niet mogelijk is om de waarden van de parameters erodeerbaarheid en kritische stress te bepalen. Dit maakt de huidige opstelling nog ongeschikt voor het bepalen van het erosiegedrag van klei. Er wordt geadviseerd om eerst de normaalspanningen en erosiesnelheden te herberekenen nadat de analyse van de resultaten van de golfoverslagproeven voltooid zijn. Ten tweede wordt geadviseerd om de spreiding in de resultaten van de brandslangmethode verder te minimaliseren, zodat deze gebruikt kan worden om de erosieparameters van klei te definiëren. Als dit mogelijk is, wordt het aangeraden om meer experimenten uit te voeren met de brandslangmethode, zodat geverifieerd kan worden of dat de testmethode gebruikt kan worden om de erosiebestendigheid van klei te bepalen.

Contents

Preface	i
Summary	ii
Samenvatting	iv
List of Abbreviations	viii
List of Symbols	ix
List of Figures	xi
List of Tables	xiv
1 Introduction	1
1.1 Theoretical background	1
1.2 Problem context	5
1.3 Research goal and research questions	6
1.4 Thesis outline	7
2 Literature Review	8
2.1 Experiments to determine the erosion resistance of clay	8
2.1.1 Small-scale experiments	8
2.1.2 Large-scale experiments	10
2.1.3 Clay categorisation based on experimental outcomes	10
3 Methodology	12
3.1 The basic setup of the fire hose method	12
3.2 Fire hose method experiments performed in the Hedwige-Prosperpolder	12
3.3 Wave overtopping experiments performed in the Hedwige-Prosperpolder	16
3.4 Calculating the hydraulic load	17
3.4.1 Calculating the hydraulic loads occurring during fire hose method experiments	17
3.4.2 Calculating the hydraulic loads occurring during wave overtopping experiments	19
3.5 Finding relations in the fire hose method results	20
3.6 Analysing the results of the fire hose method experiments and wave overtopping experiments	24
4 Results	25
4.1 Measured erosion during the fire hose method experiments	25
4.1.1 Best suitable parameter to describe the erosion rate	26
4.2 Analysing the results of the wave overtopping experiments	29
4.3 Comparison of the fire hose method experiments and the wave overtopping experiments	29

5	Discussion	33
5.1	Suitability of existing clay classifications for Dutch safety standards	33
5.2	Uncertainties caused by the setup of the fire hose method	34
5.3	Suitability of methods used to calculate the hydraulic loads	37
5.3.1	Uncertainties in calculating the hydraulic loads occurring during the fire hose method experiments	37
5.3.2	Uncertainties in calculating the hydraulic loads occurring during the wave overtopping experiments	38
5.4	The effect of the clay structure on the ability to correlate results of the fire hose method experiments to results of wave overtopping experiments	39
6	Conclusions and Recommendations	40
6.1	Conclusions	40
6.2	Recommendations	42
6.2.1	Performing fire hose method experiments in the future	43
	Bibliography	44
A	Determining the Critical Stress and Erodibility Coefficient	47
B	Action Plan	48
B.1	Introduction	49
B.2	Materials	51
B.3	Executing the experiments	52
B.3.1	Test setup	52
B.3.2	Test plan	53
B.3.3	Location	53
B.3.4	Planning	54
B.4	Logbook	55
C	Fire Hose Method Results Per Test	56
C.1	Results Test A	57
C.2	Results Test B	59
C.3	Results Test C	61
C.4	Results Test D	63
C.5	Results Test E	65
C.6	Results Test F	67
D	Dike Cover Layer at Hedwige-Prosperpolder	69
D.1	Location of rests	69
D.2	Description of cover layer	70
E	Recommendations for Performing Fire Hose Method Experiments in the Future	72

List of abbreviations

EFA	Erosion Function Apparatus
ENW	Expertise Netwerk Water safety
GEKB	Grasbekleding erosie kruin en binnentalud (English: Grass cover erosion crest and inner slope)
JET	Jet Erosion Test
LL	Liquid Limit
PI	Plasticity Index
RCT	Rotating Cylinder Test
RETA	Rotating Erosion Testing Apparatus
TAW	Technische Adviescommissie voor de Waterkeringen (Currently known as ENW)
TRL	Technology Readiness Level
USCS	Unified Soil Classification System
WBI	Wettelijk Beoordelingsinstrumentarium (English: Legal Assessment Protocol)

List of Symbols

A	Cross-sectional area of control volume	[m ²]
A_n	Cross-sectional area of nozzle	[m ²]
A_2	Area where normal stress acts on	[m ²]
d	Distance from nozzle to impact location	[m]
d_{av}	Average height of erosion hole	[m]
E	Erosion rate	[m/s]
E_{av}	Average erosion rate	[cm/min]
E_d	Erosion rate of depth	[cm/min]
E_{max}	Maximum erosion rate	[cm/min]
E_V	Erosion rate of volume	[cm ³ /min]
f	Friction factor	[-]
F	Net force	[N]
F_n	Normal force	[N]
F_x	Net force exerted in x-direction	[N]
F_y	Net force exerted in y-direction	[N]
h	Height of nozzle	[m]
k	Erodibility coefficient	[m ³ /sN]
Q	Flow rate	[m ³ /s]
Q_p	Pump rate	[L/min]
T_n	Normal stress	[N/m ²]
T_s	Shear stress	[N/m ²]
u or U	Flow velocity	[m/s]
u_{max}	Maximum flow velocity	[m/s]
V	Overtopping volum	[m ³ /m]
α	Power coefficient	[-]
α_i	Angle of incidence	[degrees]
α_s	Angle of nozzle	[degrees]
α_1	Angle of slope of start control volume	[degrees]
α_2	Angle of slope of end control volume	[degrees]

ρ or ρ_w	Density of water	[kg/m ³]
σ_n	Normal stress	[N/m ²]
s	Shear stress	[N/m ²]
τ	Stress	[N/m ²]
τ_c	Critical stress	[N/m ²]
τ_s	Shear stress	[N/m ²]

List of Figures

1.1	Clay categorisation as proposed by TAW (1996).	3
1.2	Clay categorisation as proposed by Schematiseringshandleiding grasbekleding (2021).	4
1.3	Setup of the fire hose method experiment.	6
2.1	Schematic overview of (a) submerged JET, (b) EFA, and (c) RCT (Hanson & Cook, 2004; Briaud et al., 2017; van Steeg & Mourik, 2020).	9
2.2	USCS erosion chart.	11
3.1	Visualisation of the adjustable nozzle.	12
3.2	Fire hose method experiment performed in the Hedwige-Prosperpolder.	13
3.3	Visualisation of removed grass cover and the angle of incidence of the jet.	14
3.4	Points used from raster to calculate average depth over middle 10 centimeters.	14
3.5	Determining the (a) erosion rate of the depth (E_d), (b) maximum erosion rate (E_{max}), and (c) erosion rate of the volume (E_V).	15
3.6	Wave overtopping experiment performed in the Hedwige-Prosperpolder.	16
3.7	The dike profile (a) visualised using photogrammetry, and (b) before waves of 500 L/m were released at 4 measuring locations (Ebrahimi, 2022).	16
3.8	Profile of the erosion hole after each interval of test C.	18
3.9	Profile of erosion hole during interval 4 of test C between 10 and 30 cm.	19
3.10	The erosion rate (E_d) and applied normal stress (σ_n) during (a) test A and (b) all tests at location where jet impacts.	20
3.11	The erosion rate (E_d) and applied normal stress (σ_n) during (a) test A and (b) all tests at entire length of test section.	21
3.12	The erosion rate (E_d) and applied normal stress (σ_n) during all tests visualised per flow velocity.	21
3.13	The erosion rate (E_d) and applied normal stress (σ_n) during all tests visualised using a double logarithmic scale.	22
3.14	The erosion rate (E_d) and applied normal stress (σ_n) for tests performed with small flow velocities.	22
3.15	The erosion rate (E_d) and applied normal stress (σ_n) visualised per flow velocity (u).	23
3.16	Ratio between erosion rate (E_d) and applied normal stress (σ_n) during all tests under different flow velocities (u).	23
3.17	Relation between the three parameters erosion rate (E_d), normal stress (σ_n), and flow velocity from nozzle (U).	24
4.1	Development of hole caused by erosion where the water jet causes a hole on the impact location.	25
4.2	Development of hole caused by erosion where the water flow follows the shape of the hole.	25
4.3	Measured depth erosion rate (E_d) under (a) calculated normal stresses (σ_n) and (b) flow velocity from nozzle (U) during the fire hose method experiments.	26
4.4	Measured average erosion rate (E_{av}) under (a) calculated normal stresses (σ_n) and (b) flow velocity from nozzle (U) during the fire hose method experiments.	27
4.5	Measured maximum erosion rate (E_{max}) under (a) calculated normal stresses (σ_n) and (b) flow velocity from nozzle (U) during the fire hose method experiments.	27

4.6	Measured erosion rate of the volume (E_V) under (a) calculated normal stresses (σ_n) and (b) flow velocity from nozzle (U) during the fire hose method experiments.	28
4.7	Erosion rate (E) under (a) calculated normal stress (σ_n) and (b) calculated shear stress (σ_s) during the wave overtopping experiments.	29
4.8	Picture of the erosion at the bottom of hole after the wave overtopping experiments were finished.	30
4.9	Results of wave overtopping experiments and fire hose method experiments: Erosion rate (E) caused by (a) normal stress (σ_n) and (b) flow velocity (u).	31
4.10	Results of wave overtopping experiments and fire hose method experiments: Average erosion rate (E) caused by (a) normal stress (σ_n) and (b) flow velocity (u).	32
5.1	Results of JETS in Hedwige-Prosperpolder indicating (a) the Atterberg Limits and (b) the erodibility coefficient (k) and critical stress (τ_c).	34
5.2	(a) Hole caused by jet and (b) jet causing hole.	35
5.3	Flow of wave in excavated hole during wave overtopping experiments.	35
5.4	Measuring raster used during fire hose method experiments.	36
5.5	Spreading of the flow after the jet impacts.	37
5.6	Development of erosion hole during test A (zoomed in).	38
5.7	Images used for photogrammetry (a) before and (b) after 10 waves of 2000 L/m were released.	39
A.1	Example of determining the erodibility coefficient (k) and critical stress (τ_c).	47
B.1	Prepared surface.	52
B.2	Schematisation of fire hose method setup.	53
B.3	Schematisation of prepared dike surface and angle of incidence of water jet.	53
B.4	Measuring points at erosion hole every ten centimeters.	54
C.1	Development of erosion hole during test A.	57
C.2	(a) Erosion rate of depth, (b) average erosion rate, (c) maximum erosion rate, and (d) erosion rate of volume under normal stresses during test A.	57
C.3	(a) Erosion rate of depth, (b) average erosion rate, (c) maximum erosion rate, and (d) erosion rate of volume under flow velocities during test A.	58
C.4	Development of erosion hole during test B.	59
C.5	(a) Erosion rate of depth, (b) average erosion rate, (c) maximum erosion rate, and (d) erosion rate of volume under normal stresses during test B.	59
C.6	(a) Erosion rate of depth, (b) average erosion rate, (c) maximum erosion rate, and (d) erosion rate of volume under flow velocities during test B.	60
C.7	Development of erosion hole during test C.	61
C.8	(a) Erosion rate of depth, (b) average erosion rate, (c) maximum erosion rate, and (d) erosion rate of volume under normal stresses during test C.	61
C.9	(a) Erosion rate of depth, (b) average erosion rate, (c) maximum erosion rate, and (d) erosion rate of volume under flow velocities during test C.	62
C.10	Development of erosion hole during test D.	63
C.11	(a) Erosion rate of depth, (b) average erosion rate, (c) maximum erosion rate, and (d) erosion rate of volume under normal stresses during test D.	63
C.12	(a) Erosion rate of depth, (b) average erosion rate, (c) maximum erosion rate, and (d) erosion rate of volume under flow velocities during test D.	64
C.13	Development of erosion hole during test E.	65
C.14	(a) Erosion rate of depth, (b) average erosion rate, (c) maximum erosion rate, and (d) erosion rate of volume under normal stresses during test E.	65
C.15	(a) Erosion rate of depth, (b) average erosion rate, (c) maximum erosion rate, and (d) erosion rate of volume under flow velocities during test E.	66
C.16	Development of erosion hole during test F.	67

C.17	(a) Erosion rate of depth, (b) average erosion rate, (c) maximum erosion rate, and (d) erosion rate of volume under normal stresses during test F.	67
C.18	(a) Erosion rate of depth, (b) average erosion rate, (c) maximum erosion rate, and (d) erosion rate of volume under flow velocities during test F.	68
D.1	Locations of the exploration pits on the land side slope of the dike (Koelewijn, 2022).	69
D.2	(a) Back wall and (b) side wall of ‘Proefkuil West’ (Koelewijn, 2022). The division between each layer is indicated with a white line.	70
D.3	(a) Back wall and (b) side wall of ‘Proefkuil Oost’ (Koelewijn, 2022). The division between each layer is indicated with a white line.	71

List of Tables

1.1	Requirements for clay usage in dikes as proposed by TAW(1996).	3
3.1	Flow velocities during the six fire hose method experiments performed in the Hedwige-Prosperpolder.	13
B.1	Flow velocities during the six fire hose method experiments performed in the Hedwige-Prosperpolder.	53
D.1	Description of exploration pit ‘Proefkuil West’ per layer (Koelewijn, 2022).	70
D.2	Description of exploration pit ‘Proefkuil Oost’ per layer (Koelewijn, 2022).	71

Chapter 1

Introduction

The Netherlands is protected against flooding by almost 18.000 kilometers of dike (*Onderzoek Grasbekleding Dijken*, n.d.). The assessment of these dikes is described in the WBI 2017 (Dutch: Wettelijk Beoordelingsinstrumentarium) (*Schematiseringshandleiding grasbekleding*, 2021). One of the failure mechanisms for which grass-covered dikes are assessed is wave overtopping, during which waves overtop the crest of a dike during an extreme event and flow down the landward slope (van Bergeijk, Verdonk, et al., 2021; van Bergeijk et al., 2019). The waves cause high hydraulic loads on the dike cover and when these loads exceed the strength of the cover material, the cover will erode. The strength of the cover of grass-covered dikes is assessed by the protocol GEKB (Dutch: Grasbekleding erosie kruin en binnentalud) of the WBI 2017. This protocol describes that a dike has failed when the top layer has eroded over a depth more than 0.2 meter (Rijkswaterstaat, 2012). The top 0.2 meter of the top layer consists of a clay layer supported by the root system of grass. This root system protects the clay layer against erosion and significantly reduces the erosion rate. When the root system is eroded, the clay aggregates wash out more easily and the erosion rate increases. When the erosion hole develops and expands upstream, it can lead to a dike profile which is lower than the water level outside the dike. In this case, a breach has formed and the dike completely fails ('t Hart et al., 2016).

Even though the dike still has residual strength from the remaining cover layer after the grass cover has eroded, the strength of the residual cover layer and core of the dike is not taken into account in the protocol GEKB. Grass-covers are visually inspected and classified based on its coverage (Rijkswaterstaat, 2012). However, the knowledge is missing on the erosion processes and strength of clay and therefore the clay layer is not included in the protocol. Because of this exclusion, the calculated failure probability by wave overtopping is conservative, since the strength of the cover layer is not taken into account (Breteler, 2021; 't Hart et al., 2016). By performing experiments, the erosive behaviour of the cover materials can be determined to make more accurate estimates in the erosion processes during wave overtopping (Wopereis & van Steeg, 2021).

1.1 Theoretical background

Clay is used as a building material of dikes in the cover layer and in the core of the dike. Clay used in dikes in the Netherlands is classified into three categories, which are based on its capacity to resist erosion. Category 1 is classified as erosion resistant, Category 2 as moderately erosion resistant, and Category 3 as little erosion resistant (TAW, 1996). Which clay category may be used for the structure depends on the function of the structure. For example, water-retaining structures with a bare clay cover are only allowed to be covered with erosion resistant clay. Whereas structures with a well-developed grass cover can also be covered with moderately to little erosion resistant clay (de Vries & de Bruijn, 2021). The requirements of each category are described in 'Technisch rapport klei voor dijken' (TAW, 1996). This report describes that the erosion resistance of clay can be determined by the Atterberg limits and sand content of the clay. The Atterberg limits are a measure for the plastic properties of cohesive soils and describe the water-retaining capacity of the clay by means of the plasticity index and the liquid limit (TAW, 1996).

The clay categorisation advised by the Technische Adviescommissie voor de Waterkeringen (TAW, currently known as the Expertise Network Water safety (ENW)) is based on field and laboratory experiments performed between 1985 and 1987 by Grondmechanica Delft and are described in the report ‘Onderzoek naar het beoordelen van de geschiktheid van kleigrond voor bekleding van dijken met grasbekleding’ (Kruse et al., 1988). Experiments are performed on (samples of) grass-covered dikes, which are constructed entirely out of clay or have a clay cover layer over the sand core. The aim of the research was to develop requirements for clay used in grass-covered dikes. Rotating Cylinder Tests (RCT) have been performed on 30 clay samples of dikes spread over the Netherlands (Postma & Dekker, 1985). The samples were taken at a depth of 0.4 to 0.5 meters, had a diameter and height of 6.7 cm and 5 cm respectively. During the RCT, the erosion resistance of a sample is tested by increasing the rotational speed of the outer cylinder in intervals. The rotation of the outer cylinder causes the water between the soil sample and the outer cylinder to flow at high velocity. This results in shear stress on the sample and leads to erosion of the sample. At the start of the experiments, the rotational speed of the outer cylinder was set to 100 rpm. For one hour, the rotational speed is incrementally increased with 100 rpm every 10 minutes. When a rotational speed of 600 rpm is reached, this rate is kept constant for one hour. After this time, the rotational speed is further incrementally increased in intervals with 100 rpm every 10 minutes. When a rotation rate of 1200 rpm is reached, this rate is held constant till the experiment is stopped. During the experiment, the weight of the sample is measured with intervals of 5 to 15 minutes. The magnitude of the shear stress is measured by the testing apparatus simultaneously.

The results of the RCT generally show three stages during the erosion process (Postma & Dekker, 1985). During the first stage, the sample is quite smooth which results in barely any shear stresses on the sample. During this stage, individual particles become loose from the sample, which results in a slightly higher shear stress. During the second stage, the shear stresses increases linearly and a slight increase in mass loss is observed. The third stage is often observed when by a sharp increase of the shear stress due to the increase in rotational speed. A progressive mass loss is observed. The critical rotational speed and critical shear stress are obtained from the acquired data. In the report of Grondmechanica Delft (1988), the critical shear stress and critical rotational speed are defined as the shear stress and rotational speed where 30% of the initial mass at the start of the experiment is eroded. Based on the experiments performed by Grondmechanica Delft (1988), the erosion classes are defined. Samples of which 30% of the mass has eroded when the rotational speed is smaller than 900 rpm is categorised as very sensitive for erosion. Samples with a critical rotational speed between 900 and 1150 rpm are classified as moderately sensitive for erosion. Samples with a critical rotational speed of 1150 and above are classified as little sensitive for erosion (Kruse et al., 1988). These results are plotted in a plasticity chart. The chart indicates that samples which are little sensitive for erosion overall have a liquid limit (LL) above 45% and a plasticity index (PI) above the line described by the equation $PI=0.73(LL-20)$, and are classified by the TAW as erosion resistant. Samples which are indicated as moderately sensitive for erosion, generally have a plasticity index above 18% and a liquid limit below 45%. These samples are classified as moderately erosion resistant. The samples outside of these ranges are classified by Grondmechanica Delft as very sensitive for erosion, which resulted in the classification of the TAW as little erosion resistant. Besides the plasticity index and liquid limit, other strong correlations between the erosion resistance of the sample and soil characteristics were found. Based on these findings, the classification of clay by the TAW contains requirements on the Atterberg limits, grain size distribution, organic matter content, salt content, water content, chalk content, colouring, and odour. An overview of the requirements per clay category is shown in Figure 1.1 and Table 1.1.

To base the categorisation of clays on these soil characteristics seems logical since this conclusion is also supported by other studies. In 1947, Casagrande found relations between the geotechnical behaviour of fine-grained soil samples and the liquid limit and plasticity index of the sample (Moreno-Maroto et al., 2021). Casagrande (1947) made a division between inorganic clays and other fine-grained materials, using the equation $PI = 0.73(LL-20)$. This dividing line is called the "A-line". This A-line is also used as a dividing line in the clay categorisation proposed by the TAW in 1996, as can be seen in Figure 1.1

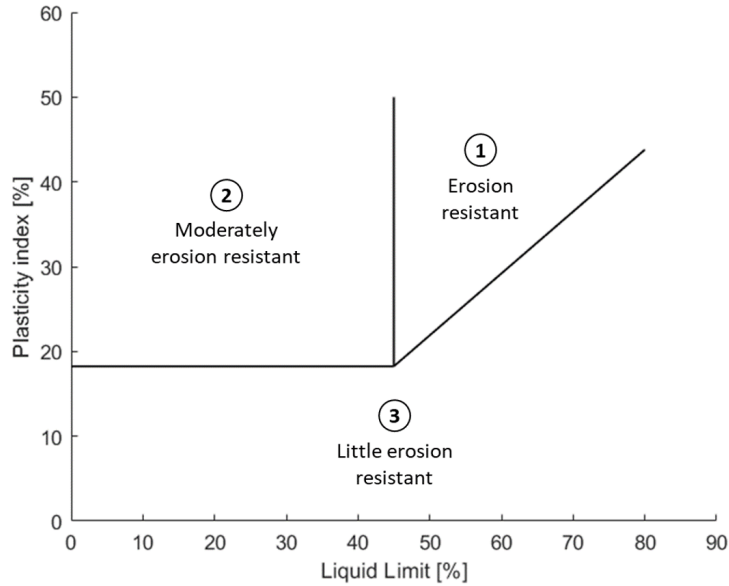


Figure 1.1: Clay categorisation as proposed by TAW (1996).

Table 1.1: Requirements for clay usage in dikes as proposed by TAW(1996).

Category	Thresholds for classification tests		
	Liquid limit LL [%]	Plasticity index PI [%]	Sand content [%]
1) Erosion resistant clay	>45	>0.73(LL - 20)	<40
2) Moderately erosion resistant clay	<45	>18	<40
3) Little erosion resistant clay	<0.73(LL - 20)	<18	>40
For all categories hold			
Organic matter content [%]	<5		
Salt content [g/L]	<4		
Chalk content [%]	<25		
No extreme discoloration during excavation or drying			
No deviant strong odour			

and is also commonly used internationally for soil classifications standards (Kruse et al., 1988). The division between low and high compressible clay is set by Casagrande at a liquid limit of 50%. This differs from the boundary of the liquid limit set by the TAW, which is 45%. This implicates that clay is more often classified as erosion resistant when using the categorisation proposed by the TAW.

The report of Briaud et al. (2019) summarises different studies on relations between soil characteristics and the erosion resistance of clays and other soils. Based on the results of flume tests, Gibbs (1962) found that the critical shear stress is proportional to the liquid limit and proposed four erosion categories based on the plasticity index and liquid limit. 45 case studies were assessed, which resulted in the following categories: ‘Highest resistance to erosion’, ‘Slight erosion expected’, ‘Moderate erosion expected’, and ‘Low resistance to erosion’. The categorisation is similar to the categorisation proposed by Casagrande. Above the A-line, the ‘Highest resistance to erosion’ and ‘Slight erosion expected’ categories are situated. However, it is remarkable that the category ‘Highest resistance to erosion’ has a range of the liquid limit between 30% and 40%. Outside this range, clays are classified as ‘Slight erosion expected’. This is in contrast with the categorisation of Casagrande in which clays with a liquid limit above 50% are classified as erosion resistant instead of 45%.

From flume tests performed by Lyle and Smerdon (1965) could be concluded that parameters such as void ratio during compaction, plasticity index, percentage of organic matter, average particle size, Ca/Na-ratio, and percentage of clay are, amongst others, influencing parameters on the erosion

resistance of clay. Shaikh et al. (1988) proposed empirical correlations between the percentage of clay and the erosion rate coefficient. Submerged JET tests performed by Hanson (1992) and Hanson and Robinson (1993) and open channel tests performed by Robinson (1990) showed that the erosion resistance of unsaturated soil samples increases with an increase in moisture content during compaction, whereas the opposite relationship holds for saturated soil samples. Briaud (2008) concluded that for fine-graded soils no direct relationship is present between the critical velocity and critical shear stress and the mean particle size, but the relation between the critical velocity/shear stress and mean particle size can be described by upper and lower boundary equations. Shan et al. (2015) proposed a relationship for cohesive soils between the critical shear stress and the water content, unconfined compressive strength, plasticity index, and fine-grained soil content. Sing and Thompson (2015) indicated that the critical shear stress varies with the moisture content of the soil, but is proportional to the soil moisture content until the level is below the plastic limit.

Since the advice of TAW was released in 1996, new insights have been found regarding the functioning and the assessment of clay soils in dikes. These new insights are used to optimise the use of clay in dikes and are based on numerical simulations, large-scale experiments, field observations, and additional analyses regarding the effects of parameter values on the performance of clay (van Meurs & Kruse, 2017). This resulted in four recommendations on the classification of clay in dikes, the development of damage in clay on dikes (Rijkswaterstaat, 2018). The first recommendation is adjusting the classification boundaries of the clay, by shifting the boundary of the liquid limit between classes 1 and 2 from 45% to 40%. This way, more clay is classified as erosion resistant. Second: the advice is given to allow a bandwidth in the assessment of clay samples. This reasoning is supported by the following: 1) the accuracy of the liquid limit is limited, and 2) geotechnical parameters are heterogeneous by nature. By implementing the second recommendation, it is prevented that clays are unnecessarily disapproved. These recommendations lead to a new classification figure (Figure 1.2). The third and fourth recommendation are related to use less conservative, and thus more realistic values for the permeability of clay and to improve the consolidation process of the clay layers during construction.

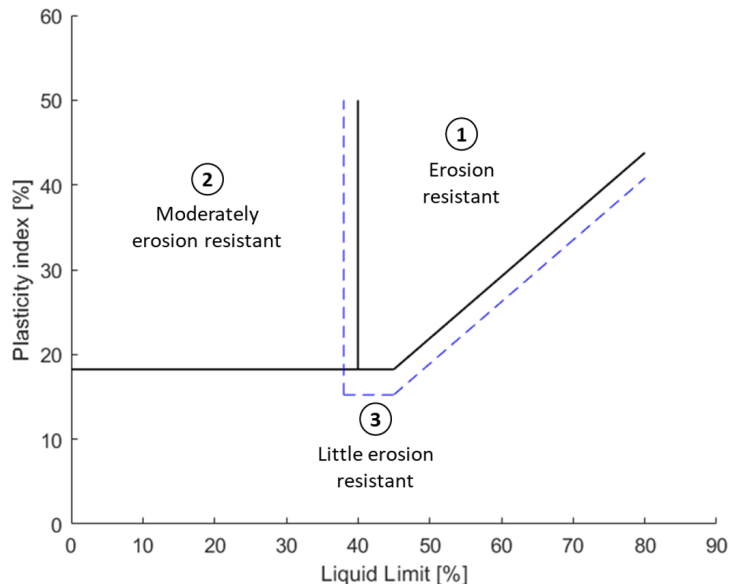


Figure 1.2: Clay categorisation as proposed by Schematiseringshandleiding grasbekleding (2021).

The ability of clay to resist erosion depends on the characteristics of the clay, such as the soil structure, cohesion, friction angle, plastic and liquid limit, porosity, sand and organic matter content, and compaction (Briaud et al., 2019; Hoffmans et al., 2009; TAW, 1996; Yagisawa et al., 2019). The erosion resistance of cohesive soils is commonly described by two erosion parameters, namely the erodibility coefficient (k) and the critical stress (τ_c) (Mazurek, 2010). The critical stress is the stress

at which the soil starts to erode. The erodibility coefficient represents the susceptibility of a soil to erode by an exogenic force (Wang et al., 2013). These coefficients are used in the erosion relation (Hanson & Cook, 2004):

$$E = \begin{cases} k(\tau - \tau_c)^\alpha & \text{if } \tau > \tau_c \\ 0 & \text{if } \tau \leq \tau_c \end{cases} \quad (1.1)$$

Where

E	Erosion rate	[m/s]	
k	Erodibility coefficient	Unit depends on α	(For $\alpha = 1 : [m^3/sN]$)
τ	Stress	[N/m ²]	
τ_c	Critical stress	[N/m ²]	
α	Power coefficient	[-]	

The erosion relation is widely used to determine the erosion resistance of clay (Briaud et al., 2019). Via experiments, the erosion resistance is measured to verify the strength of the existing dike. However, it is not possible to measure the erodibility coefficient and critical stress directly. Depending on the type of experiment, the applied stress or flow velocity and the resulting erosion rate is measured. Using the erosion relation, the erodibility coefficient and critical stress is derived from the observed erosion rate and the flow velocity or stresses caused by the water (Appendix A). From the data, the critical stress is first calculated. This is the stress acting on the clay at the moment the soil starts to erode or erosion no longer occurs, depending on the type of test (van Damme et al., 2021). When fitting a line through the data points, the erodibility coefficient is indicated by the slope of the line. A linear relation is assumed when $\alpha = 1$ is used. When using an other value for the power coefficient, a non-linear relation is assumed. However, this can lead to over-fitting of the data (Wahl, 2021).

1.2 Problem context

The strength of clay against erosion caused by overtopping waves is currently not taken into account in the assessment protocol of dikes, due to the lack of knowledge on the erosion processes and strength of clay layers. Consequently, the calculated failure probability by wave overtopping is conservative. Knowledge about the erosive behaviour and erosion resistance of clay is needed to include clay erosion in the assessment protocol. To gain these insights, it is needed to perform experiments.

Experiments used to determine the erosion resistance of clay in dikes are divided into small- and large-scale experiments. Common small-scale experiments are for example the Jet Erosion Test (JET), Erosion Function Apparatus (EFA), and Rotating Cylinder Test (RCT). On the other hand, large scale tests are: flume experiments and wave overtopping experiments (Briaud et al., 2019). The small-scale experiments are performed on clay samples in laboratories or on a small test area in the field. The advantage of small-scale experiments is that they are often less expensive and less logistically challenging than large-scale experiments (Briaud et al., 2019; van Steeg & Mourik, 2020). The disadvantage of such experiments is that the scale is too small to include the heterogeneous character of the clay and samples are easily disturbed leading to unrepresentative results. Many experiments have to be performed to gain insight in the erosion character of the clay. These problems are overcome with large-scale experiments (Breteler, 2021; van Steeg & Mourik, 2020). However, these experiments are often costly and logistically challenging.

The fire hose method is designed by Deltares to overcome problems which occur during commonly performed small- and large-scale test methods (Figure 1.3). The test method is designed to quantify the strength of grass covers and transitions of dikes against wave overtopping in situ. The goal during the design phase of the fire hose method was to create a low-threshold test method, which gives insights in the effect of structured clay on its resistance to wave overtopping or to classify the strength of the dike cover (van Steeg & Mourik, 2020). The hydraulic load caused by the setup of the fire hose method is at a scale of decimeters instead of centimeters as is the case for other small-scale test methods. Hence,

the fire hose method should be able to take the complex heterogeneous character of clay into account in a better way. Since the setup is relatively small compared to large-scale experimental setups, the fire hose method is less logistically challenging and less costly.

The fire hose method has already been used on a couple of occasions. The first tests have been performed on grass on the terrain of Deltares to get an indication about a possible setup (van Steeg & Mourik, 2020). Since then, tests have been performed on blocks originating from grass-covered dikes and on the Waddenzeedijk in Friesland. These have been performed to test the effect of different setups, like differences in flow velocity and angle of incidence (van Steeg, 2021; Wopereis & van Steeg, 2021). Fire hose method experiments have mainly been performed on clay, covered with grass under different flow velocities ranging between 4.5 and 7.5 m/s, and with angles of incidence between 5 and 20 degrees. Erosion was measured over different intervals, and was used to indicate the erosion rate over the length, width, and depth of the erosion hole. One test was performed on bare clay. During this test, the flow velocity was held constant at 7 m/s and the angle of incidence was 20 degrees. The erosion rate under these conditions was extremely high and the test had to be aborted after 3 minutes (van Steeg, 2021). To be able to perform more measurements on a test section, the erosion rate of clay must be reduced. Here for, the fire hose method setup must be adjusted.

Next to a better setup to test clay covers, more insight is needed on how results of the fire hose method can be used to determine the erosion resistance of covers or to classify them. This is done by analysing the results of the fire hose method experiments and results from large-scale tests performed on the same dike section. These results are used to correlate the outcome to the fire hose method to those of the wave overtopping experiments.



Figure 1.3: Setup of the fire hose method experiment.

1.3 Research goal and research questions

The goal of this thesis is to indicate to what extent the fire hose method can be used to accurately determine the erosion resistance of clay in dikes against wave overtopping. Small-scale fire hose method experiments and large-scale wave overtopping experiments are performed in the Hedwige-Prosperpolder. To analyse the results of the fire hose method experiments, the flow velocity and the erosion profile of the hole are used to determine the hydraulic loads on the clay and resulting erosion rate. Data from the wave overtopping experiments, such as depth of the excavated hole and the wave volumes, are used to determine the erosion rate and hydraulic forces occurring during large-scale experiments. The analysis of these test results is used to correlate the outcome of the fire hose method experiments to the outcome of the wave overtopping experiments in order to reach the goal of this study. As a result, the main research question and sub-questions are formulated as follows:

Main research question:

How can the fire hose method be used to accurately determine the erosion resistance of clay in dikes against wave overtopping?

Subquestions:

1. Which test outcomes lay at the basis of clay categorisation and how is dealt with the spread in these outcomes?
2. What experimental setup of the fire hose method is most appropriate to determine the critical stress and erodibility coefficient of clay?
3. To what extent are the forces, that are exerted on the clay during the fire hose method experiments, representative for wave overtopping?
4. To what extent can the results of the fire hose method be correlated to wave overtopping experiments performed on the same clay?

1.4 Thesis outline

Chapter 2 describes the results of the literature review to answer the first subquestion. The methodology used to answer the latter three subquestions is described in Chapter 3. This chapter describes how the Fire Hose Method can be adjusted, such that the optimal setup is found to determine the erosion resistance of clay, how the experiments with the Fire Hose Method and Wave Overtopping Simulator are performed in the Hedwige-Prosperpolder and how their results are used to determine the hydraulic loads and erosion rates during these tests. This chapter also describes how these results are used to determine to what extent the stresses, exerted on the clay during the fire hose method experiments, are representative for wave overtopping and to what extent the results of the fire hose method experiments can be correlated to the results of wave overtopping experiments. Chapter 4 describes the results of the study and Chapter 5 discusses the study. Finally, the conclusions on this study and recommendations for future studies is given in Chapter 6.

Chapter 2

Literature Review

2.1 Experiments to determine the erosion resistance of clay

A literature study is performed to gain insight in experiments which are commonly performed to test the erosion resistance of clay. This has indicated how test results are used to categorise clay. Furthermore, it is indicated how data is analysed and how is dealt with the spread of the outcome. First, the small-scale experiments Jet Erosion Test (JET), Erosion Function Apparatus (EFA), and Rotating Cylinder Test (RCT) are discussed. Secondly the large-scale experiments such as tests using the wave overtopping simulator and Delta Flume are discussed.

2.1.1 Small-scale experiments

During submerged JETs, a small jet of water is aimed perpendicular at a submerged sample of the clay (Figure 2.1a) (van Damme et al., 2021). Due to the stresses exerted on the clay by the jet, the soil erodes. When the bed level of the soil lowers, the stresses exerted on the bed decrease. During the experiment, the changes in scour depth are measured, which is used to calculate the erosion rate for the corresponding time interval and the applied stress. Using the data about the erosion depth during the experiment, the critical stress and erodibility coefficient are often calculated using the Blaisdell Method (Hanson & Cook, 2004). Also other methods such as the Iterative Method and Scour Depth Method are used to predict the equilibrium scour range and to find the linear relation between the critical shear stress and erodibility constant (Wahl, 2016). The Blaisdell Method tends to overestimate the equilibrium scour depth, resulting in small values for the critical shear stress (Karamigolbaghi et al., 2017). The other two methods significantly over-predict the value for the critical shear stress, resulting in unrealistic values. Due to the assumptions made for the JET results and the various methods, the predicted erosion parameters are uncertain (Karamigolbaghi et al., 2017). This results in uncertainties in the accuracy of the derived values for the critical shear stress and erodibility coefficient and their physical representation. That is why, results for the erosion parameters from the JET are often presented with a retained value and a confidence interval (GeophyConsult, 2021).

Tests performed with the EFA use a soil sample to determine its erosion rate under different flow velocities (Briaud et al., 2017). During the test, the soil sample is placed in a Shelby tube of which the top is connected to the bottom of a flume (Figure 2.1b). Water flows through the flume with a predefined flow velocity over the top of the sample. The water flow causes a shear stress on the top of the sample, resulting in erosion of the sample when it is above the critical flow velocity. The level of the top of the eroding sample is held constant by the piston on which the sample is placed. During the test, the flow velocity of the water and the pushing rate of the piston are measured. Initially, the flow velocity is set low, such that no erosion occurs. The velocity is increased incrementally till the sample starts to erode. This velocity is defined as the critical flow velocity. Then, the flow velocity is further increased in steps to determine the erosion rate for different flow velocities. During the test, the amount of eroded soil and time span are recorded such that the erosion rate can be calculated. The flow velocity is used to calculate the shear stress on the sample (Equation 2.1). Multiple assumptions have to be made for these calculations, such as the friction factor of the top of the sample and the flow

profile through the flume. Wrong assumptions can result in under- or over-prediction of the erosion parameters (Larsen, 2008).

$$\tau_s = \frac{1}{8} f \rho_w u^2 \quad (2.1)$$

Where:

τ_s	Bed shear stress	[N/m ²]
f	Friction factor obtained from Moody chart	[-]
ρ_w	Water density	[kg/m ³]
u	Flow velocity	[m/s]

The RCT is the only apparatus that directly provides the shear stress on a sample. The apparatus consists of two cylinders between which water is situated (Figure 2.1c). The inner cylinder contains the soil sample. During the test, the outer cylinder rotates and causes the water between the cylinders to generate a couette flow. This causes shear stresses on the sample. A pin is located at the centre of the sample and connected to an arm above the outer cylinder. This arm is positioned against a torsion meter. When shear stresses act on the sample, the central pin will slightly rotate, which is translated by a displacement of the arm and is measured by the torsion meter. The measured torsion is used to determine the applied shear stress. (Chapuis & Gatién, 1986; Lim, 2006; Kruse et al., 1988). A calibration procedure prior to testing is performed, to determine the corresponding shear stress to the measured torsion. By weighing the sample, the amount of eroded soil is determined, which indicates the erosion rate under the applied stress conditions. The RCT is often performed by increasing the rotational speed of the outer cylinder to measure the erosion rate under increasing shear stress conditions. The shear stress during which significant erosion starts taking place is defined as the critical shear stress. The accuracy of the shear stress measurements depends on the sensitivity of the components of the torque meter, the accuracy of the calibration of these components, and the size of the soil sample (Lim, 2006).

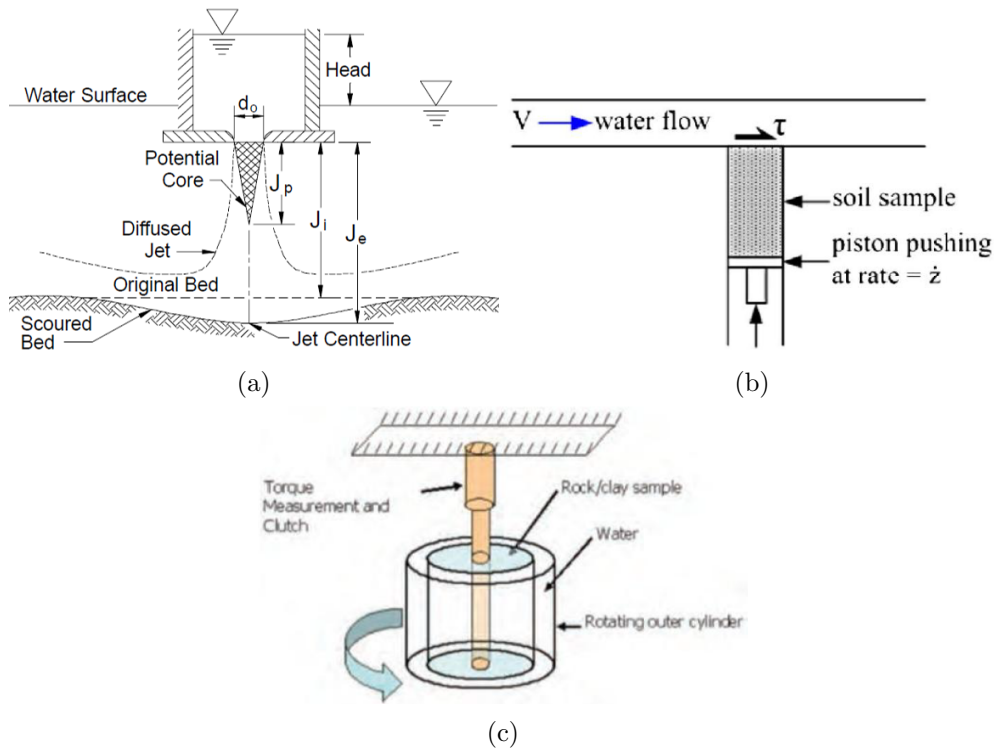


Figure 2.1: Schematic overview of (a) submerged JET, (b) EFA, and (c) RCT (Hanson & Cook, 2004; Briaud et al., 2017; van Steeg & Mourik, 2020).

The loads exerted on the soil (sample) with small-scale experiments are often smaller than the loads exerted on the dike during wave overtopping. JET results have indicated that the erosive behaviour of clay differs under different stress conditions (van Damme et al., 2021). When lower stresses are acting on the soil, a lower critical shear stress and erosion rate are observed. This can be caused by the bi-linear behaviour which is often observed during JET and RCT. During these tests, when lower stresses act on the soil, lower erosion rates are observed, and when higher stresses act on the soil, higher erosion rates are observed. This phenomenon occurs because grain particles tend to erode under low stresses and clods of soil tend to erode under higher stresses (GeophyConsult, 2021). Hence, to determine the erosion resistance of the clay (sample) of a dike, it is important that stresses exerted on the soil are similar to stresses caused by wave overtopping to indicate the accurate critical shear stress and erodibility coefficient.

The main downside of small-scale experiments is their inability to include the heterogeneous character of the soil. Forces exerted on the clay (sample) act on a relatively small area in the order of centimeters. However, the differences in soil erodibility of clay occur at the length scale of decimeters (Wichman, 2021). To reduce uncertainty in the values for critical shear stress and erodibility coefficient obtained for a dike section, tests have to be performed on (samples of) various places and depths of the dike. This is also done for tests performed on clay in the Hedwige-Prosperpolder. The report of GeophyConsult (2021) describes the results from JETs performed on 20 samples. The results of these tests are visualised in diagrams showing the evolution of the scour depth over time, the erosion rate caused by the applied stresses, and scatter plots indicate the erodibility coefficient and critical shear stress of the samples visualised in a Hanson diagram. By plotting the results per dike section, the erosion parameters have been analysed per dike section and have been compared to the results of the study area overall. The results can, for example, give a mean value and dispersion of the erosion parameters per dike section or for the entire study area, but also the uncertainty related to the testing procedure can be compared to the variability of the results. Furthermore, the results can be compared to test results performed on samples from other study areas to compare the erosion resistance of the clay to other locations (GeophyConsult, 2021).

2.1.2 Large-scale experiments

Large-scale experiments such as flume experiments and field experiments using the wave overtopping simulator have been performed on dike sections. During these experiments, the loading conditions were adjusted such that they represent overtopping conditions during storms (van der Meer et al., 2009). By simulating overtopping waves, the progress of damages in the dike are measured by for example cameras, lasers, and pin profilers. The processes occurring during wave overtopping have been measured using wave gauges, pressure transducers, and velocity meters (Breteler, 2021; Piontkowitz et al., 2009). The camera's, lasers, and pin profilers measure the development of erosion holes in the dike section over time. These have been used to visualise the erosion progress of the dike profile in terms of erosion depth or volume and have been used to quantify the erosion rates under the applied wave conditions.

The stresses exerted on the soil and erosion parameters are not directly measured during these types of experiments. Models are generally used to calculate the stresses using parameters such as flow velocity and water depth, which are measured during experiments (*Schematiseringshandleiding grasbekleding*, 2021). Erosion models have been used to quantify relations between the hydraulic loads caused by overtopping waves and geometric characteristics of the dike, and erosion velocity (Mourik, 2015; van Bergeijk, 2022). The erosion parameters 'erodibility coefficient' and 'critical stress' are determined using the erosion relation (Equation 1.1).

2.1.3 Clay categorisation based on experimental outcomes

Briaud (2019) describes two methods that provides the erosion category of soil samples. The first method uses the NCHRP-Erosion database, which contains data of tested soil samples and their geotechnical properties such as Atterberg limits and the Unified Soil Classification System (USCS)

categories. By searching for samples with similar properties, the expected values for the erodibility parameters are determined, which can be used to determine an experiment plan for tests. The second method uses the USCS erosion charts for estimating the edibility of a sample. The USCS erosion charts have the erosion rate on the y-axis and the applied stress on the x-axis (Figure 2.2). By plotting the results of the tested sample in the USCS erosion chart, the corresponding USCS category is determined. This gives information about the erosion resistance of the soil sample. Furthermore, the erodibility coefficient and critical stress are shown in these graphs by the slope of the line and the intercept of the line with the x-axis respectively.

The erosion categorisation proposed by Briaud et al. is internationally widely used. However, due to the large variation in soil types included in this system, the ranges obtained for the critical shear stress and erodibility coefficient for each category is quite large and not useful for classifying the erodibility of a clay for Dutch standards (van Steeg & Mourik, 2020).

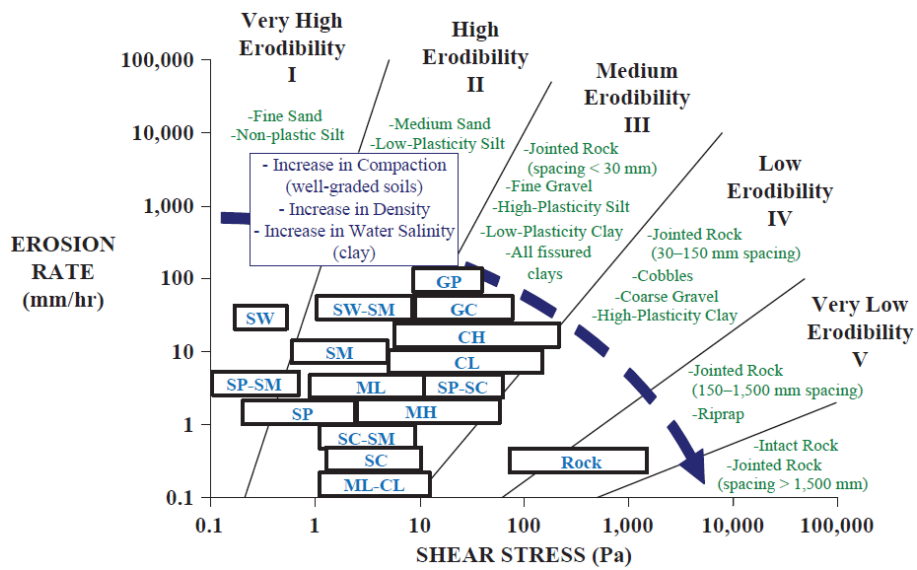


Figure 2.2: USCS erosion chart.

Chapter 3

Methodology

3.1 The basic setup of the fire hose method

The setup of the fire hose method, used during previous tests, is unsuitable to perform tests on bare clay. The high hydraulic loads exerted on the clay, resulted in high erosion rates and the test was terminated after three minutes (van Steeg, 2021). The setup of the fire hose method was adjusted during this study, such that experiments could be performed over a longer time span, which result in more data points. The adjustments made to the setup are made after conversations with the designers and users of the test method.

The settings which can be altered to the setup are the pump rate (Q_p), the height of the nozzle (h), and the angle of the nozzle (α_s) (Figure 3.1). The flow velocity of the jet (u) from the nozzle depends on the pump rate and the cross-sectional area of the nozzle (A_n). The distance from the nozzle to the impact location (d) can be calculated prior to the experiments using the angle and height of the nozzle and the flow velocity. The angle with which the water jet impacts on the surface (α_i) and the flow velocity affect the magnitude of the normal and shear stresses on the clay. The setup of the fire hose method has been adjusted, such that experiments on bare clay could be performed in the Hedwige-Prosperpolder.

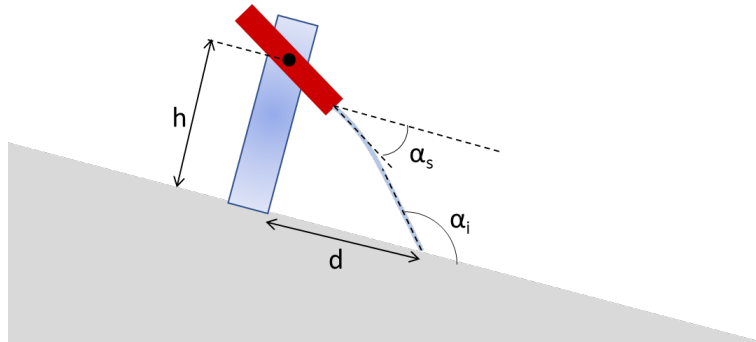


Figure 3.1: Visualisation of the adjustable nozzle.

3.2 Fire hose method experiments performed in the Hedwige-Prosperpolder

The fire hose method experiments were performed from February 22nd till February 24th, 2022 (Figure 3.2). Six test sections were dug halfway of the slope of the dike. These test sections were approximately 0.5 meters wide, 1 meter long and at maximum 0.4 meters deep. The angle and height of the nozzle were kept constant during all tests, to reduced the variation in hydraulic load caused by the setup. The flow velocity of the water from the nozzle was varied to test the erosive behaviour of the clay under different stress conditions. An overview of the flow rate during each interval and the duration of each interval is shown in Table 3.1.



Figure 3.2: Fire hose method experiment performed in the Hedwige-Prosperpolder.

Table 3.1: Flow velocities during the six fire hose method experiments performed in the Hedwige-Prosperpolder.

Section A				Section B				Section C			
Interval	Time [min]	Flow rate [L/min]	Flow velocity [m/s]	Interval	Time [min]	Flow rate [L/min]	Flow velocity [m/s]	Interval	Time [min]	Flow rate [L/min]	Flow velocity [m/s]
1	5	210	1.75	1	5	150	1.25	1	5	150	1.25
2	10	210	1.75	2	5	150	1.25	2	5	150	1.25
3	15	210	1.75	3	10	150	1.25	3	5	210	1.75
4	20	210	1.75	4	10	210	1.75	4	5	300	2.50
5	15	530	4.42	5	10	210	1.75	5	5	300	2.50
				6	15	210	1.75	6	10	300	2.50
								7	10	630	5.25
Section D				Section E				Section F			
Interval	Time [min]	Flow rate [L/min]	Flow velocity [m/s]	Interval	Time [min]	Flow rate [L/min]	Flow velocity [m/s]	Interval	Time [min]	Flow rate [L/min]	Flow velocity [m/s]
1	5	150	1.25	1	5	300	2.50	1	5	390	3.25
2	5	150	1.25	2	5	300	2.50	2	5	390	3.25
3	10	150	1.25	3	10	300	2.50	3	10	390	3.25
4	15	150	1.25	4	15	300	2.50	4	15	390	3.25
5	15	150	1.25								
6	10	630	5.25								

The setup used during the fire hose method experiments is explained in more detail in the Action Plan (Appendix B). During the experiments, a hole is dug to remove the grass cover and to make the angle of incidence as close as possible to 180° (Figure 3.3). This angle of incidence is used to best quantify the magnitude of the normal and shear stresses. The grass cover is removed to solely measure the erosion resistance of the clay layer.

When the hydraulic load, caused by the jet, is larger than the critical load, the soil starts to erode. The erosion depth is measured during the experiments by using a raster of 10 by 10 cm. This ensures that during each measurement, the depth is measured at the same location. The results are noted in the logbook. The measurements are used to calculate the average depth over over the middle 10 to 20 centimeters of the hole at every 10 centimeters over its length (Figure 3.4). Based on these measurements, four indicators for the erosion rate have been determined. The erosion rate at each of these locations is indicated as the ‘depth erosion rate’ (E_d) and is calculated from the difference in the depth before and after the interval and the duration of the interval (Figure 3.5a). Furthermore, the average erosion rate over the entire length of the erosion hole is determined for each interval and is called the ‘average erosion rate’ (E_{av}). This is determined by calculating the mean of the erosion rate of the depth during an interval. The maximum depth is measured after each interval and used to calculate the ‘maximum erosion rate’ (E_{max}) (Figure 3.5b). Finally, the rate of the eroded volume is calculated (E_V). This is done for a width of 10 centimeters, by using the difference in measured

depth. The calculated erosion volume is indicated in Figure 3.5c by the blue area. It is important to note that only the points after the location where the water jet impacts are included. The four parameters are used to find relations between the applied loads and the observed erosion rates. The results of the six experiments are visualised in Appendix C and shows the depth of the erosion holes before the experiment and after each interval. Furthermore, the applied stresses and observed erosion rates of the four parameters are shown.

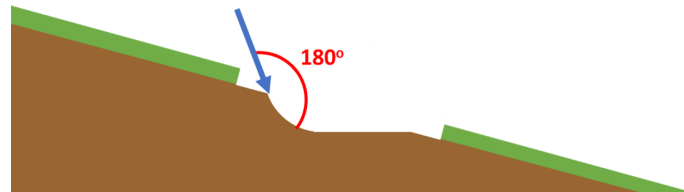


Figure 3.3: Visualisation of removed grass cover and the angle of incidence of the jet.

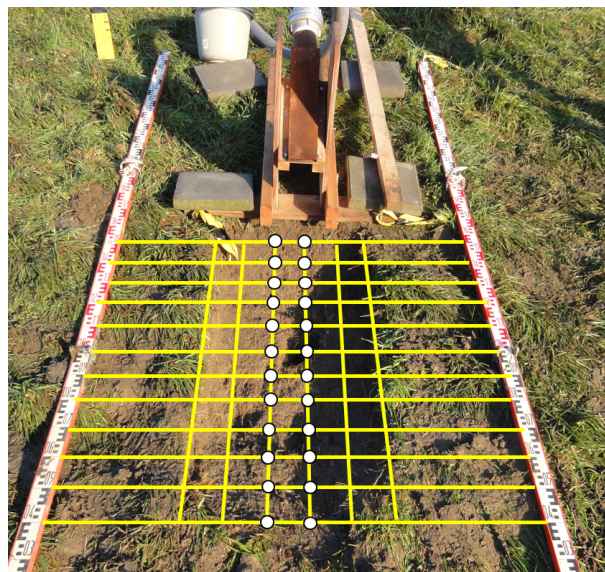
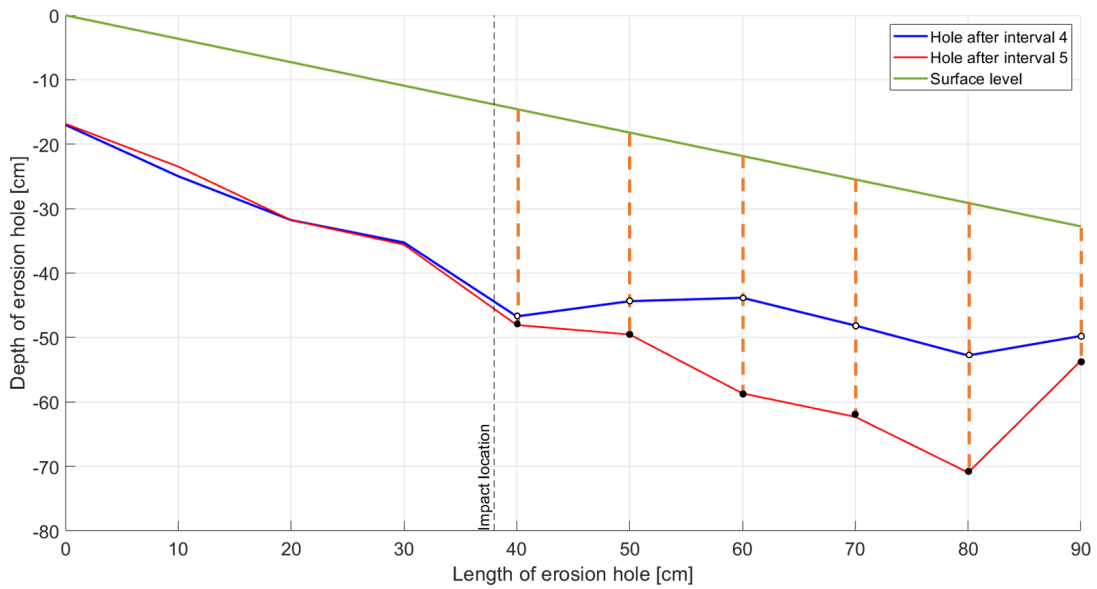
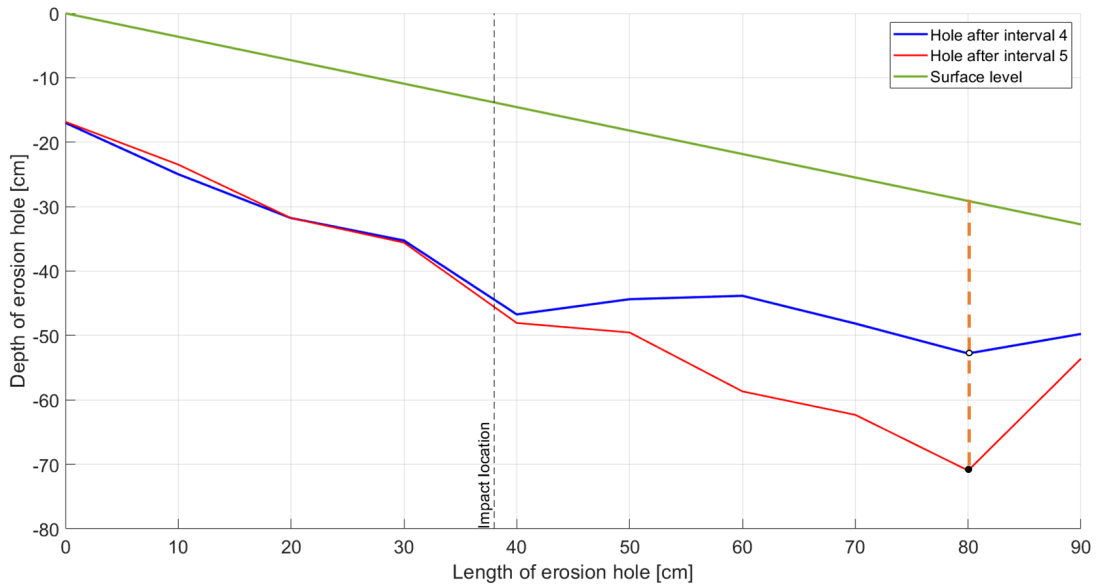


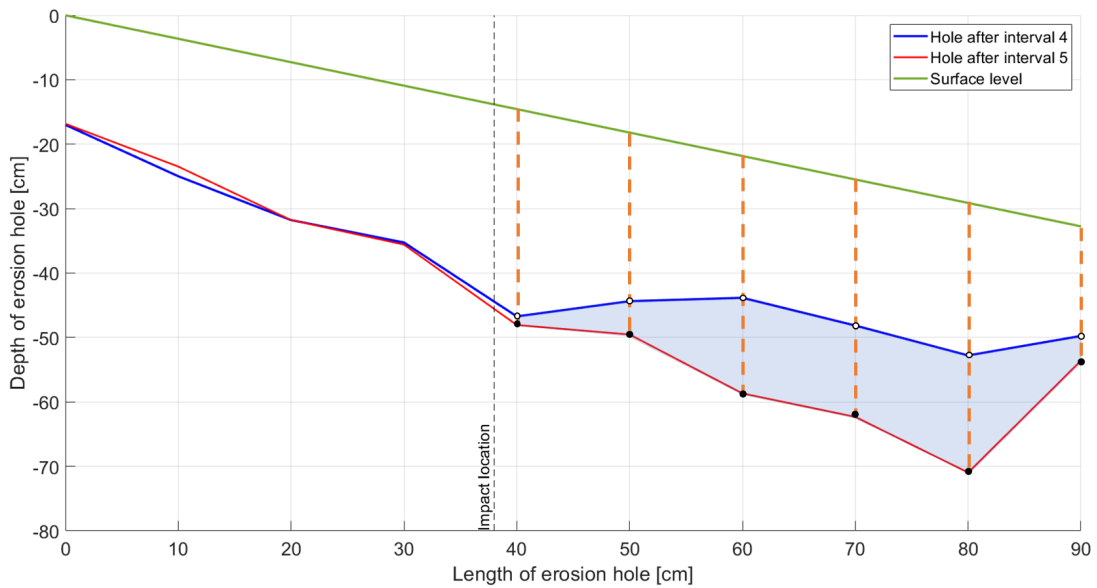
Figure 3.4: Points used from raster to calculate average depth over middle 10 centimeters.



(a)



(b)



(c)

Figure 3.5: Determining the (a) erosion rate of the depth (E_d), (b) maximum erosion rate (E_{max}), and (c) erosion rate of the volume (E_V).

3.3 Wave overtopping experiments performed in the Hedwige-Prosperpolder

Wave overtopping experiments are performed in the Hedwige-Prosperpolder as part of the Polder2C's project between February 1st and February 7th, 2022 (Rikkert et al., 2021). The wave overtopping simulator is placed at the crest of the dike above a test section of four meters wide. Wooden plates were placed on the sides of the test section to prevent spreading of the wave outside of the test area (Figure 3.6). During the experiments, the strength of the clay cover against wave overtopping was tested by excavating a hole of 3.5 meters long, 4 meters wide and 20 centimeters deep. The dike stretch was divided into three sections. The results of the lowest section are used in this study.

Nine load conditions were applied to the lowest test section. Three of these conditions were used for this study: 20 waves of 500 L/m, 10 waves of 1500 L/m and 10 waves of 2000 L/m. Prior and after each of these waves were released, the height of the top of the dike cover was captured using close-range photogrammetry. This data is analysed to determine the initial and final elevation over the test section at four stretches along the length of the dike (Figure 3.7) (Ebrahimi, 2022). These results are used to calculate the erosion rate per 10 waves for each of the three wave volumes.



Figure 3.6: Wave overtopping experiment performed in the Hedwige-Prosperpolder.

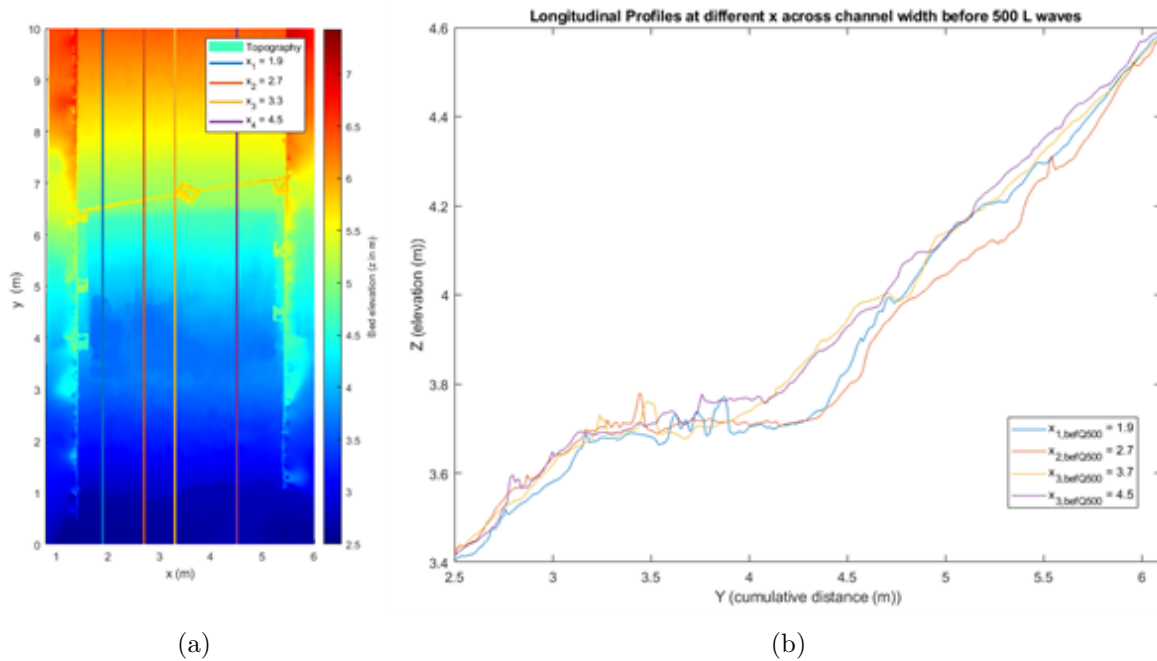


Figure 3.7: The dike profile (a) visualised using photogrammetry, and (b) before waves of 500 L/m were released at 4 measuring locations (Ebrahimi, 2022).

3.4 Calculating the hydraulic load

The jet of water exerted on the clay during the fire hose method experiments, and the overtopping waves released during the wave overtopping experiments cause high hydraulic loads on the clay. These loads can be divided into shear and normal stresses and are calculated during this study. First, an explanation is given of how the normal and shear stresses are calculated for the fire hose method experiments. Then, is explained how the normal and shear stresses are calculated for the wave overtopping experiments.

3.4.1 Calculating the hydraulic loads occurring during fire hose method experiments

During the fire hose method experiments, the hole develops due to the normal and shear stresses caused by the hydraulic load. The shape of the hole is used to determine the magnitude of these stresses. Assuming that the hole has a rounded shape, the stresses acting on the clay are determined. The shear stress is complicated to calculated due to uncertainties in the friction coefficient of the bed and layer thickness of the water flow. However, the flow velocity is the main factor contributing to the magnitude of the shear stress and is thus used to define the shear stress. The normal stress is the main contributor to the deepening of the hole and is calculated from the momentum equation. Hereby, the forces are expressed in the x- and y-direction, where ‘x’ indicates the horizontal direction and ‘y’ the vertical direction. The forces in x- and y-direction exerted in a bend are calculated as follows (Fox et al., 2016):

$$F_x = \int \rho_2 Q_2 u_2 u_{x2} dA_2 - \int \rho_1 Q_1 u_1 u_{x1} dA_1, \quad (3.1a)$$

$$F_y = \int \rho_2 Q_2 u_2 u_{y2} dA_2 - \int \rho_1 Q_1 u_1 u_{y1} dA_1, \quad (3.1b)$$

where:

F	Net force exerted in x- or y-direction	[N]
ρ	Density	[kg/m ³]
Q	Flow rate	[m ³ /s]
u	Flow velocity in x- or y-direction	[m/s]
A	Cross-sectional area of control volume	[m ²]
1 and 2 indicate the end and start of control volume respectively		

The profile of erosion hole C is used to elaborate on the method used to calculate the normal stresses (Figure 3.8). The normal stress is calculated for each measuring location where the water jet impacted and further downstream. Figure 3.9 shows how the normal stress is calculated at location ‘Length of erosion hole = 20 cm’. The left slope in the figure indicates the start of the control volume and the right slope the end of the control volume. It is assumed that the water flows parallel to slope 1 and causes stress on the entire length of slope 2, which is assumed to be 10 cm wide. Furthermore it is assumed that the flow velocity, discharge and density of the water from the jet are constant. Therefore, Equations 3.1a and 3.1b have been written to:

$$F_x = \rho Q u (\cos(\alpha_2) - \cos(\alpha_1)) \quad (3.2a)$$

$$F_y = \rho Q u (\sin(\alpha_2) - \sin(\alpha_1)) \quad (3.2b)$$

where:

F	Net force exerted in x- or y-direction	[N]
ρ	Density	[kg/m ³]
Q	Flow rate	[m ³ /s]
u	Flow velocity from nozzle	[m/s]
α	Angle of slope	[degrees]

Using Equations 3.2a and 3.2b, the normal force and normal stress on the clay are calculated using Equations 3.3 and 3.4 respectively.

$$F_n = \sqrt{F_x^2 + F_y^2} \quad (3.3)$$

$$\sigma_n = \frac{F_n}{A_2} \quad (3.4)$$

where:

F_n	Normal force	[N]
F_x	Net force exerted in x-direction	[N]
F_y	Net force exerted in y-direction	[N]
σ_n	Normal stress	[N/m ²]
A_2	Area where normal stress acts on	[m ²]

During each interval, the flow velocity from the nozzle was held constant. However, due to the change in depth of the erosion hole, the stresses acting on the soil were different between the start and end of the interval. The average normal stress during interval n was calculated using the profile of interval of $n-1$ as the start condition and the profile of interval n as the end condition. Hereby, the flow velocity during interval n was considered for both conditions.

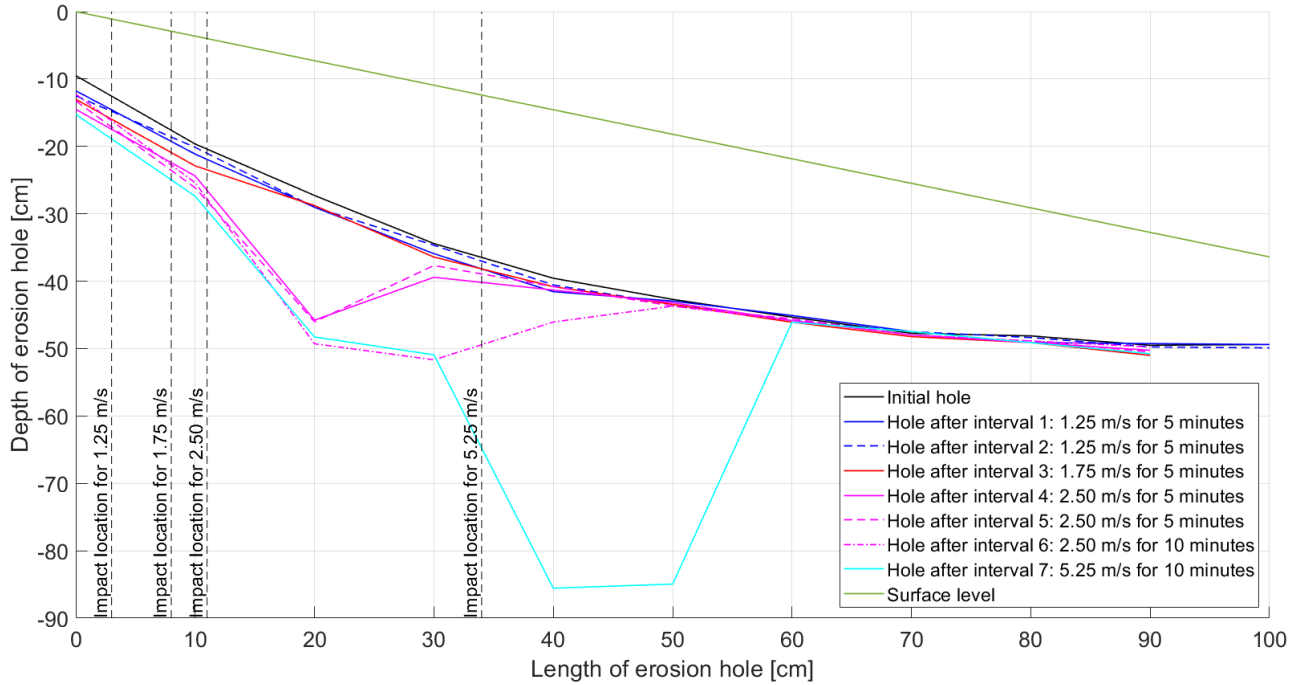


Figure 3.8: Profile of the erosion hole after each interval of test C.

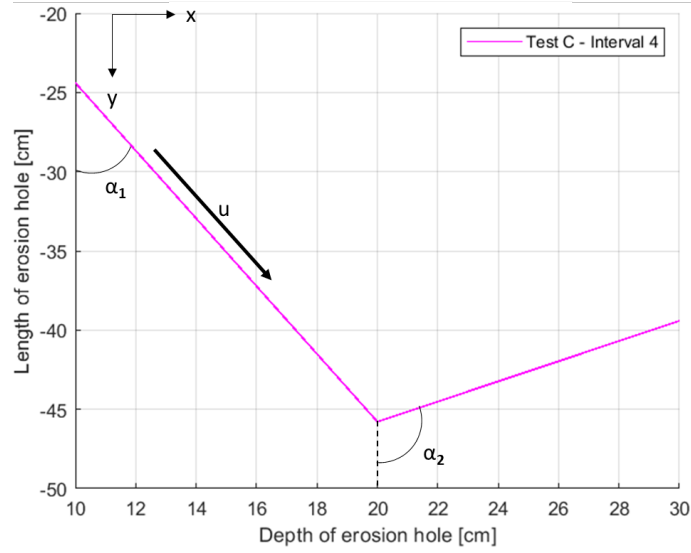


Figure 3.9: Profile of erosion hole during interval 4 of test C between 10 and 30 cm.

3.4.2 Calculating the hydraulic loads occurring during wave overtopping experiments

The normal and shear stresses on the clay, that occurred during the wave overtopping experiments, is calculated using the measured profile of the excavated hole (Figure 3.7). The average height of the slope is calculated for every 0.5 meters along the length of the slope. This is done for all four locations along the width of the test section to maximise the amount of data for the three wave volumes. The normal and shear stresses acting on the clay are calculated using the formulas proposed by van Bergeijk (Chapter 5) to calculate the maximum load at vertical height transitions:

$$T_n = \max(11.8d_{av}^{1/3}U^2 - 108.0) \quad (3.5)$$

$$T_s = \max(29.4d_{av}^{1/3}U^2 - 443.0) \quad (3.6)$$

where:

T_n	Normal stress	[N/m ²]
T_s	Shear stress	[N/m ²]
d_{av}	Average height of erosion hole over 0.5 m	[m]
U	Flow velocity	[m/s]
Units of coefficients: 29.4 kg/m ^{10/3} , 443 N/m ² , 11.8 kg/m ^{10/3} , and 108 N/m ²		

Since data on the flow velocity was not available, the maximum flow velocity is calculated using (van der Meer et al., 2011):

$$u_{max} = 5.00V^{0.34} \quad (3.7)$$

where:

u_{max}	Maximum flow velocity	[m/s]
V	Overtopping volume	[m ³ /m]

3.5 Finding relations in the fire hose method results

The results of the fire hose method experiments are analysed to study the best relation between the applied hydraulic load and measured erosion rate. This chapter describes the steps that are taken to do this. The outcome of this analysis is used in Section 4.1 to find the best parameter of the erosion rate to describe the linear relation between the calculated normal and shear stress and the observed erosion rate.

Preparing data

During the experiments, the depth of the erosion hole and the duration of the interval is noted in the logbook. This information is used to calculate the erosion rate and to visualise the development of the erosion hole during each interval (Figure 3.8).

Appendix C shows the results of the different erosion rates and the calculated hydraulic loads per test. Every first interval of each test is excluded from the data. Loose material, which is caused by digging the hole, is washed out during the first interval. As a result, an erosion rate is calculated which is significantly higher than during the other intervals with the same flow velocity and is not representative for erosion normally observed in the field.

Erosion rate at locations where jet impacts

To start, the erosion rate and applied normal stress is calculated for the locations where the jet impacts on the hole. This data is analysed to check if, for example, a linear or quadratic relation can be observed from data (Figure 3.10a). After this, the results of all tests is combined in a graph to increase the number of data points (Figure 3.10b). However, from this data no clear conclusion can be drawn about the erodibility coefficient, critical stress and the value of factor α used in Equation 1.1.

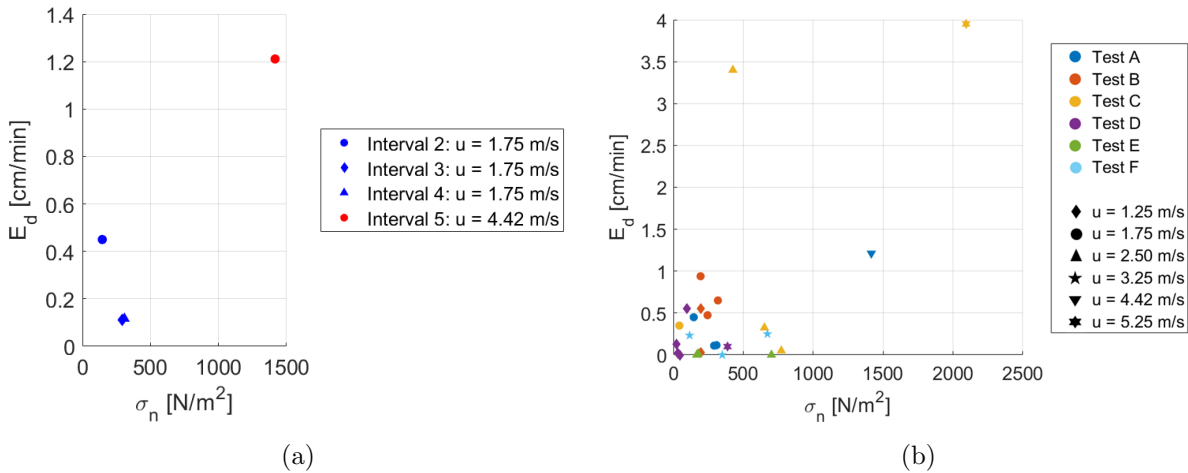


Figure 3.10: The erosion rate (E_d) and applied normal stress (σ_n) during (a) test A and (b) all tests at location where jet impacts.

Erosion rate over entire length of hole

To increase the amount of data, the hydraulic load at every point over the length of the hole where the water flows is calculated and visualised in a plot with the corresponding erosion rate (Figure 3.11). Over all can be concluded from the figure that higher normal stresses act on the clay when the flow velocity of the jet is higher. The spread of the erosion rate during each test is quite large, due to variations in flow velocity during the test. Hence, the relation between the applied normal stress and observed erosion rate can better be visualised by showing the test results based on the applied flow velocities instead of the type of test. In that case, Figure 3.11b, is adjusted to Figure 3.12.

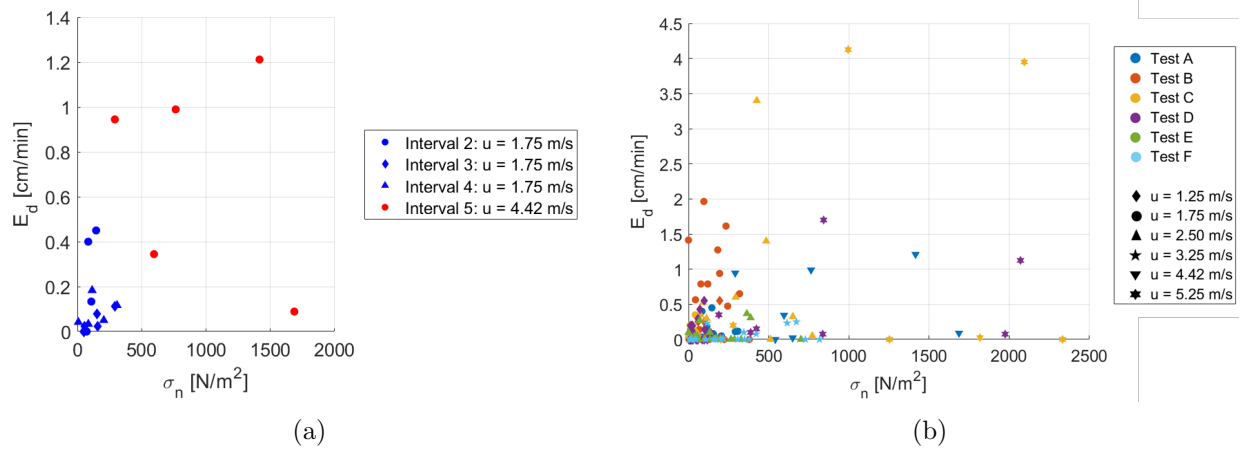


Figure 3.11: The erosion rate (E_d) and applied normal stress (σ_n) during (a) test A and (b) all tests at entire length of test section.

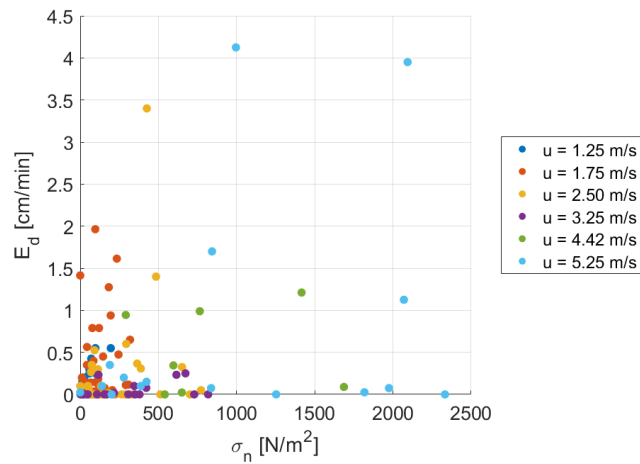


Figure 3.12: The erosion rate (E_d) and applied normal stress (σ_n) during all tests visualised per flow velocity.

Changing to a double logarithmic scale

Most data points show a relatively low erosion rate (below 1 cm/min) and relatively low normal stress (below 500 N/m²) (Figure 3.12). Consequently, to determine the erosion caused by relatively low normal stresses is hard to define from the graph, which is needed to define the critical stress. To overcome this problem, the x- and y-axis are both adjusted to a logarithmic scale. As a result, the data points with smaller values are better taken into account (Figure 3.13). However, the main downside of this method is that no zero values can be included for the erosion rate and stress (Briaud et al., 2019). To now define a critical stress, a low erosion rate must be defined as the critical erosion rate. The results of JET-tests performed in the Hedwige-Prosperpolder by GeophyConsult have indicated that the critical erosion rate of the clay is equal to 0.2 cm/min.

Only using small flow velocities

Most data is collected for flow velocities smaller than 3 m/s. Figure 3.14 shows the applied normal stress and observed erosion rate for only small flow velocities. Results for flow velocities above 3 m/s are excluded, due to the small amount of data and the high erosion rate that is calculated, which reduces the reliability of the results. However, this did not result in a smaller spread in results and no clear conclusion can be drawn from the new figure.

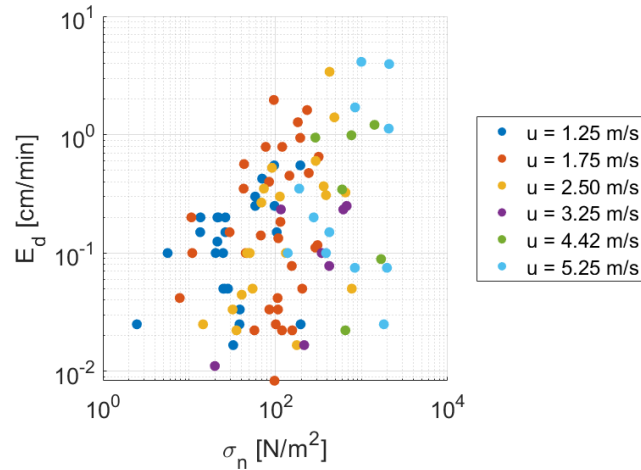


Figure 3.13: The erosion rate (E_d) and applied normal stress (σ_n) during all tests visualised using a double logarithmic scale.

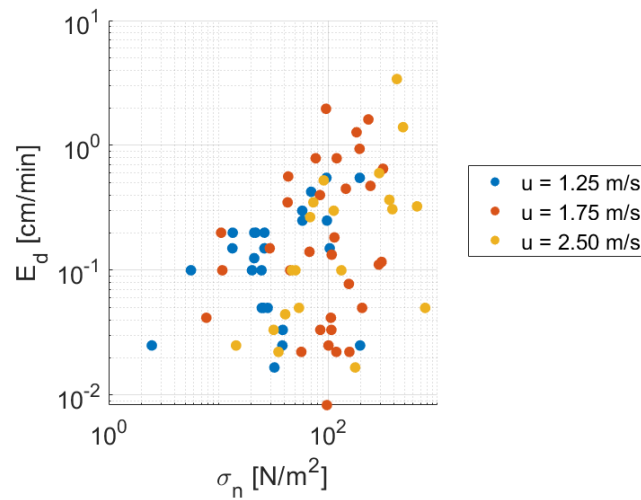


Figure 3.14: The erosion rate (E_d) and applied normal stress (σ_n) for tests performed with small flow velocities.

Plotting results per flow velocity

The large spread in the results of previous steps cause that no clear relation between the hydraulic load and erosion rate is found. Figure 3.15 shows the results per flow velocity individually. This shows that higher flow velocity generally result in a higher normal stress and the maximum erosion rate also increases with higher flow velocities. However, the large spread in the results hinder the ability to define a relation.

Ratio between erosion rate and normal stress

By calculating the ratio between the erosion rate and normal stress and plotting it against the flow velocity, one can study in what manner the flow velocity affects the ratio between the two parameters. This is visualised in Figure 3.16. In the figure can be seen that a negative trend is visible between the flow velocity and the ratio between the erosion rate and normal stress. However, due to the large spread in the data, no clear conclusions can be drawn.

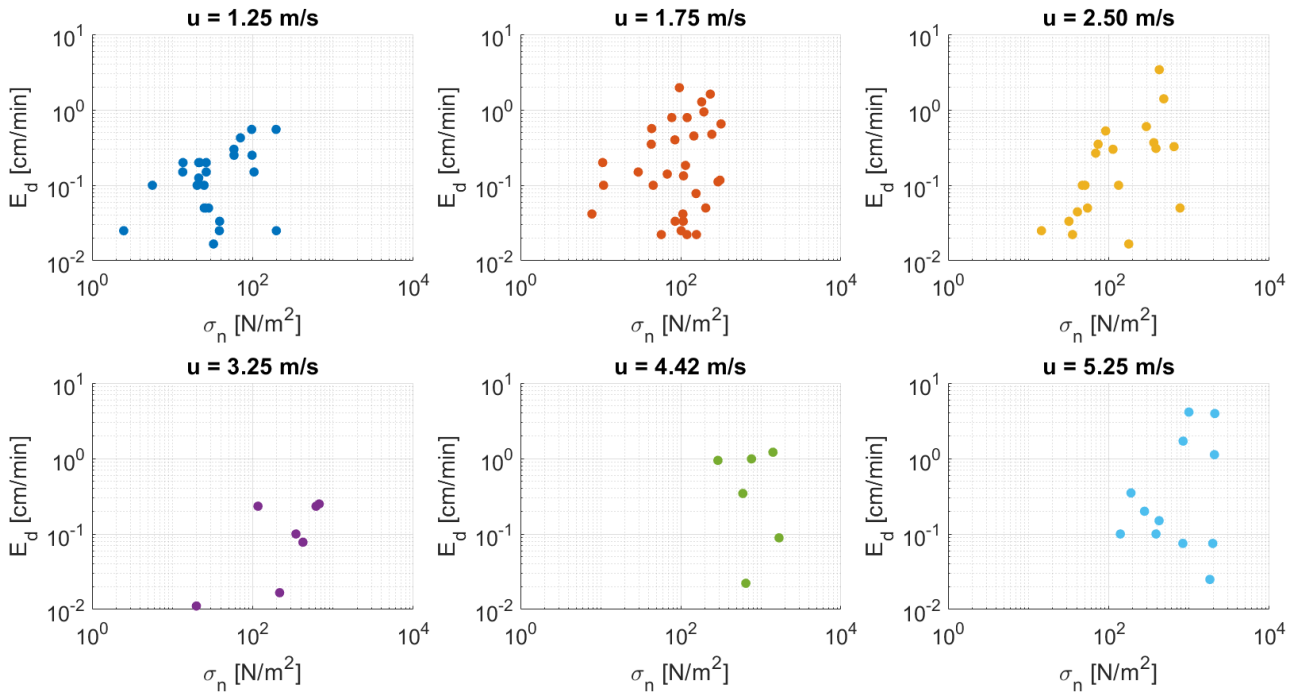


Figure 3.15: The erosion rate (E_d) and applied normal stress (σ_n) visualised per flow velocity (u).

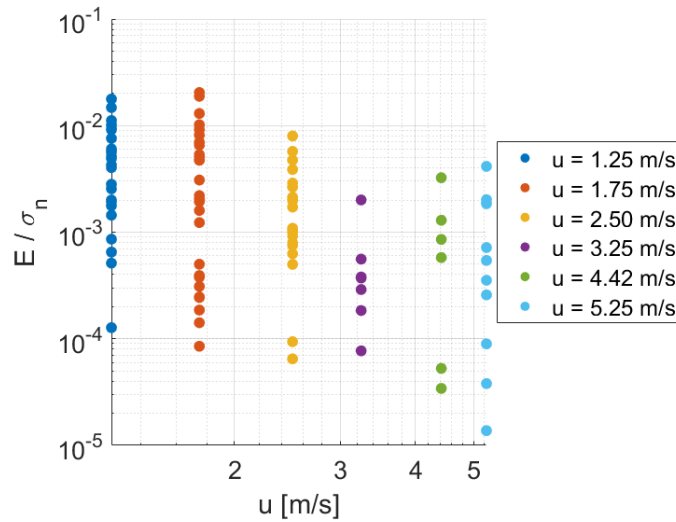


Figure 3.16: Ratio between erosion rate (E_d) and applied normal stress (σ_n) during all tests under different flow velocities (u).

Relation between erosion rate, normal stress and flow velocity

Lastly, a figure is created showing the relation between the erosion rate, normal stress and flow velocity (Figure 3.17). From this figure a positive trend can be observed between the flow velocity and observed erosion rate, the flow velocity and calculated normal stress, and the normal stress and erosion rate. This is what one would expect beforehand. The applied flow velocity is calculated using the discharge and flow velocity from the nozzle, which means that if these two increase, the normal stress increases as well (Equation 3.2). Higher normal stresses should also cause more erosion, which is what should be measuring in the field. However, the spread in the data is too large to define a clear relation between the normal stress and erosion rate, and the flow velocity and erosion rate.

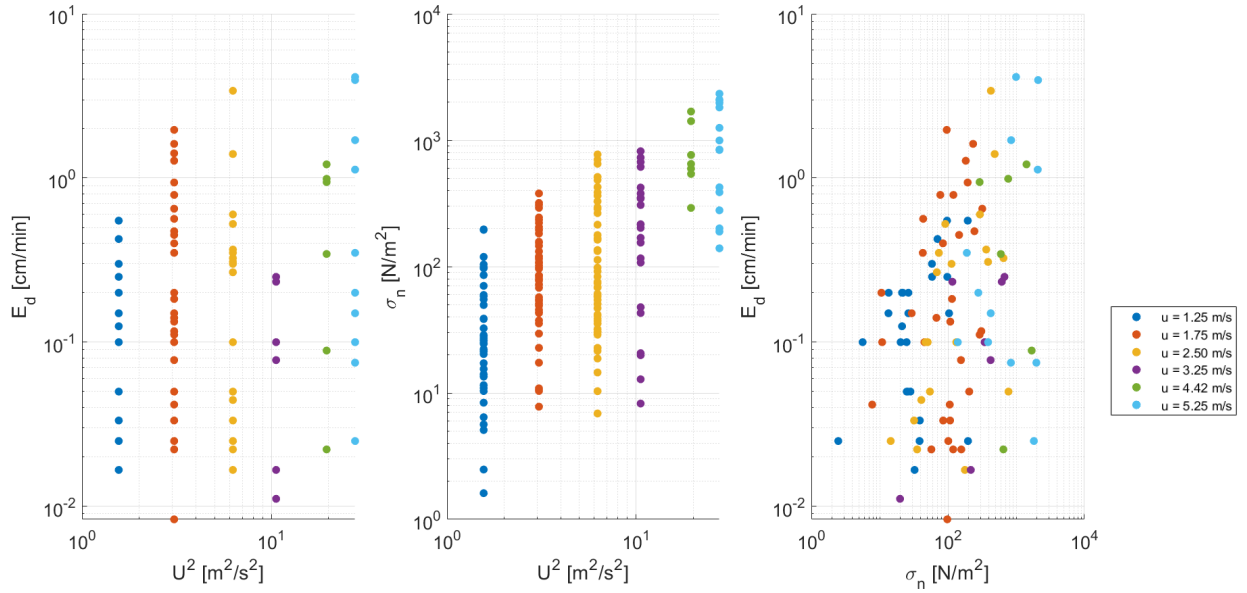


Figure 3.17: Relation between the three parameters erosion rate (E_d), normal stress (σ_n), and flow velocity from nozzle (U).

Finding relations for the observed average erosion rate, maximum erosion rate, and erosion rate of the volume

The steps previously described in this chapter are also performed for the average erosion rate (E_{av}), maximum erosion rate (E_{max}), and erosion rate of the volume (E_V) to define the best parameter to describe the erosion rate for the fire hose method test. The graph showing the applied normal stress and measured erosion rate using the double logarithmic scale can best be used to show the results of the fire hose method experiments. The obtained figures for the erosion rate and applied shear stress, and for the erosion rate and applied flow velocity are shown in Section 4.1.

3.6 Analysing the results of the fire hose method experiments and wave overtopping experiments

To use the fire hose method in practise, the outcome of the method must be correlated to the results of the wave overtopping experiments. The wave overtopping experiments are representative for what would occur in reality when the dike cover erodes due to wave overtopping, and its results can better be used in the assessments for dike safety when the strength of the clay cover would be included (Wopereis & van Steeg, 2021). When the results of the fire hose method are ‘translated’ to results of wave overtopping experiments, this small-scale test method could also be used to define the strength of clay covers.

The calculated normal and shear stresses for the fire hose method are compared to those calculated for the wave overtopping experiments, to verify whether the stresses exerted on the clay during the fire hose method experiments are representative for the stresses occurring during wave overtopping. Furthermore, the observed erosion rate caused by these stresses are visualised and compared for both experiments. This is done by visualising the erosion rate of the depth, average erosion rate, maximum erosion rate, and erosion rate of the volume and the ensuing normal stress. Since the shear stress could not be calculated for the fire hose method experiments, the four erosion parameters are visualised with their ensuing flow velocity. This is done to find a relation between the applied hydraulic loads and observed erosion rates. These results are elaborated in the next chapter.

Chapter 4

Results

4.1 Measured erosion during the fire hose method experiments

While performing the experiments, two types of erosion developments were observed. During Test F, the water flow followed the shape of the hole after the water jet impacted. During the other tests, the impact of the water jet caused a hole, where significant erosion took place. This can also be observed when visualising the development of the erosion holes (Figures 4.1 and 4.2).

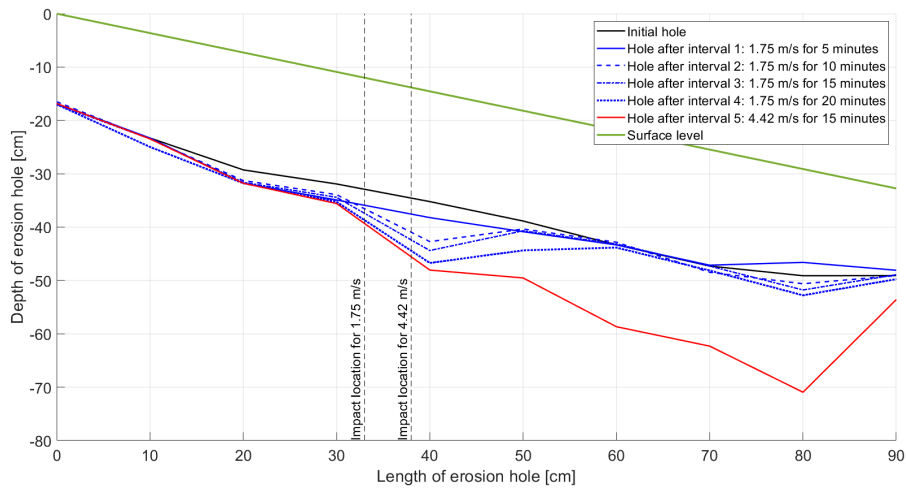


Figure 4.1: Development of hole caused by erosion where the water jet causes a hole on the impact location.

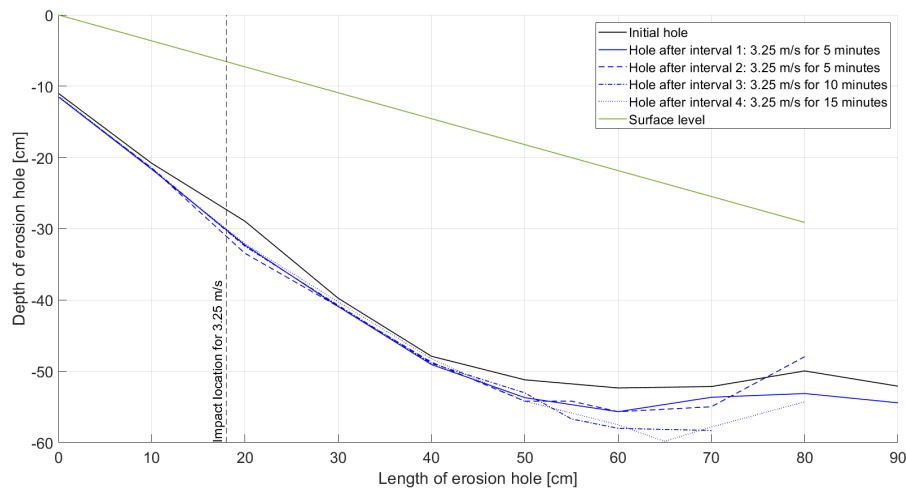


Figure 4.2: Development of hole caused by erosion where the water flow follows the shape of the hole.

4.1.1 Best suitable parameter to describe the erosion rate

The development of the hole is used to determine the normal and shear stresses and ensuing erosion rate. The erosion rate is described using the erosion rate of the depth (E_d), average erosion rate (E_{av}), maximum erosion rate (E_{max}), and erosion rate of the volume (E_V). The steps described in Section 3.5 have been performed for all four types of erosion rates. The analysis has indicated that visualising the results of the calculated normal stress and measured erosion rate on a double logarithmic scale, for all points measured after the location where the jet has impacted, is the best method to show a relation between the two parameters. The section below describes these results.

Erosion rate of depth (E_d)

The results of the six fire hose method experiments are combined to maximize the number of data points. Figure 4.3 shows the erosion rate measured vertically downwards during all these tests. This figure shows a positive trend between the calculated normal stress and the erosion rate which results in a correlation coefficient of 0.37. However, the spread in the data is too large to define a relation between the applied normal stress and observed erosion rate and thus to define the erodibility coefficient and critical normal stress of the clay.

The same data has been used to find a relation between the applied flow velocity and observed erosion rate. Here, also a slight trend is visible in which the erosion rate slightly increases with an increasing flow velocity. But also the spread in these observations is too large to define a proper relation between the two parameters. Hereby, a correlation coefficient of 0.24 is calculated.

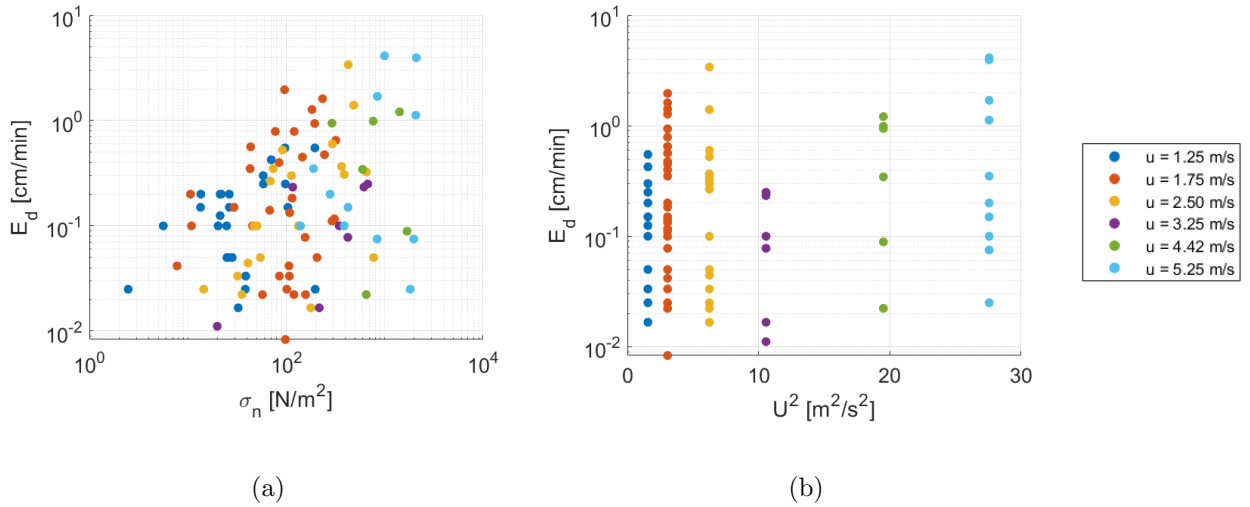


Figure 4.3: Measured depth erosion rate (E_d) under (a) calculated normal stresses (σ_n) and (b) flow velocity from nozzle (U) during the fire hose method experiments.

Average erosion rate (E_{av})

The average erosion rate for each interval is calculated from the data points analysed above. Figure 4.4 shows the relationship between the average calculated normal stress and average erosion rate measured. Due to the averaging of the data, the number of data points significantly decreases. The figure shows a positive trend between the applied normal stress and observed erosion rate and analysing the data resulted in a correlation coefficient of 0.56.

A positive relation between the applied flow velocity and the observed erosion rate with a coefficient of variation of 0.44 is also visible in Figure 4.3. However, due to the few data points for flow velocities above 3 m/s, the trend is quite uncertain.

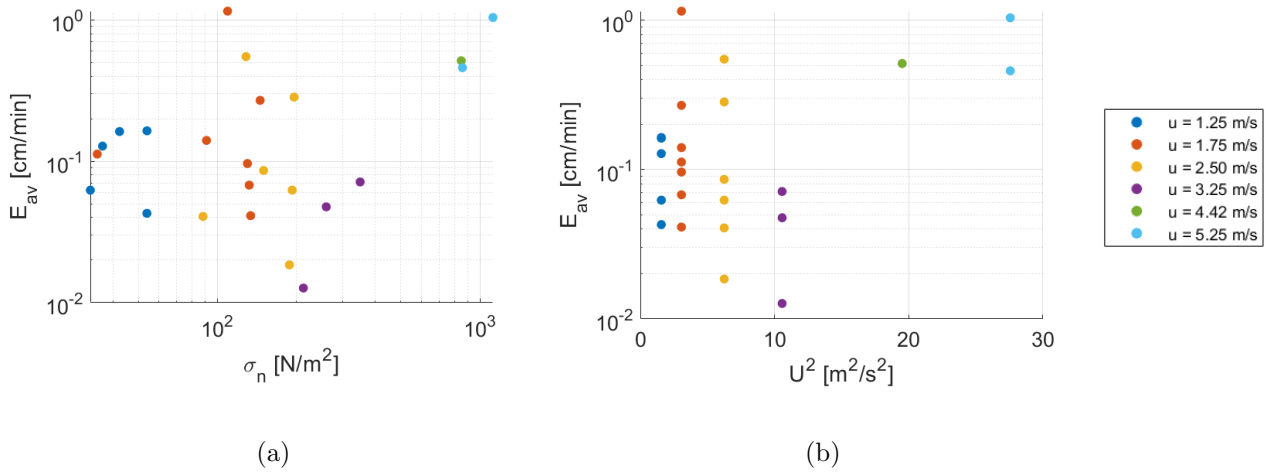


Figure 4.4: Measured average erosion rate (E_{av}) under (a) calculated normal stresses (σ_n) and (b) flow velocity from nozzle (U) during the fire hose method experiments.

Maximum erosion rate (E_{max})

After each interval, the maximum depth is measured. This is used to calculate the maximum erosion rate. Figure 4.5 shows the calculated normal stress and corresponding maximum erosion rate observed. A correlation coefficient of -0.08 is calculated. This indicates almost no linear relation between the applied load and observed erosion rate. The same holds for the correlation between the applied flow velocity and the observed erosion rate. Hereby, a correlation coefficient of -0.12 is calculated. The negative correlation coefficient implicates that an increasing hydraulic load would cause a lower erosion rate, which is contradicting to what is observed during large-scale field experiments and to theory.

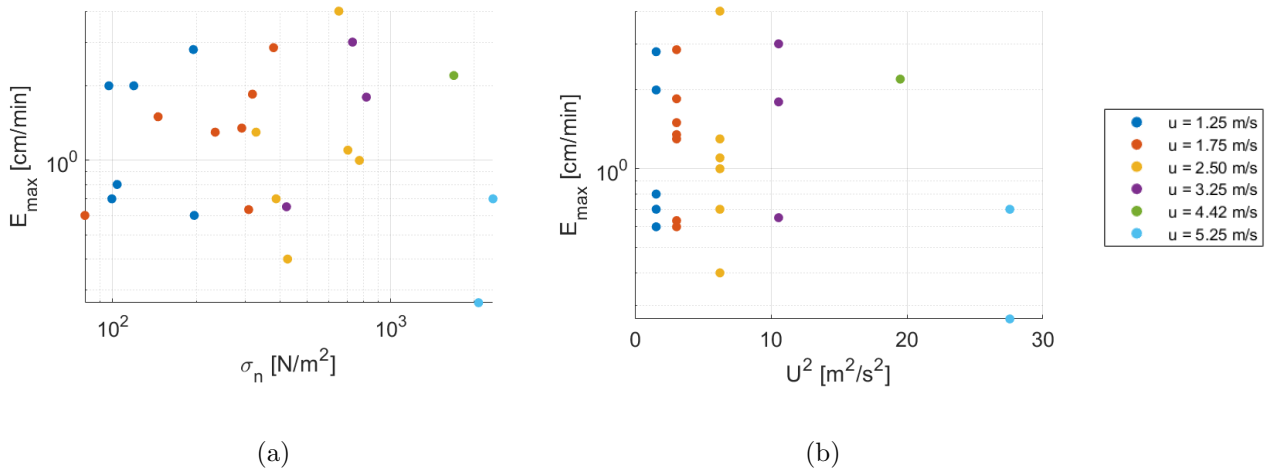


Figure 4.5: Measured maximum erosion rate (E_{max}) under (a) calculated normal stresses (σ_n) and (b) flow velocity from nozzle (U) during the fire hose method experiments.

Erosion rate of volume (E_V)

The eroded volume is calculated from the erosion depth data. Figure 4.6 shows the applied normal stress (a) and flow velocity (b) and the observed erosion rates during all tests. Hereby, again a large spread in data is found. The correlation coefficients for the applied normal stress and observed erosion rate, and the applied flow velocity and observed erosion rate are calculated. These values are -0.18 and -0.13 respectively. As explained in the previous section, the negative coefficient indicates an decreasing erosion rate under increasing hydraulic forces, which is contradicting to what is expected.

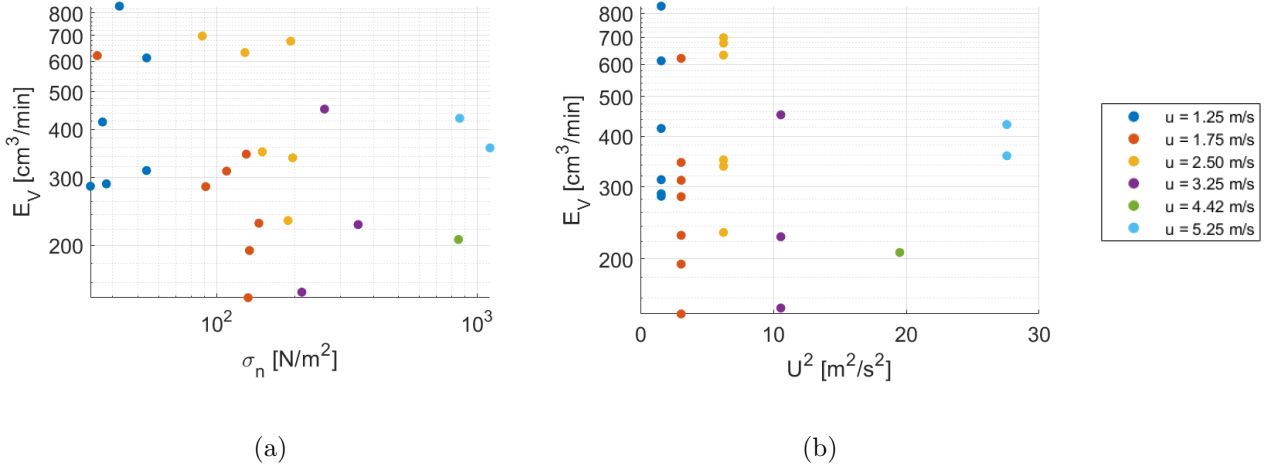


Figure 4.6: Measured erosion rate of the volume (E_V) under (a) calculated normal stresses (σ_n) and (b) flow velocity from nozzle (U) during the fire hose method experiments.

Most suitable parameter for the erosion rate

Using the maximum erosion rate and erosion rate of the volume results in a negative trend between the normal stress and erosion rate, and the flow velocity and erosion rate. This contradicts what is observed in the field. Hence, these parameters are not suitable for any further analysis. Using the average erosion rate to define a relation between the applied normal stress and measured erosion rate is the best option considering the correlation coefficient. However, due to the large decrease in the amount of data compared to using the erosion rate of the depth, the reliability of these findings is questionable. This is mainly the case for the relation between the flow velocity and average erosion rate. Due to the few data points for flow velocities above 3 m/s and the fact that the erosion rate for $u = 3.25$ m/s is much smaller than the erosion rates for $u = 4.42$ m/s and $u = 5.25$ m/s, it is hard to define a trend. Using the erosion rate of the depth, this problem is overcome. However, when the data must be correlated to the results of wave overtopping experiments using the erosion rate of the depth, no expected value for the erosion rate can be defined due to the large spread in the outcome.

In Section 4.3 the results using the average erosion rate and the erosion rate of the depth will be compared to the outcome of the wave overtopping experiments, explained in Section 4.2, to find the best alternative.

4.2 Analysing the results of the wave overtopping experiments

Figure 4.7 shows the calculated normal and shear stresses and the observed erosion rates during the wave overtopping experiments. The magnitude of the normal stress does not differ much per wave volume. When comparing the magnitude of the stresses between the three wave volumes there is a much larger difference, as would be expected. The range of the erosion depth for waves of 500 and 1500 L/m is relatively large, whereas the spread in erosion rate for the wave volume of 2000 L/m is quite small. Also, the maximum erosion rates for the two smaller wave volumes is larger than the maximum erosion rate observed after the waves of 2000 L/m were released. This is contradicting to theory, but can be explained by the method which is used to measure the erosion. After the waves were released, water remained present at the bottom of the excavated hole (Figure 4.8). Using photogrammetry, the height of the bottom is measured. However, the method cannot distinguish water from soil. As a result, the top of the remaining water is captured as the height of the hole (Ebrahimi, 2022).

The wave overtopping experiments were executed starting with the smallest wave volume and increasing the volume incrementally on the same test section. Prior to releasing the waves of 500 L/m, less erosion took place compared to the larger wave volumes and less water remained present after the waves of 500 L/m were released. Consequently, the height of the bottom of the hole could better be measured for smaller wave volumes than for the larger wave volumes. While performing the wave overtopping experiments, most erosion was observed at the bottom of the hole and serious damage was seen after the waves of 2000 L/m were released. Probably, this erosion is not measured correctly due to the remaining water. This would explain the lower erosion rate in the data for the larger wave volumes.

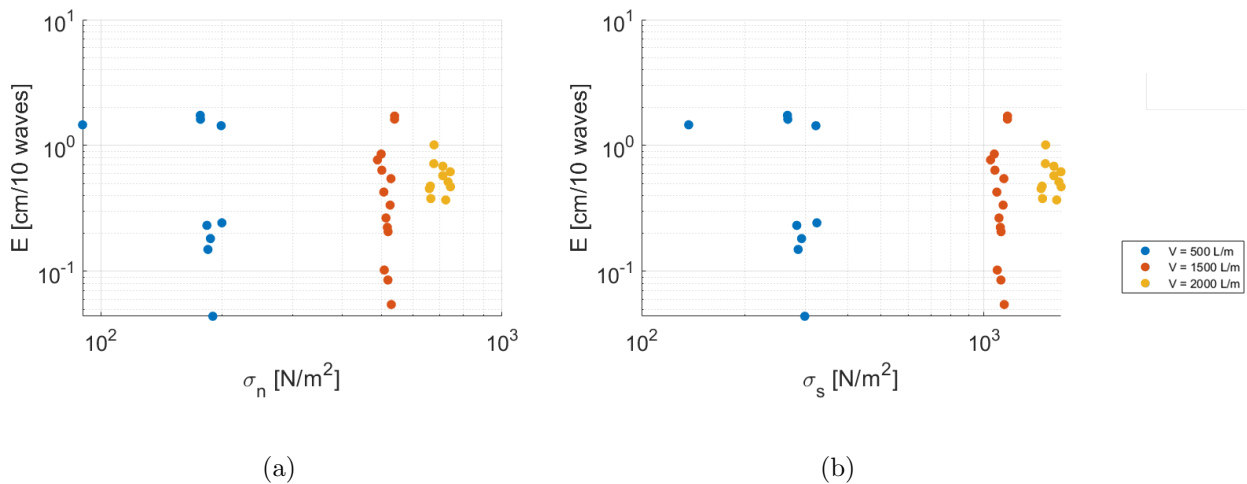


Figure 4.7: Erosion rate (E) under (a) calculated normal stress (σ_n) and (b) calculated shear stress (σ_s) during the wave overtopping experiments.

4.3 Comparison of the fire hose method experiments and the wave overtopping experiments

Figure 4.9a shows the calculated normal stress and observed erosion rate for the wave overtopping experiments and fire hose method experiments in one figure. From the figure can be seen that the spread in the observed erosion rate is quite large for both experiments. The normal stresses exerted on the clay are for the wave volumes of 1500 L/m and 2000 L/m of the same magnitude as for those of the fire hose method using a flow velocity of 2.50 m/s and above. The magnitude of the normal stress exerted by the wave overtopping experiments with a wave volume of 500 L/m is almost equal to a flow velocity of 1.75 m/s during the fire hose method experiments.



Figure 4.8: Picture of the erosion at the bottom of hole after the wave overtopping experiments were finished.

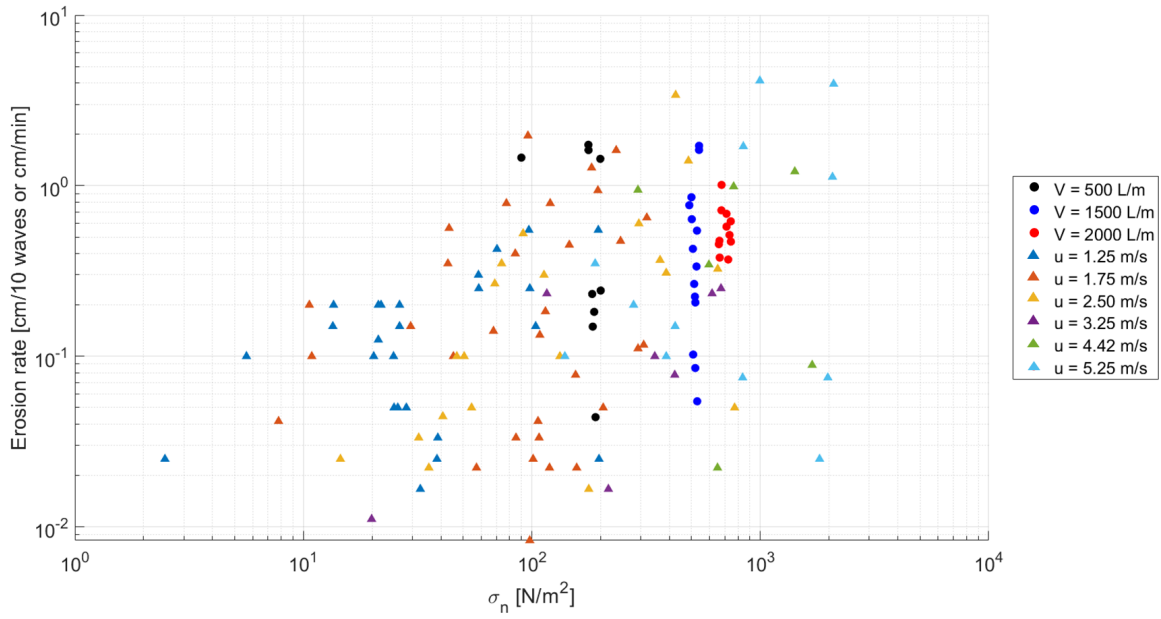
Because the shear stresses during the fire hose method are unknown, the applied shear stresses are represented using the calculated flow velocity for each test in Figure 4.9b. The figure shows that the range of the erosion rate for the wave overtopping test with a wave volume of 2000 L/m is smaller than the other test results. However, this range is expected to be larger due to the inaccuracies of the measuring method. The range of the erosion rate observed during the wave overtopping experiment using 1500 L/m is comparable to the range observed with the fire hose method using a flow velocity of 5.25 m/s. Since the flow velocities do not differ much, the shear stresses are expected to have the same order of magnitude. The observed erosion rate using wave volumes of 1500 L/m is higher than the erosion rates observed for flow velocities of 3.25 m/s and 4.42 m/s used during the fire hose method experiments.

Figure 4.10a shows the calculated normal stress and observed erosion rate for the wave overtopping experiments and the average normal stress and average erosion rate during each interval executed with the fire hose method experiments. The normal stresses calculated for the wave overtopping experiments still fall within the range of the normal stresses calculated for the fire hose method experiments. However, the range of the erosion rate measured during wave overtopping experiments is larger than these of the fire hose method experiments, especially for the larger wave volumes.

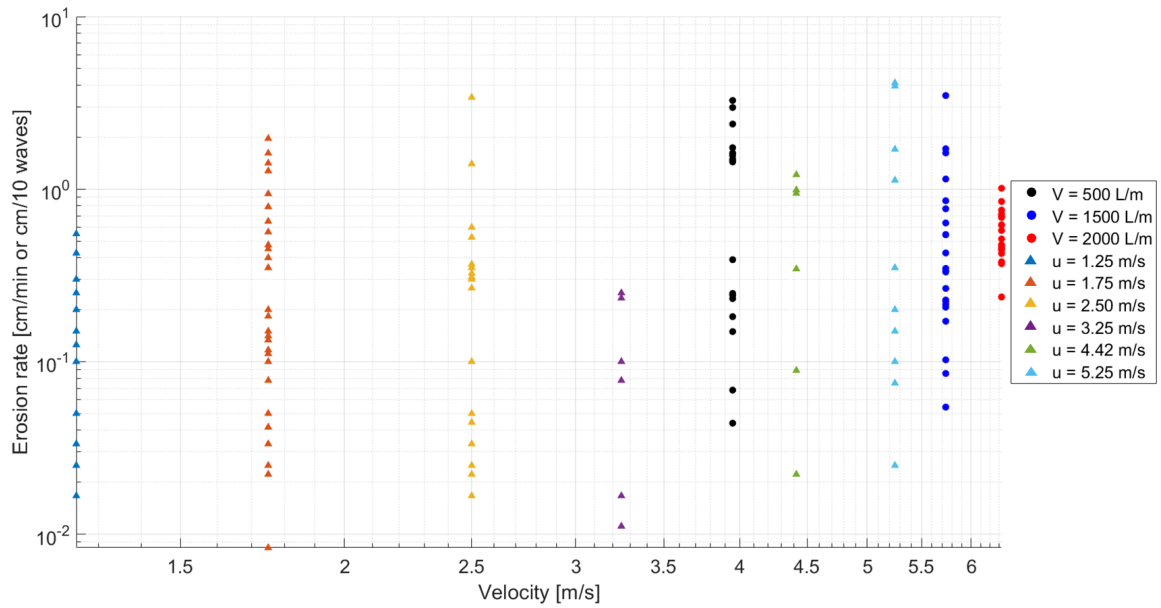
The calculated flow velocity and observed erosion rate are shown in Figure 4.10a. Because the average erosion rate is calculated by taking the mean of the erosion rate of the dept, the range of the observed erosion rate is decreased, but also the amount of data is decreased. The figure shows the observed erosion rate for wave volumes of 500 L/m and 2000 L/m is not comparable to any other results of the fire hose method experiment, due to the same reasons as explained for Figure 4.9b. However, the observed erosion rate and expected shear stress for wave volumes of 1500 L/m during wave overtopping experiments are comparable to the results of using a flow velocity of 5.25 m/s during the fire hose method experiments.

Using the erosion depth during the fire hose method experiments, one cannot obtain a clear relation between the applied normal stress and observed erosion rate, due to the large spread in the results. However, the spread in these results do correspond to those observed during the wave overtopping experiments. When looking at the data in Figure 4.9a, one can see some kind of diagonal boundary above which no erosion occurs. When the hydraulic load on the clay is known, one could read a range for the erosion rate which could be expected beforehand using the graph. However, it is questionable if this would indicate useful information for the user. The data of the average erosion rate in Figure 4.10a has a smaller spread. However, the spread in the results of the wave overtopping experiments is much larger, which makes the average erosion rate less useful. Besides that, the erosion rate measured during the wave overtopping experiments is expected to be higher than that was actually the case during the experiments. By using the photogrammetry, the reliability of the measurements at locations

where water remains present is relatively low and a higher erosion rate is probably observed in the field. This would result in much bigger deviations between the erosion rate measured during the fire hose method and the measurements of the wave overtopping experiments.

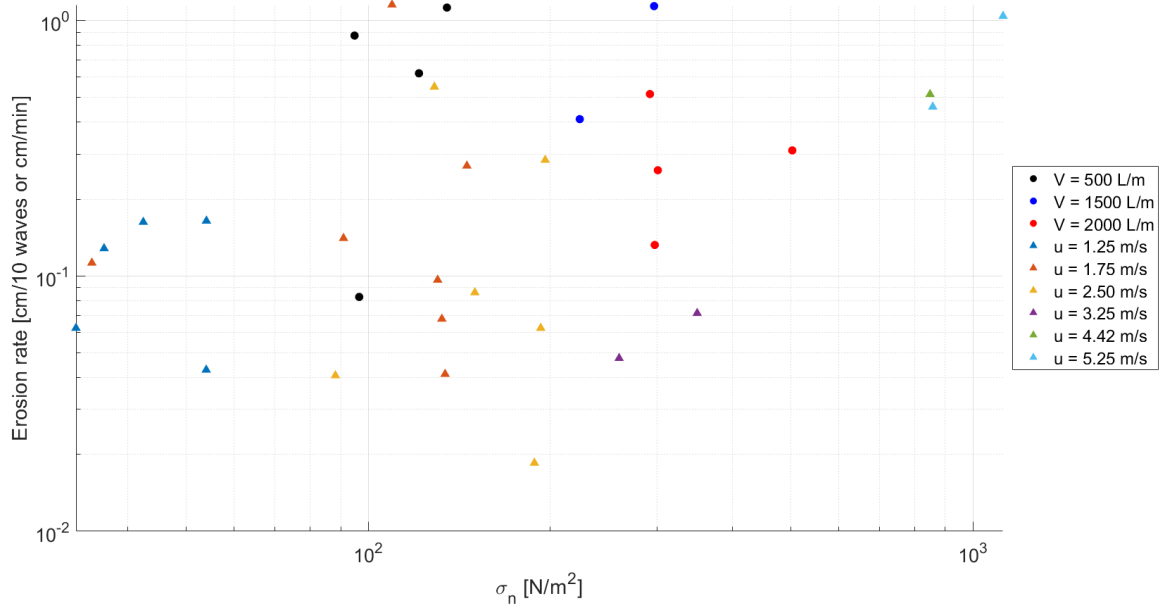


(a)

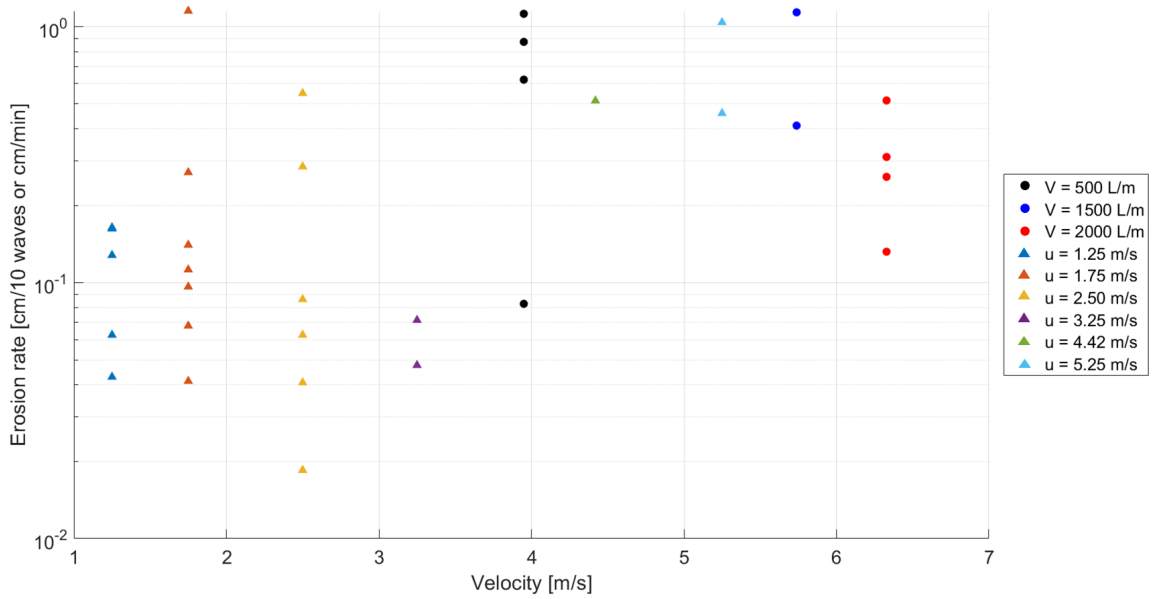


(b)

Figure 4.9: Results of wave overtopping experiments and fire hose method experiments: Erosion rate (E) caused by (a) normal stress (σ_n) and (b) flow velocity (u).



(a)



Chapter 5

Discussion

5.1 Suitability of existing clay classifications for Dutch safety standards

The Dutch clay classification system is based on Rotating Cylinder Tests performed by Grondmechanica Delft between 1985 and 1987 (Kruse et al., 1988). The erosion resistance of thirty clay samples has been tested. Hereby, the clay samples were divided into three categories, based on the rotation rate of the apparatus during which 30% of the initial mass of the clay sample had eroded. However, during RCTs, generally two stages regarding the erosion resistance are observed (Chapuis & Gatién, 1986). During the first stage, the erosion rate is quite low. Small particles come loose from the surface due to the flowing fluid. No significant erosion occurs during this stage. During the second stage, larger aggregates are picked up by the flowing water and the erosion rate rapidly increases. During this stage, significant erosion occurs and the shear stress applied on the sample when this stage is initiated is often defined as the critical shear stress. This phenomenon was not taken into account when the data of the RCTs performed by Grondmechanica Delft was analysed. Only the difference in weight between the start and end of the test was considered. Hence, it is questionable whether the critical shear stress of each sample is indicated correctly. By reanalysing the results obtained by Grondmechanica Delft and indicating the rotation speed at which the erosion rate significantly increases, the critical rotation speed can more accurately be determined.

During the RCTs, the torque is constantly measured and used to determine the average torque during a stage with a constant rotation speed. Because erosion takes place, the shear stress on the sample varies during each stage. The sample becomes smaller due to erosion, and thus the shear stress on the sample lowers as well (Chapuis & Gatién, 1986). This is not taken into account during the analysis of Grondmechanica Delft. In 2012, the Rotating Erosion Testing Apparatus (RETA) was developed, which is an updated device of the RCT (Tran, 2018). The difference between the tests is that when using the RETA, the torque is kept constant during a stage by varying the rotation speed. This way, the erosion rate under the applied shear stress can more accurately be determined.

The type of test affects the outcome of test results and thus the conclusion drawn about the erosion resistance of the tested soils. For example, when results of different small-scale experiments are compared to each other or results of small-scale experiments are related to large-scale experiments, different values for the erosion parameters are obtained (Wahl, 2010; Wichman, 2021). Also, the method used to analyse the data affects the outcome of the erosion parameters as is, for example, the case for the different methods available for JETs (Wahl, 2021). The classification of clay is based on RCTs and resulted in a classification system based on the Atterberg Limits of the samples. However, when analysing the results of the JETs performed in the Hedwige-Prosperpolder, no clear relation can be found between the Atterberg limits and the calculated critical stress and erodibility coefficient (Figure 5.1). Which shows that different test methods can result in different recommendations regarding the erosion resistance of clay.

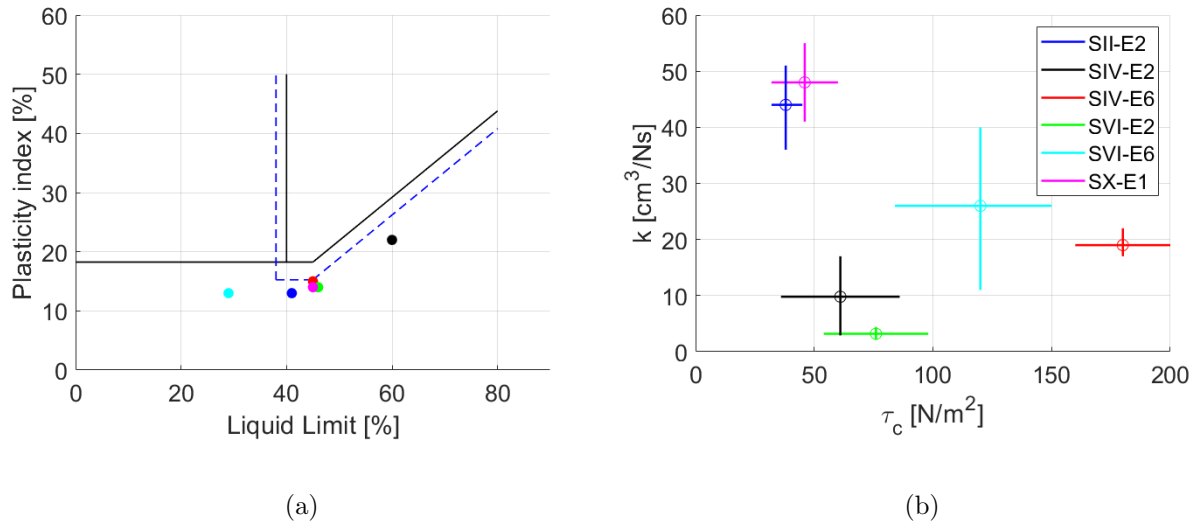


Figure 5.1: Results of JETS in Hedwige-Prosperpolder indicating (a) the Atterberg Limits and (b) the erodibility coefficient (k) and critical stress (τ_c).

The internationally used soil classification system described by Briaud et al. classifies all types of soils, including clay. The benefit of this classification system is that it is based on numerous test results obtained by both large and small scale tests. However, due to the large variation in soil types included in this system, the ranges obtained for the critical shear stress and erodibility coefficient is quite large and not useful for classifying the erodibility of a clay for Dutch standards (van Steeg & Mourik, 2020).

5.2 Uncertainties caused by the setup of the fire hose method

The setup of the fire hose method was adjusted to be able to perform experiments on clay (van Steeg, 2021). The setup of the method affects the magnitude of the normal and shear stresses on the clay. This is also observed during tests performed on grass (Wopereis & van Steeg, 2021). When the tests were performed in the Hedwige-Prosperpolder, the angle and height of the nozzle were kept similar to decrease the variation in hydraulic loads. However, due to variations in the shape of the dug hole, the angle of incidence varies, which causes variations in the magnitude of the applied stresses while using the same flow velocity. The largest variation in hydraulic load was caused by the variation in flow velocity of the jet, which was intentional to observe the erosion rate under different stresses. To best define the magnitude of the normal and shear stresses, the jet had to impact with an angle of incidence of 180° and should then flow over the rest of the hole. However, this is hard to control prior to the test and eventually this was only the case during test F. During the other tests, the impact of the jet caused a small hole in the clay (Figure 5.2). However, the normal and shear stresses were calculated the same way.

Using an angle of incidence of 180° is not representative for wave impact on clay. Normally, the waves flow over the grass cover and impact on the clay with an angle of incidence smaller than 180° on the horizontal cliff (Figure 5.3) (van Bergeijk, Warmink, & Hulscher, 2021). Consequently, the results of the fire hose method experiments are not representative for the results of the wave overtopping experiments at the top of the excavated hole. However, at the bottom of the excavation of the wave overtopping experiments, the wave follows the contour of the hole (Figure 5.3), which is similar to what occurs during the fire hose method experiments. Hence, the results of the fire hose method experiments represent the hydraulic loads better for the bottom of the excavated hole than the top of the hole during wave overtopping experiments.



(a)

(b)

Figure 5.2: (a) Hole caused by jet and (b) jet causing hole.

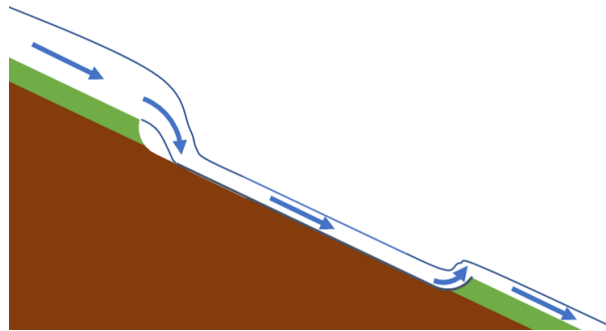


Figure 5.3: Flow of wave in excavated hole during wave overtopping experiments.

Inaccuracies in the test results were also caused by the method used to measure the erosion. During the experiments, an imaginary raster was created by laying two rulers next to the hole over its length and placing a wooden beam over the width of the hole (Figure 5.4). The raster was used to measure the same locations in the hole as much as possible. However, it could be that the measuring points differ a bit after each interval due to small shifts of placement of the wooden beam. The depth at each location was measured using a ruler and was read with an accuracy of 0.5 centimeters. But human error could result in some inaccuracies. This was also observed in the results, where sometimes the depth of the hole would be measured as smaller after the experiment was performed compared to before the experiment was performed. When analysing the results, the erosion rate at measuring locations where this phenomenon occurred was set to 0 cm/min. This way, inaccuracies caused by measuring the depth was minimised and it is expected that this does not affect the results of the measured erosion rate of the depth, average depth, and maximum depth. However, it could lead to larger inaccuracies when determining the erosion rate of the volume.

The depth of the hole is measured over its entire width. However, only the centre 2 or 3 measuring points were used to calculate the average depth over the width of the hole. At holes where the centre of the nozzle was situated in between two lines of measuring locations, 2 measuring points are included. At holes where the centre of the nozzle was situated at a line of measuring locations, 3 measuring points are included. This is done such that only locations where the water flows are taken into account. The difference in the depth of the erosion hole prior and after the interval and the duration of the interval are used to calculate the the erosion rate of the depth, average erosion rate, maximum erosion rate and the erosion rate of the volume. Because the depth of the hole is only measured every 10 centimeters, the shape of the hole is not represented as accurate as would have been the case when a smaller grid size was chosen. However, measuring the depth of the hole is a time consuming undertaking, and a grid size of 10 centimeters was seen as the best balance between accuracy and time savings. A



Figure 5.4: Measuring raster used during fire hose method experiments.

more detailed shape of the erosion hole can be obtained when using equipment like laser scanners or cameras to measure the depth. However, due to the presence of the water and the narrow shape of the hole where the water jet impacts, it is questionable whether accurate results are obtained this way. The measuring accuracy could better be improved by measuring the depth over a smaller width and a smaller grid size, such that the shape of the hole is captured more accurately but the number of measuring points does not increase significantly. During this study, the shape of the hole is determined by using linear interpolation between two measuring points over the length of the hole. Using higher order interpolation could be useful to better represent the curve of the hole. However, the top and bottom of the hole is rather straight and higher order interpolation can result in more inaccuracies regarding the shape of the hole at these locations. It is expected, that using a smaller grid size already results in a more accurate representation of the shape of the hole.

The duration of the intervals varied between 5 and 20 minutes. An advantage of performing the interval for a shorter time span is that more measurements can be performed. The disadvantage is that inaccuracies in measuring the depth and the duration of the test result in larger inaccuracies for shorter time intervals. These inaccuracies reduce when the time span is increased.

While executing the experiments, the discharge from the nozzle was read from the discharge meter, which was placed between the 3-way manifold and the nozzle. The discharge meter has an accuracy of $\pm 2\%$ (van Steeg & Mourik, 2020). Setting the correct discharge could only be done at the start of each interval by adjusting the openings of the 3-way manifold. While setting the openings correctly to reach the correct discharge, the discharge from the nozzle was sometimes higher or lower than the discharge indicated as the discharge applied during the interval. This could have caused a higher or lower erosion rate as when the correct discharge would have been used from the beginning. Furthermore, fixing kinks in the hose is done during the interval, which has also caused some small variations in the discharge. However, both were fixed rather quickly and did not affect the outcome significantly.

5.3 Suitability of methods used to calculate the hydraulic loads

The methods used to calculate the hydraulic load affect the outcome of the calculations. Different methods are used to analyse the results of the fire hose method experiments and the wave overtopping experiments. The uncertainties during the calculations are explained in the next sections.

5.3.1 Uncertainties in calculating the hydraulic loads occurring during the fire hose method experiments

As explained in the previous section, the flow velocity from the nozzle varied a little during each interval, but this is not taken into account when the normal and shear stresses were calculated. Additionally, other assumptions are made to calculate the normal stress. It is assumed that the water flows parallel to the surface of the hole. As can be seen in Figure 5.2, at the location where the jet impacts, the angle of incidence is smaller than 180° . For this location, the normal stress was probably higher than calculated. Furthermore, it is assumed that the flow velocity and discharge were constant over the entire length of the dug hole. Due to the variation of the discharge in the beginning of the interval and the bed friction of the clay, this is not the case. As depicted in Figure 5.5, the water spreads after the jet impacts on the clay. The discharge flowing over a part of 10 centimeters wide - which is the width over which the normal stress is calculated - at that part of the hole is lower than at the location where the jet impacts. As a result, the normal stress at the lower section of the hole is overestimated. When a small erosion depth is measured, it is shown in the scatter plots as a data point with a high critical stress and low erosion rate. This causes a large spread in the results.



Figure 5.5: Spreading of the flow after the jet impacts.

The normal stress during an interval is calculated by taking the average between the calculated normal stress based on the shape of the erosion hole prior to the interval and based on the shape of the erosion hole after the interval. However, it is unknown whether the erosion rate was constant during the interval and whether the change in normal stress occurs linear. The disadvantage of using this method to calculate the average normal stress and corresponding erosion rate is that the assumptions greatly affect the outcome. This can be explained when zooming in on Figure C.1, as is done in Figure 5.6. At location ‘length of erosion hole = 40 cm’ the angular displacement after interval 1 is only 4° . After interval 2 this changes to 55° and after interval 3 to 65° . According to Equations 3.2 and 3.3, the normal force increases when the angular displacement increases. As a result, when comparing the average normal stress during interval 2 to interval 3, interval 2 gives a lower average normal stress. However, as Figure 5.6 shows, the erosion rate during interval 2 is much higher than during interval 3. This contradicts expectations and can be caused by the method used to calculate the normal stress. However, the lower normal stress on the clay can also be caused by the fact that water remained present at the erosion hole after interval 2 due to the shape of the hole. The remaining water can weaken the impact of the water jet (van Bergeijk, 2022).

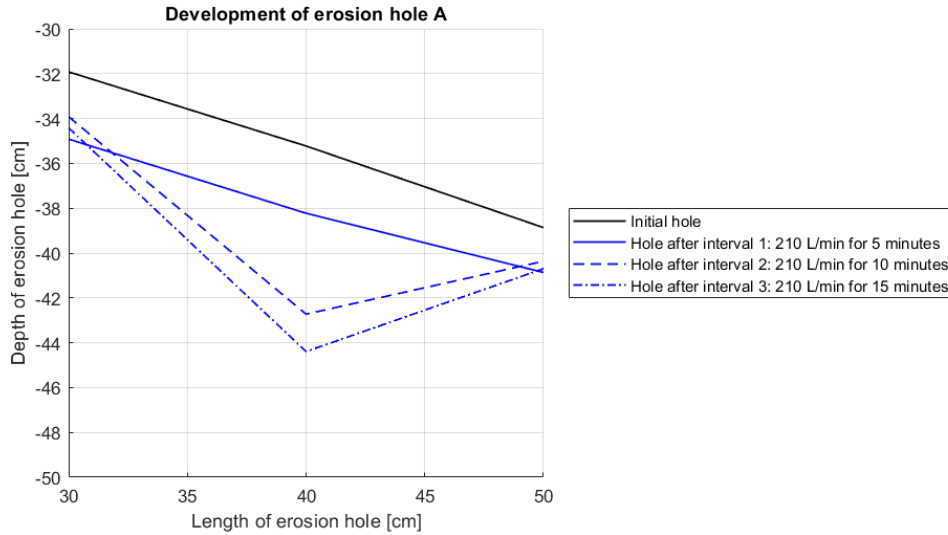


Figure 5.6: Development of erosion hole during test A (zoomed in).

5.3.2 Uncertainties in calculating the hydraulic loads occurring during the wave overtopping experiments

Most wave overtopping experiments have been performed on dike sections with a grass cover. During the experiments performed in the Hedwige-Prosperpolder, a 20 centimeter deep section has been excavated to test the erosion resistance of the clay. However, no common formulas are known for calculating the flow velocity, normal stresses, and shear stresses on clay and thus formulas for wave overtopping over grass are used. The roughness of clay covers is smaller than the roughness of grass covers, which can lead to under prediction of the flow velocity and thus under prediction of the hydraulic load when using these equations (van Bergeijk et al., 2020). Several assumptions were made when using this formula. The flow velocity at the hole is unknown and thus the maximum flow velocity is calculated. However, it is uncertain whether these flow velocities did actually occur. Consequently, also the normal and shear stresses calculated are uncertain. Furthermore, the equations used to calculate the normal and shear stresses are based on experiments performed to study the effects of vertical transitions. Also these formulas are based on experiments performed on grass-covered dikes.

Data on the height of the dike cover was given for four locations over the width of the hole covering the entire length of the slope of the dike. The average height is calculated for every 0.5 meters over its length for all four locations and used to calculate the erosion rate during each experiment. This is not the common procedure for calculating the erosion rate during large-scale experiments. For example, during experiments performed in the Delta Flume, first an overview of the median cross section of the test section is made after each test. This gives a clear overview of the erosion progress. The migration of the cliff is measured and used to calculate the erosion rate (Wichman, 2021). Another method commonly used to define the erosion rate is to calculate the eroded volume (Wichman, 2021). Using these methods, the erosion rate is measured more accurately. However, this is not done in this study due to limited time.

The spread observed in the erosion rate is significantly smaller for the 10 waves of 2000 L/m compared to the other two wave volumes. This can have two causes. The first cause can be the method used to measure the erosion depth, namely photogrammetry. During the experiments, most erosion took place at the bottom of the excavated hole. However, water at the bottom of the hole could not flow out (Figure 5.7). Using photogrammetry to determine the depth of the hole, leads to uncertainties since water cannot be distinguished from clay. Because most erosion took place at the bottom, it is possible that the erosion is not measured correctly, which leads to an underestimation of the erosion rate. During the experiments, the depth of the hole was also measured using the GPS system RTK GNSS. These data can be used to quantify the erosion during the wave overtopping experiments more

accurately. The second cause of the smaller spread during higher wave volumes is explained by the bi-linear behaviour of clay (GeophyConsult, 2021). During erosion tests, clay shows a decrease in the values of the critical stress and the erosion rate when a lower stress is applied. This is caused by the predominance of two erosion mechanisms. Erosion by clods occurs under higher hydraulic stresses, and results in high erosion rates. Erosion by grains occurs under lower hydraulic stresses, and results in low erosion rates. When larger wave volumes are released from the simulator, erosion by clods is the main erosion mechanism, whereas the contribution of erosion by grains is more dominant when smaller wave volumes are released. Because of the dominance of erosion by clods occurring when large waves are released, the spread in the data becomes smaller.



Figure 5.7: Images used for photogrammetry (a) before and (b) after 10 waves of 2000 L/m were released.

5.4 The effect of the clay structure on the ability to correlate results of the fire hose method experiments to results of wave overtopping experiments

A large spread in the results of the fire hose method and wave overtopping experiments is observed. This can be caused by the heterogeneous character of clay. Prior to the tests, two pits were excavated to check the structure of the dike cover. These results are elaborated in Appendix D. The excavations indicate that the cover layer consists of different clay layers each between 10 to 50 centimeters deep and with a structure ranging from a loose, fine structure to a closed, coarse structure. Clay with a loose, fine structure is more susceptible to erosion due to the smaller critical stress and under similar load conditions, a higher erosion rate would be observed for clay layers with a loose, fine structure as compared to a clay layer with a more closed, coarse structure (van Steeg & Mourik, 2020). Roots were present till a depth of 1.40 meters. Which means that not only clay was tested on its erosion resistance, but also the erosion resistance of the roots is included in the test results. During both tests, the depth of the holes varied between approximately 20 and 70 centimeters. This implicates that different clay structures were tested during the tests and the erosion rates of all structure layers are analysed simultaneously. This could explain the large spread in the results, however this is not analysed in this study. The large spread in the data causes that no clear relation was found between the normal and shear stresses and the observed erosion rate. Furthermore, the critical normal and shear stress and erodibility coefficient cannot be determined from these data, which makes it questionable whether the test results can be used for to determine the clay quality class.

Chapter 6

Conclusions and Recommendations

A literature study is performed to gain insight in the origin of clay categorisation in the Netherlands and internationally, and to retrieve information about how small- and large-scale tests are performed and generates outcomes used to determine the erosion resistance of clay. This information is used to improve the original setup of the fire hose method. The improved setup is used during experiments performed in the Hedwige-Prosperpolder and the results are analysed to calculate the normal and shear stresses and erosion rate during the tests. The results are used to answer the research questions stated in Section 1.3. The section below answers the four subquestions individually, which are used to answer the main research question. Section 6.2 describes the recommendations for further research. These recommendations are based on the drawn conclusions and the main findings described in the Discussion.

6.1 Conclusions

The first subquestion was: *‘Which test outcomes lay at the basis of clay categorisation and how is dealt with the spread in these outcomes?’*

The Dutch clay categorisation system is based on Rotating Cylinder Tests performed by Grondmechanica Delft. The results of 30 tested samples were analysed. The samples were divided into three categories based on the rotational speed of the outer cylinder when 30% of the initial mass of the sample was eroded. An analysis on the characteristics of these samples has indicated that the category of a sample can be determined by the Atterberg Limits of the sample.

By defining the critical rotational speed as the speed where 30% of the initial mass is eroded, the two stages where first only small particles erode and secondly larger aggregates erode is not considered. The initiation of the second stage is commonly used to define the critical shear stress. Also should be noted that the shear stress on the sample is calculated by the average shear stress over each interval. When erosion occurs during an interval, the shear stress on the sample decreases. In 2012, the RCT is updated to the RETA where the shear stress on the sample during an interval is kept constant by adjusting the rotation speed, to determine the critical shear stress more accurately.

In 2017, the Dutch clay categorisation system was updated, based on results of numerical simulations, large-scale experiments, field observations, and additional analysis regarding the effects of parameter values on the performance of clay. By shifting the classification boundaries between categories 1 and 2 from 45% to 40% and creating a bandwidth around category 1, more samples are classified as ‘Erosion resistant’ and the heterogeneous character of clay is better taken into account.

The soil classification system of Briaud is internationally widely used. This system has incorporated the results of various small- and large-scale experiments. By performing large-scale experiments, the heterogeneous character of clay is already taken into account. However, to take the heterogeneous character also into account with small-scale experiments, multiple experiments must be performed on the same dike section.

The second subquestion was: *‘What experimental setup of the fire hose method is most appropriate to determine the critical stress and soil erodibility of clay?’*

To determine the critical stress and soil erodibility of clay, the applied stress and erosion rate must be calculated. Even though the setup used to perform experiments in the Hedwige-Prosperpolder was better suited to perform experiments on clay compared to the setup used during experiments in 2021, the outcome resulted in a large spread in the data and therefore the values for the erosion resistance parameters could not be calculated.

The third subquestion was: *‘To what extent are the forces, that are exerted on the clay during the fire hose method experiments, representative for wave overtopping?’*

The outcome of the fire hose method experiments is compared to the results of wave overtopping experiments to check whether the stresses on the clay are of the same magnitude. The calculated normal stresses that occurred using flow velocities of 1.75 m/s and above during the fire hose method experiments are representative for the magnitude of the normal stresses that occurred during wave overtopping experiments using waves of 500 L/m, 1500 L/m, and 2000 L/m. However, it should be noted that the method used to calculate the normal stresses affect the outcome. To calculate the normal stress during the wave overtopping experiments, the flow velocity of the wave front is calculated using equations normally used for overtopping waves flowing over grass. The roughness of clay is smaller than the roughness of grass, which implicates that the flow velocity over clay is higher than over grass and thus higher normal stresses are expected to act on the clay than is calculated in this study.

The shear stress could not be calculated for the fire hose method experiments. Therefore, the magnitude of the shear stress is expressed by the flow velocity. The maximum flow velocity calculated for the waves of 500 L/m was 4.0 m/s, which is close to the flow velocities of 3.25 m/s and 4.42 m/s used in tests A and F of the fire hose method experiments. For the waves of 1500 L/m and 2000 L/m, a maximum flow velocity of 5.7 m/s and 6.3 m/s was calculated respectively. This is higher than the maximum flow velocity used during the fire hose method tests, but results of the fire hose method using 5.25 m/s in tests C and D and the wave of 1500 L/m show similarity in their results regarding the range in the observed erosion rate.

The fourth subquestion was: *‘To what extent can the results of the fire hose method be correlated to wave overtopping experiments performed on the same clay?’*

Figure 4.9 shows that the magnitude of the normal stresses is similar for fire hose method experiments and wave overtopping experiments. The calculated normal stress and erosion rate of the fire hose method using a flow velocity of 1.75 m/s till 2.50 m/s is representative for those observed during the wave overtopping experiments with a wave volume of 500 L/m. The observed normal stresses during waves of 1500 L/m and 2000 L/m can be represented by the normal stresses occurring during the fire hose method experiments using a flow velocity between 3.25 m/s and 5.52 m/s. The observed erosion rate for those flow velocities and for the waves of 1500 L/m are similar. The smaller spread in the data for waves of 2000 L/m falls within the range of the erosion rate observed during the fire hose method experiments. However, it is expected that the erosion rate observed during the wave overtopping experiments is larger than that is captured currently in the data, due to the usage of photogrammetry.

The observed erosion rate for the fire hose method experiments using a flow velocity of 5.25 m/s is representative for the observed erosion rate for overtopping wave volumes of 1500 L/m. The observed erosion rate for wave volumes of 500 L/m and 2000 L/m is not observed during any of the fire hose method experiments with a similar flow velocity. Hence, the results of the fire hose method experiments are unsuitable to correlate to the outcome of the wave overtopping experiments based on the applied flow velocity.

The answers of the subquestions are used to answer the main research question: *‘How can the fire hose method be used to accurately determine the erosion resistance of clay in dikes against wave overtopping?’*

Because an angle of incidence of 180° and a curved shape for the wall of the hole is used during the fire hose method experiments, the setup proposed in this study is able to represent the hydraulic load on the clay, which do occur at the bottom of the excavated hole during large scale experiments, well. The fire hose method generates stresses on clay which are representative for those exerted during wave overtopping. Due to the large spread in the results obtained by the experiments performed in the Hedwige-Prosperpolder, it was not possible to determine the erosion resistance for these experiments. However, the large spread is also observed in the results of the wave overtopping experiments. The magnitude of the observed erosion rates and calculated normal stresses are similar for both experiments, which could indicate that the large spread in the data is caused by the heterogeneous character of the clay.

6.2 Recommendations

Based on the outcome of this study, three recommendations are given regarding further analysis of the data of the wave overtopping experiments and the fire hose method experiments, and performing experiments in the future with the fire hose method. These recommendations are explained below.

During the wave overtopping experiments, data about the overtopping waves and the erosion of the clay is captured using photogrammetry. For this study, data about the height of the cover material for wave volumes of 500 L/m, 1500 L/m and 2000 L/m on the lowest test section is used to calculate the normal and shear stresses and the corresponding erosion rate. As explained in the discussion, it is expected that the erosion rate used in this study is smaller than the erosion rate that actually took place during the experiments due to uncertainties in the analysing method. Infram has also performed measurements on the erosion process during the experiments using the GPS system RTK GNSS. This data contains information about the coordinates and height of the measuring points and gives a more accurate overview of the height than photogrammetry. By including the data of Infram, the erosion rate can more accurately be determined.

Besides the erosion rate, Infram has calculated the flow velocity of the wave front by analysing the video footage of the experiments. The average flow velocity of the wave front over clay for the wave volumes of 500 L/m, 1500 L/m, and 2000 L/m are 3.95 m/s, 5.58 m/s, and 5.43 m/s respectively (Daamen et al., 2022). Using these flow velocities instead of the maximum flow velocities over grass, the normal and shear stresses can be calculated more accurately.

For this study, data about the wave volumes of 500 L/m, 1500 L/m, and 2000 L/m is used. These wave volumes were selected since this data was analysed first by Ebrahimi. Currently, the data of other wave volumes and other bare clay test sections are being analysed. If needed, this data can also be included to increase the amount of data and, if needed, to correlate the outcome of the fire hose method experiments to other wave volumes.

The second recommendation is to further analyse whether the spread in the data of the fire hose method experiments can be minimised. Due to time restrictions, this could not be performed during this study. For example, the data points where no significant erosion takes place can be excluded from the data set, or by only including the data points where the water jet impacts, the uncertainties in calculating the normal stress can be reduced. Appendix D shows that a clear difference in the structure of the clay is observed over the depth of the cover layer. By analysing the results per layer instead of all layers combined, it is possible that the spread in the outcome is reduced.

The normal stress can also be calculated using the information of the setup of the experiment, such as the angle of the nozzle and flow velocity, to calculate the location of impact and the stress on the clay. This way, the assumption that water flows parallel to the wall of the hole is excluded. It is possible that by using an other method to calculate the normal stress, a smaller spread in the results is obtained.

The large spread in the results of the fire hose method experiments make the method not useful to define the erosion resistance of clay. However, a large spread is also observed in the data of the wave overtopping experiments, which could, for example, indicate that the large spread is caused by the variation in the structure of the clay at the Hedwige-Prosperpolder. By first performing the recommendations previously mentioned, it can be indicated whether the normal- and shear stresses and erosion rates are calculated correctly, and whether the spread in the data can be reduced for both experiments. If the data of the fire hose method experiments and the wave overtopping experiments still show the same characteristics, it is recommended to perform the fire hose method experiments again, to verify whether data can be obtained which can indicate the erosion resistance of the clay. Even though, no conclusions could be drawn about the erosion resistance of clay from the data obtained in this study, performing tests in the future, while considering the points mentioned in the discussion, could lead to a test method that can indicate the erosion resistance of clay. The section below describes how experiments with the fire hose method can best be performed to improve the accuracy of the obtained data. In Appendix E, these adjustments to the method are explained in more detail.

6.2.1 Performing fire hose method experiments in the future

The fire hose method still needs to be developed, to find the best setup to determine the critical stress and erodibility coefficient of clay. To improve the accuracy of the calculated stresses, the assumptions made to perform the calculations must be similar to what occurs during the experiments. By placing plates at the sides of the excavated hole, the flow can be directed and does not spread out. The angle of incidence must be 180° to calculate the normal stresses correctly, when one is interested in correlating the results of erosion occurring at the bottom of the excavated hole during large scale experiments. This can be done by calculating the angle of incidence prior to the tests, based on the setup of the experiment. If one is interested in erosion caused by the impact of the wave at the top of the excavated hole, the setup of the fire hose method must be altered, such that the angle of incidence resembles the angle of incidence during wave overtopping. It is advised to perform the fire hose method experiments with larger flow velocities, during which significant erosion occurs. In that case the main erosion mechanism, which is tested, is erosion by clods. Furthermore, it is advised to measure the depth of the hole over a smaller width and length, while using a smaller grid size. This reduces the time needed to measure the depth of the hole, but increases the amount of data and the accuracy in the presented shape of the hole.

It is advised to perform future experiments on other dike sections where large-scale test have already been performed or to perform tests on homogeneous clay created in the lab. By performing experiments on dike sections where already other tests have been performed, it can be studied whether the new setup can be used to determine the erosion resistance of structured clay and the outcome of the fire hose method experiments can be correlated to the results of large-scale experiments to validate the setup. By performing tests on heterogeneous clay, it can be studied whether it is possible to reduce the spread in the outcome of the fire hose method experiments. When analysing the results, it is advised to search for relations between the stress and erosion rate of the depth or the average erosion rate, since it has been shown in this study that these are the most suitable parameters. It is also advised to study whether the erosion rate of the volume can be used for this relation, since this parameter is often used to describe erosion during large-scale experiments.

Bibliography

- Breteler, M. K. (2021). *Erosie van kleibekleding met gras op boventalud van lauwersmeerdijk meetver-slag deltagootproeven voor dijktraject lauwersmeerdijk-vierhuizergat* (Tech. Rep.). Deltares.
- Briaud, J.-L. (2008, 10). Case histories in soil and rock erosion: Woodrow wilson bridge, brazos river meander, normandy cliffs, and new orleans levees. *Journal of Geotechnical and Geoenvironmental Engineering*, 134, 1425-1447. doi: 10.1061/(ASCE)1090-0241(2008)134:10(1425)
- Briaud, J.-L., Govindasamy, A., & Shafii, I. (2017, 10). Erosion charts for selected geomaterials. *Journal of Geotechnical and Geoenvironmental Engineering*, 143, 04017072. doi: 10.1061/(asce)gt.1943-5606.0001771
- Briaud, J.-L., Shafii, I., Chen, H.-C., & Medina-Cetina, Z. (2019). Relationship between erodibility and properties of soils. *The National Academies Press*. Retrieved from <https://doi.org/10.17226/25470>. doi: 10.17226/25470
- Casagrande, A. (1947). Classification and identification of soils. *Proceedings of the American Society of Civil Engineers*, 73, 783-810.
- Chapuis, R., & Gatién, T. (1986). An improved rotating cylinder technique for quantitative measurements of the scour resistance of clays. *Canadian Geotechnical Journal*, 23, 83-87. doi: 10.1139/t86-010
- Daamen, E., Heida, L., & Mom, R. (2022). *Factual report golfoverslag- en grastrekproeven polder2c's*. de Vries, G., & de Bruijn, H. (2021). *Beoordelingskader samenstelling kaden noordwaard* (Tech. Rep.). Deltares.
- Ebrahimi, M. (2022). *Close-range photogrammetry application to wave overtopping erosion progression measurements* (Tech. Rep.). Université catholique de Louvain.
- Fox, R., McDonald, A., Pritchard, P., & Mitchell, J. (2016). *Fluid mechanics* (9th ed.). John Wiley & Sons.
- GeophyConsult. (2021). *Jet erosion tests carried out in the framework of interreg polder2c's project* (Tech. Rep.).
- Gibbs, H. (1962). *A study of erosion and tractive force characteristics in relation to soil mechanics properties : Earth research program*. Office of Assistant Commissioner and Chief Engineer, Division of Engineering Laboratories.
- Hanson, G. (1992). Erosion resistance of compacted soils. *Journal of the Transportation Research Board*, 2630.
- Hanson, G., & Cook, K. (2004). *Apparatus, test procedures, and analytical methods to measure soil erodibility in situ* (Tech. Rep.).
- Hanson, G., & Robinson, K. (1993). The influence of soil moisture and compaction on spillway erosion. *Transactions of the ASABE*, 36, 1349-1352.
- Hoffmans, G., Akkerman, G., Verheij, H., van Hoven, A., & van der Meer, J. (2009, 5). The erodibility of grassed inner dike slopes against wave overtopping. , 3224-3236. doi: 10.1142/9789814277426_0267
- Karamigolbaghi, M., Ghaneeizad, S., Atkinson, J., Bennett, S., & Wells, R. (2017). Critical assessment of jet erosion test methodologies for cohesive soil and sediment. *Geomorphology*, 295, 529-536. doi: 10.1016/j.geomorph.2017.08.005.
- Koelewijn, A. (2022). *Test plan wave overtopping reference test living lab hedwigeprosperpolder (llhpp)*.
- Kruse, G., Dekker, J., & van Deen, J. (1988, 9). *Onderzoek naar het beoordelen van de geschiktheid van kleigrond voor bekleding van dijken met grasdekking* (Tech. Rep.). Grondmechanica Delft.

- Larsen, R. (2008). Erosion function apparatus. *The Journal of Undergraduate Research*, 6, 51-56. Retrieved from <http://openprairie.sdstate.edu/jur/vol6/iss1/6>
- Lim, S. (2006). *Experimental investigation of erosion in variably saturated clay soils* (Tech. Rep.). School of Civil and Environmental Engineering The University of New South Wales. Retrieved from <http://unsworks.unsw.edu.au/fapi/datastream/unsworks:1112/SOURCE01?view=true>
- Lyle, W., & Smerdon, E. (1965). Relation of compaction and other soil properties to erosion resistance of soils. *Transactions of the ASAE*, 8, 419-422. doi: 10.13031/2013.40536
- Mazurek, K. (2010). *Erodibility of a cohesive soil using a submerged circular turbulent impinging jet test* (Tech. Rep.). University of Saskatchewan. Retrieved from https://acwi.gov/sos/pubs/2ndJFIC/Contents/6A2_Mazurek_3_9_2010_paper.pdf
- Moreno-Maroto, J., Alonso-Azcárate, J., & O'Kelly, B. (2021, 1). Review and critical examination of fine-grained soil classification systems based on plasticity. *Applied Clay Science*, 200, 105955. doi: 10.1016/J.CLAY.2020.105955
- Mourik, G. (2015). *Prediction of the erosion velocity of a slope of clay due to wave attack* (Tech. Rep.). Deltares.
- Onderzoek grasbekleding dijken. (n.d.). <https://www.wur.nl/nl/onderzoek-resultaten/onderzoeksinstututen/environmental-research/faciliteiten-tools/kwaliteit-grasbekleding-dijken/onderzoek-grasbekleding-dijken.htm#:~:text=Er%20ligt%20bijna%2018.000%20km,verzamelen%20en%20opslag%20van%20data.>
- Piontkowitz, T., Verhagen, H., Verheij, H., Cao, T., Dassanayake, D., Roelvink, D., ... Ploompoo, T. (2009). *Erograss: Failure of grass cover layers at seaward and shoreward slopes* (Tech. Rep.). Retrieved from www.kyst.dk/erogress
- Postma, T., & Dekker, J. (1985). *Klei onder steenzettingen oesterdam en philipsdam: onderdeel erosieproeven (centrifuge)* (Tech. Rep.). Laboratorium voor Grondmechanica. Retrieved from https://puc.overheid.nl/doc/PUC_49155_31/1
- Rijkswaterstaat. (2012). *Handreiking toetsen grasbekledingen op dijken t.b.v. het opstellen van het beheerdersoordeel (bo) in de verlengde derde toetsronde* (Tech. Rep.). Author.
- Rijkswaterstaat. (2018). *Vier quick wins grond en klei* (Tech. Rep.). Author.
- Rikkert, S., Alleon, C., Khaldi, I., Shaiek, S., Ebrahimi, M., Frazao, S. S., ... Sergent, P. (2021). *How strong are our levees? hydraulic analysis based on polder2c's project in situ testing* (Tech. Rep.).
- Robinson, K. (1990). Gully erosion in earth spillways. *Applied engineering in agriculture*, 6, pp. 279-284-1990 v.6 no.3. Retrieved from <http://dx.doi.org/10.13031/2013.26382> doi: 10.13031/2013.26382
- Schematiseringshandleiding grasbekleding* (Tech. Rep.). (2021, 05). Ministerie van Infrastructuur en Waterstaat.
- Shaikh, A., Ruff, J., & Abt, S. (1988, 3). Erosion rate of compacted na-montmorillonite soils. *Journal of Geotechnical Engineering*, 114, 296-305. Retrieved from [https://doi.org/10.1061/\(ASCE\)0733-9410\(1988\)114:3\(296\)](https://doi.org/10.1061/(ASCE)0733-9410(1988)114:3(296)) (doi: 10.1061/(ASCE)0733-9410(1988)114:3(296)) doi: 10.1061/(ASCE)0733-9410(1988)114:3(296)
- Shan, H., Shen, J., Kilgore, R., & Kerenyi, K. (2015). *Scour in cohesive soils* (Tech. Rep.). Retrieved from <http://www.ntis.gov>
- Sing, H., & Thompson, A. (2015). Effect of antecedent soil moisture content on soil critical shear stress in agricultural watersheds. *Geoderma*, 165-173.
- TAW. (1996). *Technisch rapport klei voor dijken* (Tech. Rep.). Technische Adviescommissie voor de Waterkeringen. Retrieved from <http://resolver.tudelft.nl/uuid:1adcbb6e-fc1a-42f2-abef-5d75635bc8fc>
- 't Hart, R., de Bruijn, H., & de Vries, G. (2016). *Fenomenologische beschrijving faalmechanismen wti* (Tech. Rep.). Deltares. Retrieved from https://puc.overheid.nl/doc/PUC_148759_31/1
- Tran, T. (2018). *Instrumentation of erosion function apparatus and evaluation of a new erosion characterization methodology*.
- TWI. (2022). <https://www.twi-global.com/technical-knowledge/faqs/technology-readiness>

-levels.

- van Bergeijk, V. (2022). *Over the dike top: Modelling the hydraulic load of overtopping waves including transitions for dike cover erosion* (Doctoral dissertation). doi: 10.3990/1.9789036553414
- van Bergeijk, V., Verdonk, V., Warmink, J., & Hulscher, S. (2021, 3). The cross-dike failure probability by wave overtopping over grass-covered and damaged dikes. *Water*, 13, 1-22. doi: 10.3390/w13050690
- van Bergeijk, V., Warmink, J., Frankena, M., & Hulscher, S. (2019). Modelling dike cover erosion by overtopping waves: The effects of transitions. *Coastal Structures*. doi: 10.18451/978-3-939230-64-9_110
- van Bergeijk, V., Warmink, J., & Hulscher, S. (2020). Modelling the wave overtopping flow over the crest and the landward slope of grass-covered flood defences. *Journal of Marine Science and Engineering*, 30. doi: doi:10.3390/jmse8070489
- van Bergeijk, V., Warmink, J., & Hulscher, S. (2021). *Experimental set-up and modelling tools for the load by overtopping waves in erosion models*.
- van Damme, M., van der Meer, M., Gerrits, A., Vos, R., & Bizzarri, A. (2021). *Incorporating the erosion sensitivity of local soils in a levee safety analysis* (Tech. Rep.). Retrieved from www.waterschaplimburg.nl
- van der Meer, J., Hardeman, B., Steendam, G.-J., Schüttrumpf, H., & Verheij, H. (2011). Flow depths and velocities at crest and landward slope of a dike, in theory and with the wave overtopping simulator. *Coastal Engineering Proceedings*, 1. Retrieved from <https://icce-ojs-tamu.tdl.org/icce/index.php/icce/article/view/1239> doi: 10.9753/icce.v32.structures.10
- van der Meer, J., Steendam, G., de Raat, G., & Bernardini, P. (2009, 05). Further developments on the wave overtopping simulator. , 4, 14. doi: 10.1142/9789814277426.0245
- van Meurs, G., & Kruse, G. (2017). *Eindrapport update inzichten gebruik van klei voor ontwerp en uitvoering van dijkversterkingen* (Tech. Rep.). Deltares. Retrieved from https://www.deltaexpertise.nl/images/e/eb/Eindrapport_Update_inzichten_gebruik_van_klei_voor_ontwerp_en_uitvoering_van_dijkversterkingen.pdf
- van Steeg, P. (2021). *Testen op grasbekleding met brandslangmethode* (Tech. Rep.).
- van Steeg, P., & Mourik, G. (2020). *Ontwikkeling brandslangmethode* (Tech. Rep.). Deltares.
- Wahl, T. (2010). Relating jet and jet test results to internal erosion field tests. *Joint Federal Interagency Conference on Sedimentation and Hydrologic Modeling*, 12.
- Wahl, T. (2016). The submerged jet erosion test: Past-present-future. , 12. Retrieved from https://www.usbr.gov/tsc/techreferences/hydraulics_lab/pubs/PAP/PAP-1133.pdf
- Wahl, T. (2021). Methods for analyzing submerged jet erosion test data to model scour of cohesive soils. *American Society of Agricultural and Biological Engineers*, 64, 785-799. doi: 10.13031/trans.14212
- Wang, B., Zheng, F., Römkens, M., & Darboux, F. (2013). Soil erodibility for water erosion: A perspective and chinese experiences. *Geomorphology*, 187, 1-10. Retrieved from <https://www.sciencedirect.com/science/article/pii/S0169555X1300055X> doi: 10.1016/j.geomorph.2013.01.018.
- Wichman, B. (2021). *Dijkerosie 2021-de2 vaststelling erosieparameters en lengte-effecten buitentalud* (Tech. Rep.). Deltares.
- Wopereis, L., & van Steeg, P. (2021). *Meetverslag grasbekledingsproeven brandslangmethode waddenzeedijk* (Tech. Rep.). Deltares.
- Yagisawa, J., van Damme, M., Pol, J., & Bricker, J. (2019). *Verification of a predictive formula for critical shear stress with large scale levee erosion experiment* (Tech. Rep.). Delft University of Technology.

Appendix A

Determining the Critical Stress and Erodibility Coefficient

By performing tests, the erosion parameters *erodibility coefficient* (k) and *critical stress* (τ_c) of clay can be determined. Both parameters cannot directly be measured in the field. However, when using the erosion relation (Equation 1.1), these can be derived.

Figure A.1 shows an example of how test results can be used to determine the erosion parameters. The figure shows 12 erosion rates observed under two hydraulic loads. The blue data points are obtained using a low flow velocity and the orange data points using a higher flow velocity. Through the data points, a line can be fitted. A linear relation can best be assumed ($\alpha = 1$), because higher values can lead to over-fitting of the data (Wahl, 2021). The location where the line intercepts the x-axis indicates the critical stress. The slope of the line indicates the erodibility coefficient.

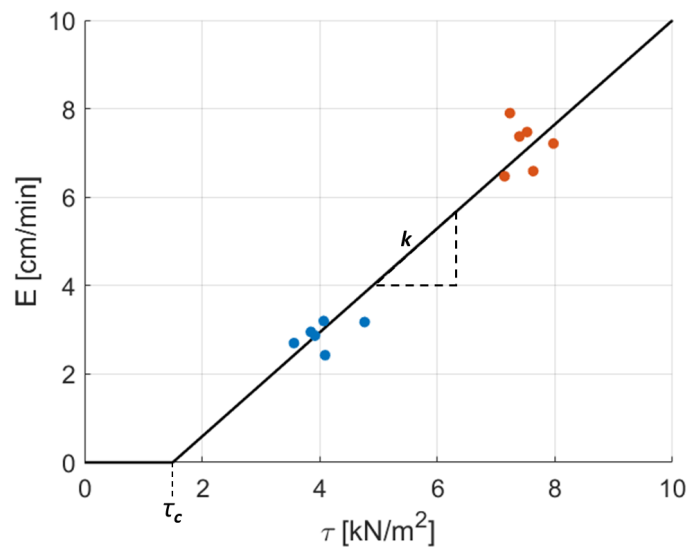


Figure A.1: Example of determining the erodibility coefficient (k) and critical stress (τ_c).

Appendix B

Action Plan

Clay Erosion Experiments using the Small-Scale Fire Hose Method

B.1 Introduction

Small scale erosion experiments are performed on bare clay to determine the erosion resistance of clay by using the fire hose method. This test method is designed by Deltares to overcome problems regarding other small- and large-scale erosion experiments (van Steeg & Mourik, 2020). The method is designed to perform tests in a short time while taking the heterogeneous character of the soil into account. The erosion experiments are performed as part of the master thesis ‘Relations for clay erosion by wave overtopping based on the fire hose method’, during which is being examined whether the fire hose method is an accurate test method to determine the erosion resistance of clay. The results of these experiments are used to correlate the results of the fire hose method experiments to the large-scale wave overtopping experiments. Both experiments are performed on the same dike section located in the Hedwige-Prospolder.

The goal of the fire hose method experiments is to determine the erosion resistance of clay by using the small-scale fire hose method. The erosion resistance of clay can be expressed in the critical stress (τ_c) and the erodibility coefficient (k). These parameters are used in the erosion equation to calculate the erosion rate caused by the excess stress (Hanson & Cook, 2004):

$$E = \begin{cases} k(\tau - \tau_c)^\alpha & \text{if } \tau > \tau_c \\ 0 & \text{if } \tau \leq \tau_c \end{cases} \quad (\text{B.1})$$

Where

E	Erosion rate	[m/s]	
k	Erodibility coefficient	Unit depends on α	(For $\alpha = 1 : [m^3/sN]$)
τ	Stress	[N/m ²]	
τ_c	Critical stress	[N/m ²]	
α	Power coefficient	[-]	

It is not possible to measure the erodibility coefficient and critical stress directly during the fire hose method. However, it is possible to measure the erosion rate of the clay, which is caused by the excessive force acting on the clay. During the fire hose method, the excessive force is caused by the water jet aimed at the clay layer. The stress caused by this jet cannot be measured directly and is calculated using the flow velocity of the water jet. Hence, it is important to record the erosion rate and flow velocity accurately during the execution of the experiments to determine the erodibility coefficient and critical shear stress of the clay.

The relationship between the erosion rate, and normal and shear stresses is determined by testing the clay under different hydraulic loads. This is done by performing the experiment for different flow velocities. Each flow velocity is applied to the regular clay at different locations to consider the heterogeneous character of clay. Preferably, the flow velocities exerted on the clay during the fire hose method are comparable to those during wave overtopping experiments to gain the best insight into its erosive behaviour. However, the erosion rate of the clay must be sufficiently low to perform the experiment for a sufficiently long time.

The critical stress is the stress under which the clay starts to erode. The optimal way to determine the critical stress is by exerting a small flow velocity on the clay initially, when the clay does not erode, the flow velocity is increased slightly. These steps are repeated until the clay starts to erode. Hereby, the rate at which erosion occurs, is defined as 1 cm/5 minutes. Whether this method can be used in the field, depends on the minimum flow velocity of the test setup and the critical flow velocity of the clay.

The goals of the fire hose experiments can shortly be summarised to:

- The erosion speed of clay is determined under different hydraulic loads, which should comply with the following:
 - Minimal 3 different flow velocities will be used as the hydraulic load on the clay, varying between 1 m/s and 7 m/s.
 - Every flow velocity is applied to 2 different locations on the dike.
 - During every interval, the flow velocity must be constant.
 - The tests must be performed on bare clay. Hence, the grass cover (top 20 cm) should be removed.
- The erosion speed is determined by the erosion volume of the erosion hole (depth, length, and width) after a predetermined time step. The following should hold:
 - The dimensions of the erosion hole are measured as accurately as possible.
 - The depth of the erosion hole is measured after each interval at the same locations by using a raster with a grid size of 10x10cm. Also the maximum depth is measured.
- The critical flow velocity is determined by increasing the flow velocity in steps slowly. The critical flow velocity is the flow velocity under which the clay starts to erode with a speed of

B.2 Materials

- 2x Sewage pump [$54m^3$]: rented from Boels - code: 10217
- 1x Sewage pump [$96m^3$]: rented from Boels - code: 10214
- Flow meter: rented from Metesco - type: Flowmaster 250DL
- Three-way manifold [4'']: rented from Boels
- Buoy: to prevent the inlet from suctioning up soil
- Suction hose with inlet [4'' – 6m]: rented from Boels - code: 10284
- Suction hose with inlet [3'' – 6m]: rented from Boels - code: 10283
- 2x Hose [4'' – 25m]: rented from Boels - code 10254
- 4x Hose [3'' – 10m]: rented from Boels - code 10212
- Coupler [3'' to 4'']: rented from Boels - code 10296
- Storz key: to (de)couple the hoses
- Frame to hold nozzle: designed by Deltares
- Nozzle (2 by 10 cm): desinged by Deltares
- 4x Tiles: to weigh down the frame
- Buckets
- Raster to measure
- Tent peg
- Basic tools and mounting materials - e.g. screw driver, hammer, screws, tie wraps, duct tape
- Spade
- Logbook
- Pen/markers
- Camera
- Laptop
- Petrol for pumps

B.3 Executing the experiments

B.3.1 Test setup

Preparation of the Surface

The experiments were performed on bare clay. Before the experiments were started, the grass layer (approximately the top 20 cm) was removed. Secondly, a hole was dug, which formed a bend in the clay (Figure B.1). The bottom of the hole was kept horizontally or descending such that water could flow out of the hole. The dimensions of the hole are measured to map the initial shape of the hole.



Figure B.1: Prepared surface.

Preparation of the setup

The pump was placed on the side of the road next to the water. The suction hose was connected to the pump and placed in the water. The pressure hose was passed through a pipe located under the road, such that the road remained clear. A three-way manifold was connected to the pressure hose and connected to another pressure hose on one of the outlets. A discharge meter was connected to this pressure hose, such that the flow velocity could be calculated. A nozzle was connected to the end of the pressure hose which was aimed at the dug hole. An overall impression of the setup is shown in Figure B.2.

The frame and nozzle were placed above the dug hole, to prevent the water to flow back into the hole. The nozzle was aimed such that the angle of incidence with respect to the wall of the hole is as close to 180° as possible. This way, the stresses can best be defined into shear and normal stress components and normal stress component. A schematisation of this position is shown in B.3

Measuring the erosion hole

The dimensions of the erosion hole are measured before the start of the experiment and at the end of each interval. This is done using a raster and a ruler to measure the development of the erosion hole during each interval at the same locations. Also, the maximum depth of the hole is noted. The logbook will be used to note the measurements. The raster is used to measure the depth of the hole at the same locations after each time interval. These locations are situated 10 centimeters apart of each other. Figure B.4 shows an example of the measuring locations using a raster.

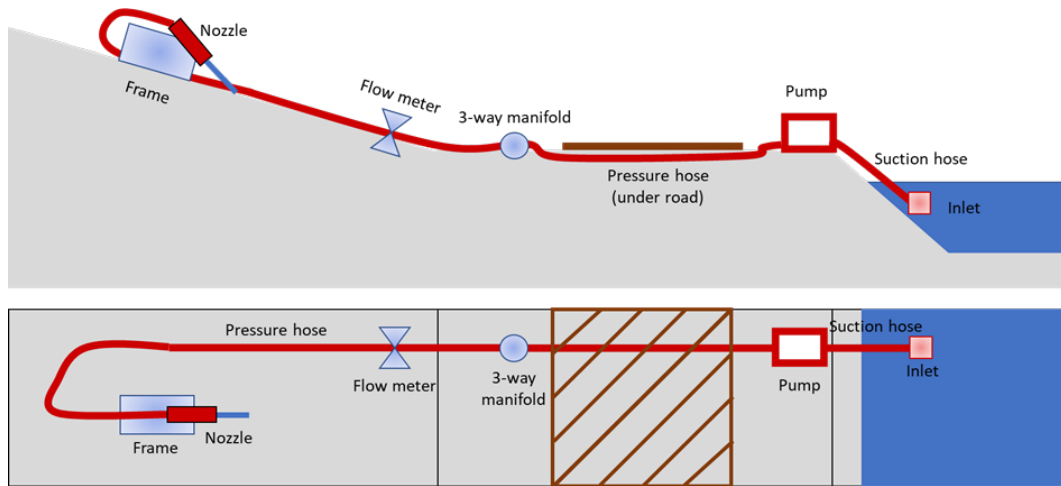


Figure B.2: Schematisation of fire hose method setup.

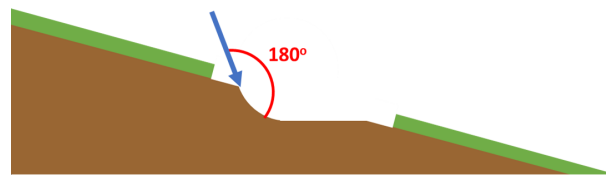


Figure B.3: Schematisation of prepared dike surface and angle of incidence of water jet.

B.3.2 Test plan

Six test sections are dug and used to perform the experiments. Table B.1 gives an overview of the six tests and the duration of their intervals and corresponding flow velocities.

Table B.1: Flow velocities during the six fire hose method experiments performed in the Hedwige-Prosperpolder.

Section A				Section B				Section C			
Interval	Time [min]	Flow rate [L/min]	Flow velocity [m/s]	Interval	Time [min]	Flow rate [L/min]	Flow velocity [m/s]	Interval	Time [min]	Flow rate [L/min]	Flow velocity [m/s]
1	5	210	1.75	1	5	150	1.25	1	5	150	1.25
2	10	210	1.75	2	5	150	1.25	2	5	150	1.25
3	15	210	1.75	3	10	150	1.25	3	5	210	1.75
4	20	210	1.75	4	10	210	1.75	4	5	300	2.50
5	15	530	4.42	5	10	210	1.75	5	5	300	2.50
				6	15	210	1.75	6	10	300	2.50
								7	10	630	5.25
Section D				Section E				Section F			
Interval	Time [min]	Flow rate [L/min]	Flow velocity [m/s]	Interval	Time [min]	Flow rate [L/min]	Flow velocity [m/s]	Interval	Time [min]	Flow rate [L/min]	Flow velocity [m/s]
1	5	150	1.25	1	5	300	2.50	1	5	390	3.25
2	5	150	1.25	2	5	300	2.50	2	5	390	3.25
3	10	150	1.25	3	10	300	2.50	3	10	390	3.25
4	15	150	1.25	4	15	300	2.50	4	15	390	3.25
5	15	150	1.25								
6	10	630	5.25								

B.3.3 Location

The experiments are performed in the Hedwige-Prosperpolder. The experiments are performed on the same dike section as where the wave overtopping experiments were performed to be able to correlate the results of the fire hose experiments to the results of the wave overtopping experiments.



Figure B.4: Measuring points at erosion hole every ten centimeters.

B.3.4 Planning

The experiments are performed from February 22nd till February 24th, 2022. The goal was to perform at least 6 experiments. Prior to these tests, a test has been performed to get familiar with the experimental setup.

B.4 Logbook

Experiment:

Angle of nozzle:

Measurement/interval:

Angle of incidence:

Flow rate:

Distance nozzle to surface:

Location:

Distance frame to hole:

	-15	-10	-5	0	5	10	15
0							
10							
20							
30							
40							
50							
60							
70							
80							
90							
100							

Maximum depth:

Coordinates:

Remarks:

Appendix C

Fire Hose Method Results Per Test

This appendix shows the individual results of the six tests performed in the Hedwige-Prosperpolder between February 22nd, 2022, till February 24th, 2022. For each test is shown: the development of the erosion profile during each interval, the calculated normal stresses and observed erosion rates per interval, and the flow velocity from the water jet and observed erosion rates per interval.

C.1 Results Test A

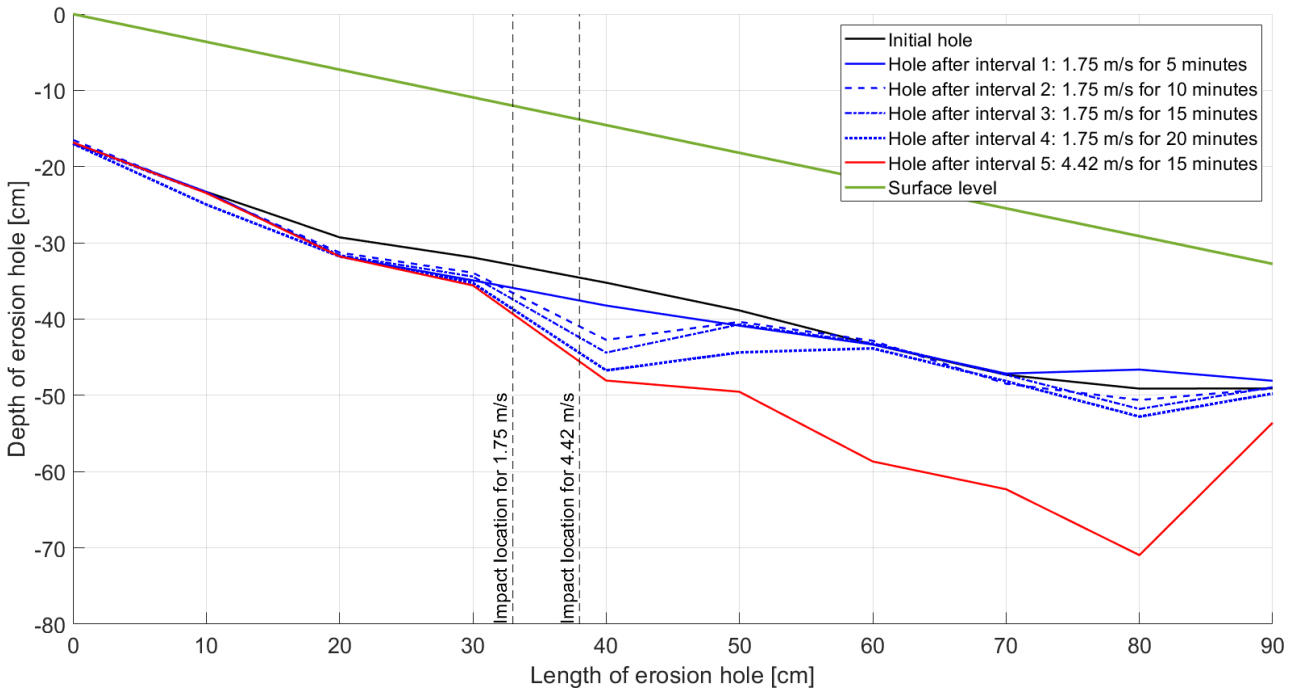


Figure C.1: Development of erosion hole during test A.

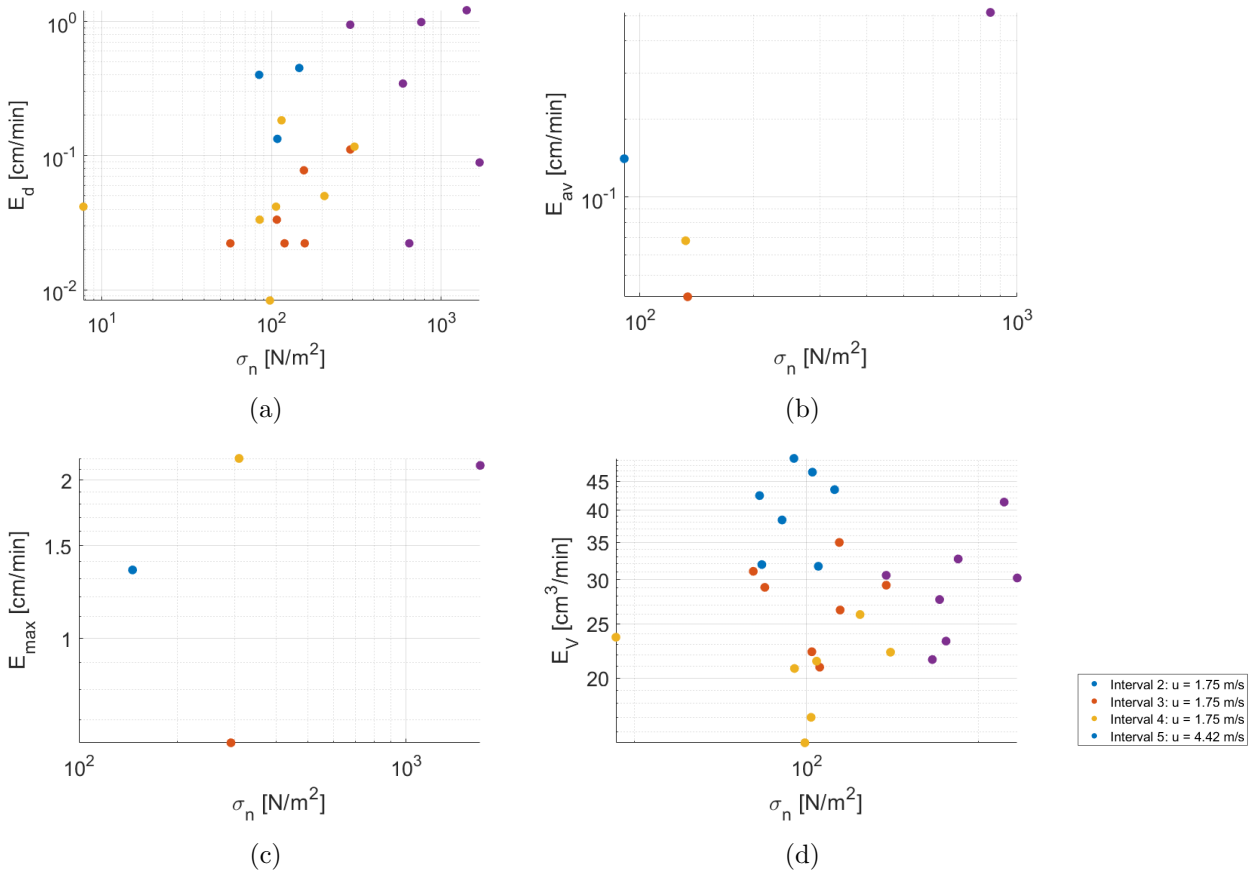


Figure C.2: (a) Erosion rate of depth, (b) average erosion rate, (c) maximum erosion rate, and (d) erosion rate of volume under normal stresses during test A.

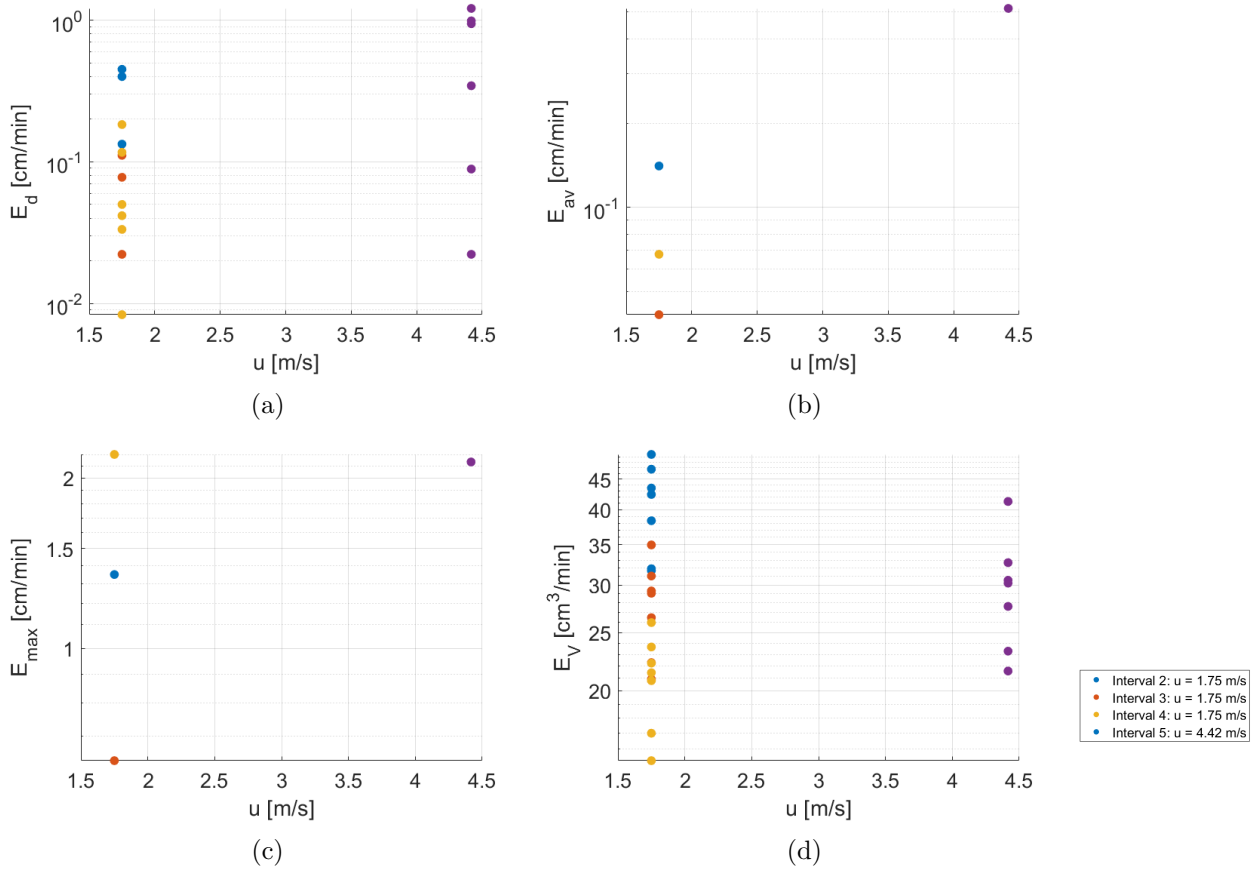


Figure C.3: (a) Erosion rate of depth, (b) average erosion rate, (c) maximum erosion rate, and (d) erosion rate of volume under flow velocities during test A.

C.2 Results Test B

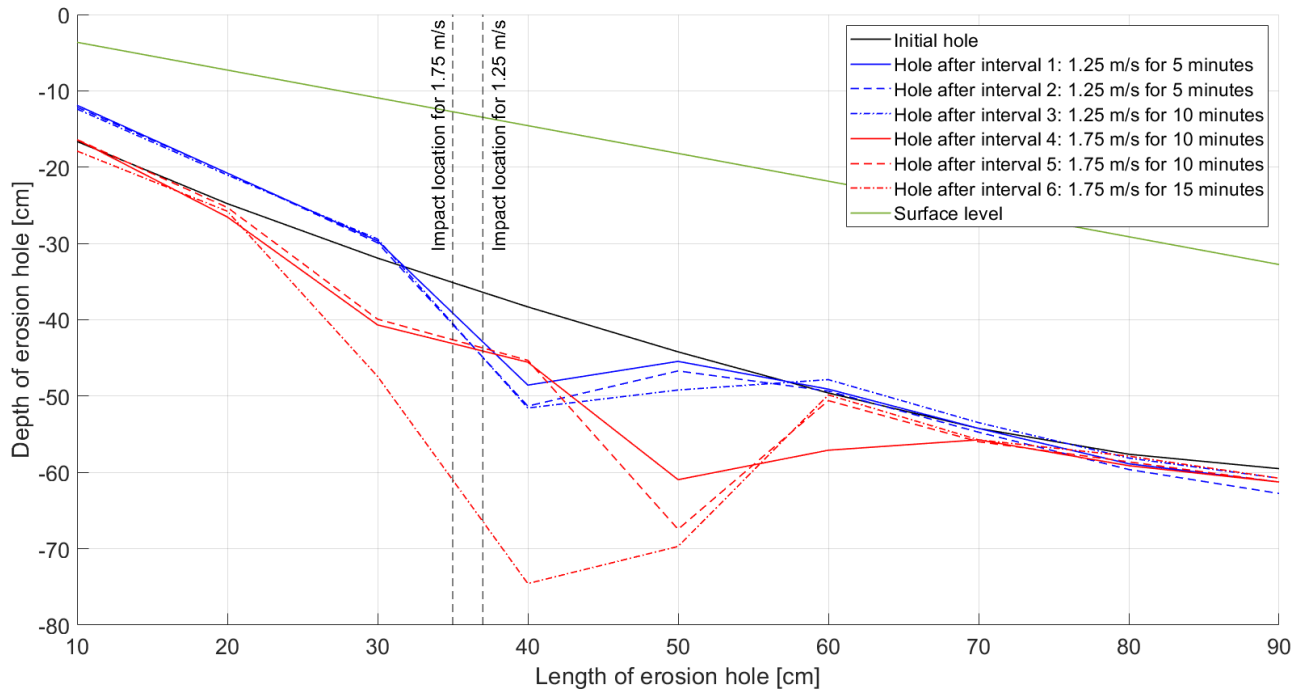


Figure C.4: Development of erosion hole during test B.

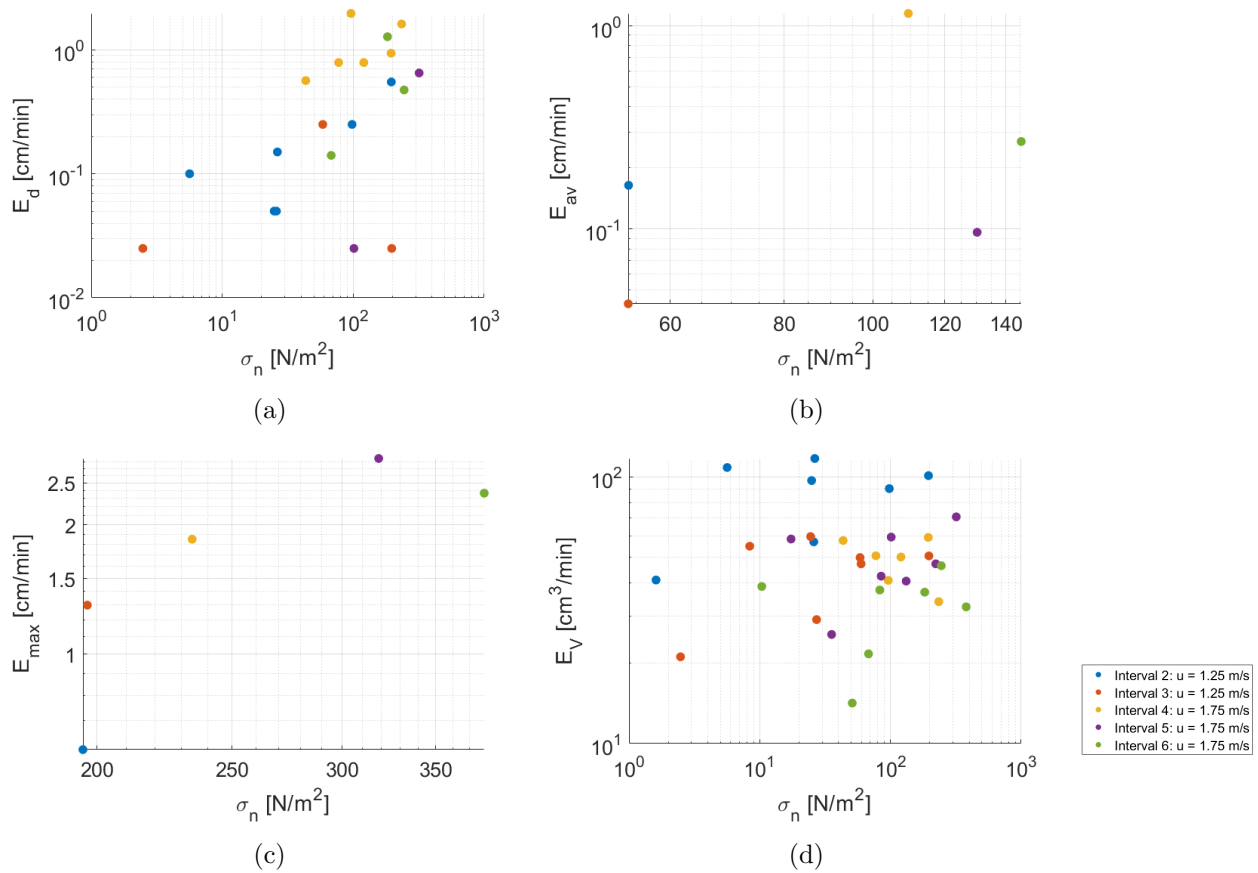


Figure C.5: (a) Erosion rate of depth, (b) average erosion rate, (c) maximum erosion rate, and (d) erosion rate of volume under normal stresses during test B.

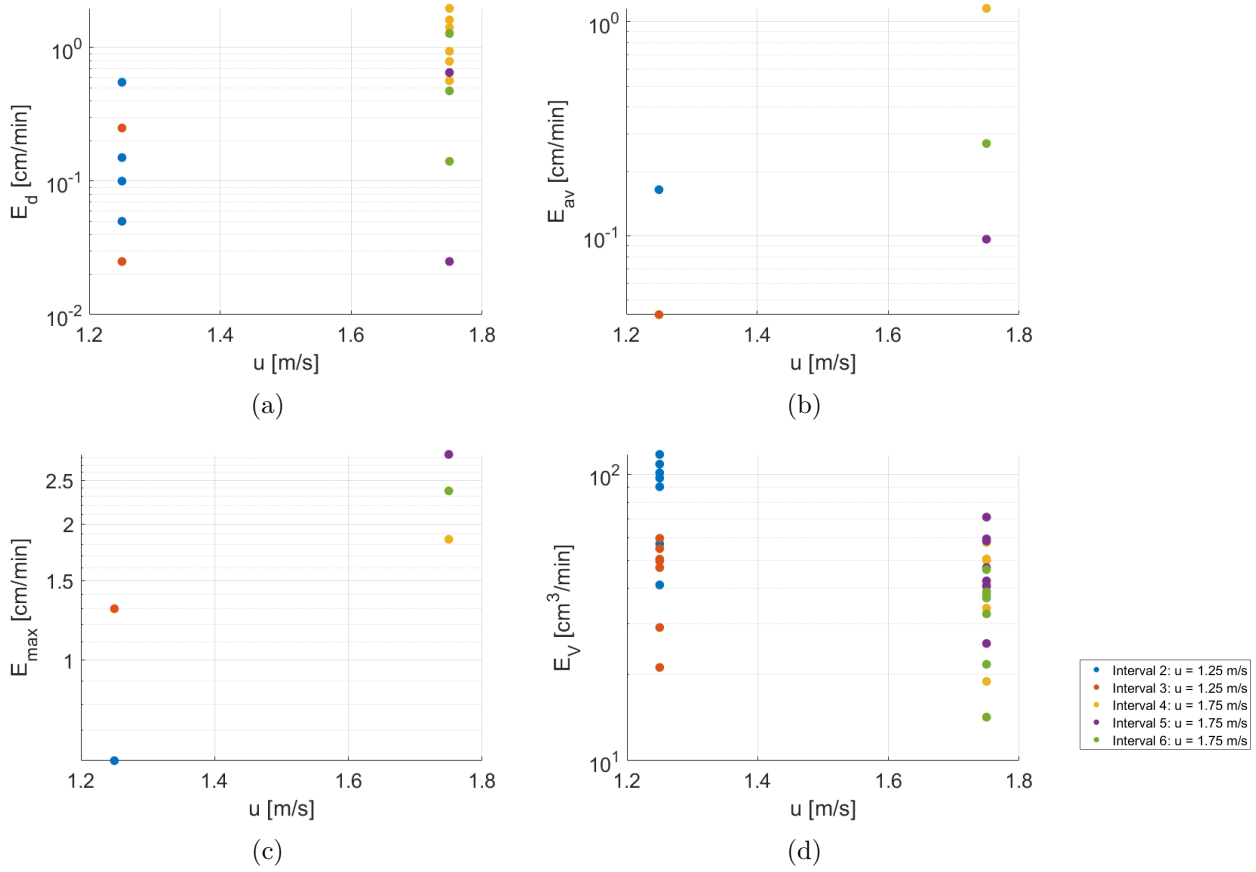


Figure C.6: (a) Erosion rate of depth, (b) average erosion rate, (c) maximum erosion rate, and (d) erosion rate of volume under flow velocities during test B.

C.3 Results Test C

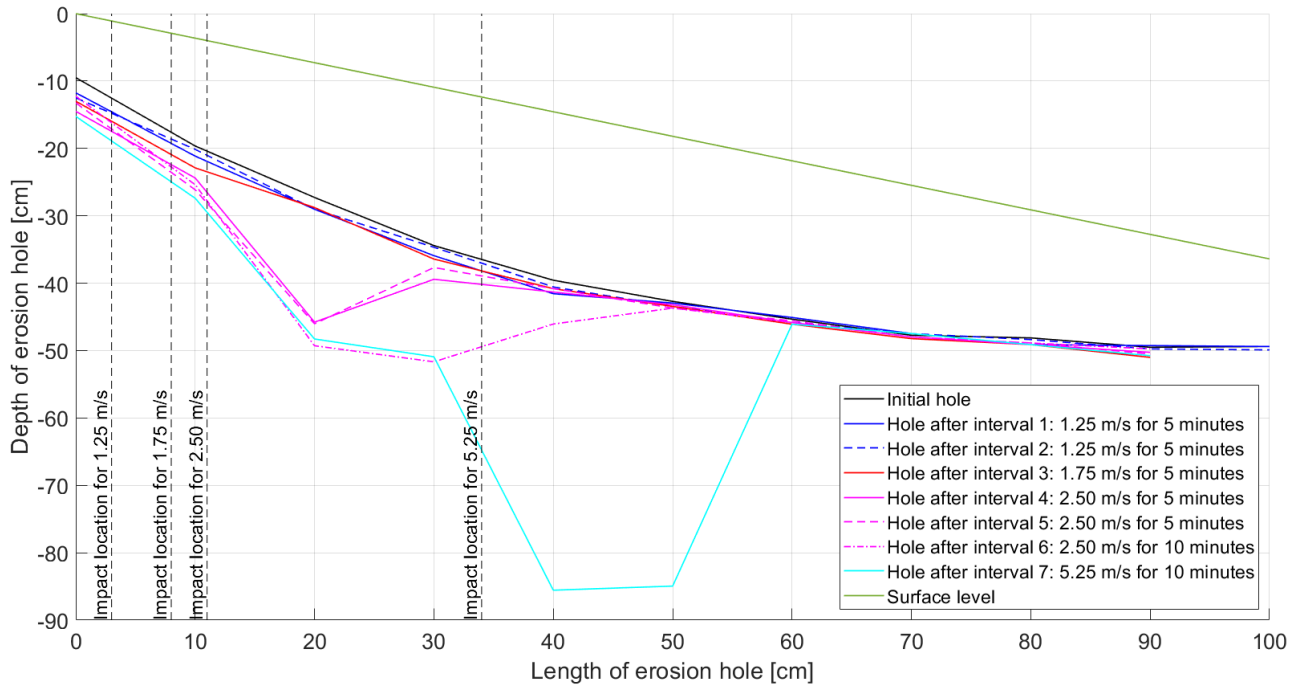


Figure C.7: Development of erosion hole during test C.

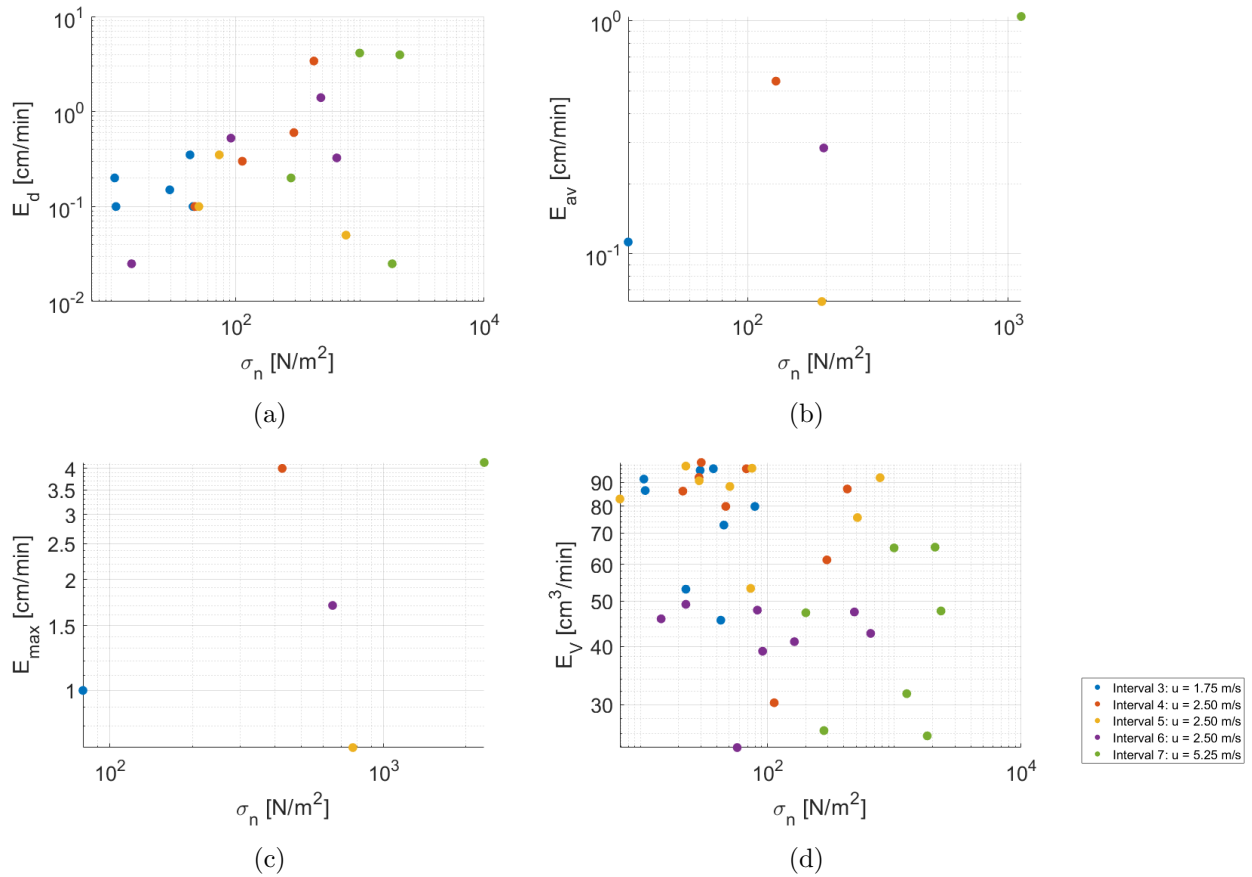


Figure C.8: (a) Erosion rate of depth, (b) average erosion rate, (c) maximum erosion rate, and (d) erosion rate of volume under normal stresses during test C.

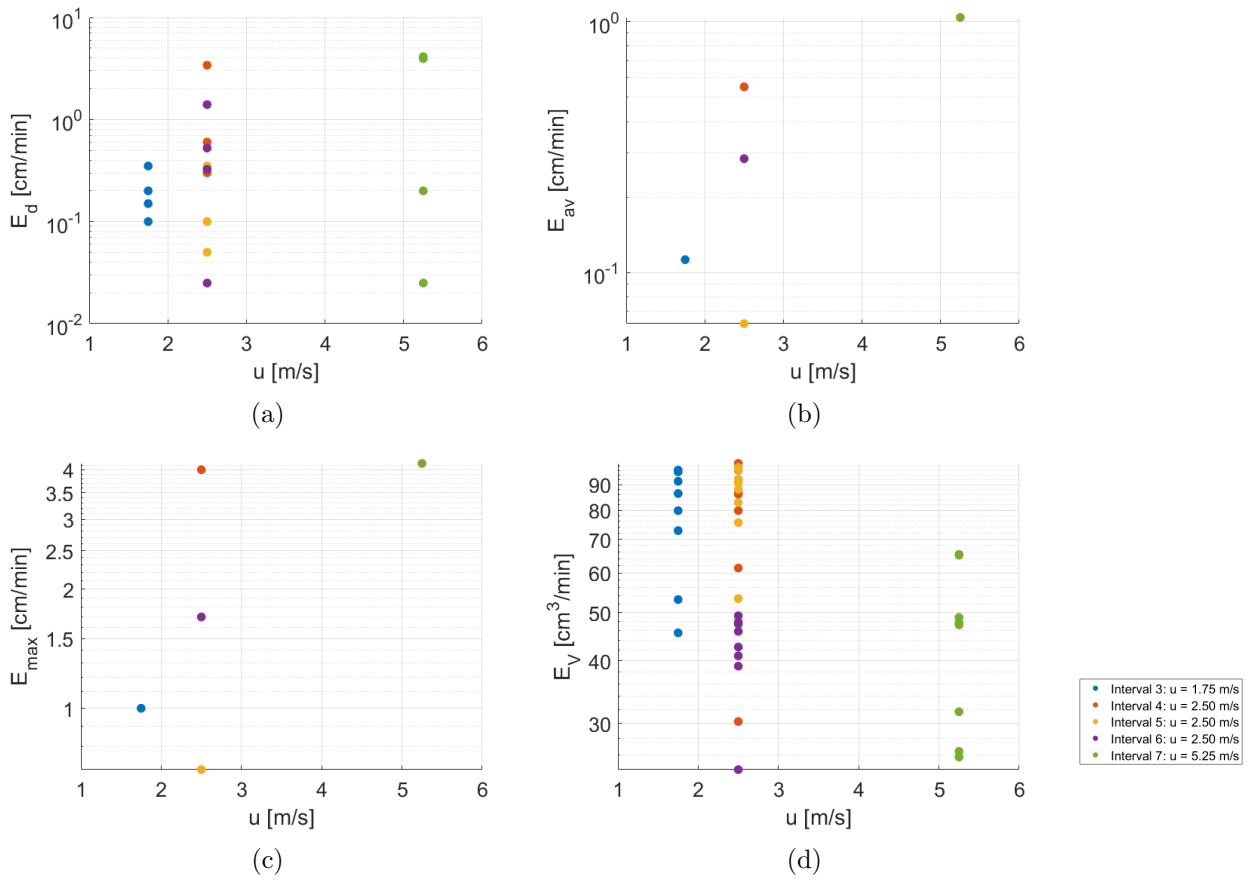


Figure C.9: (a) Erosion rate of depth, (b) average erosion rate, (c) maximum erosion rate, and (d) erosion rate of volume under flow velocities during test C.

C.4 Results Test D

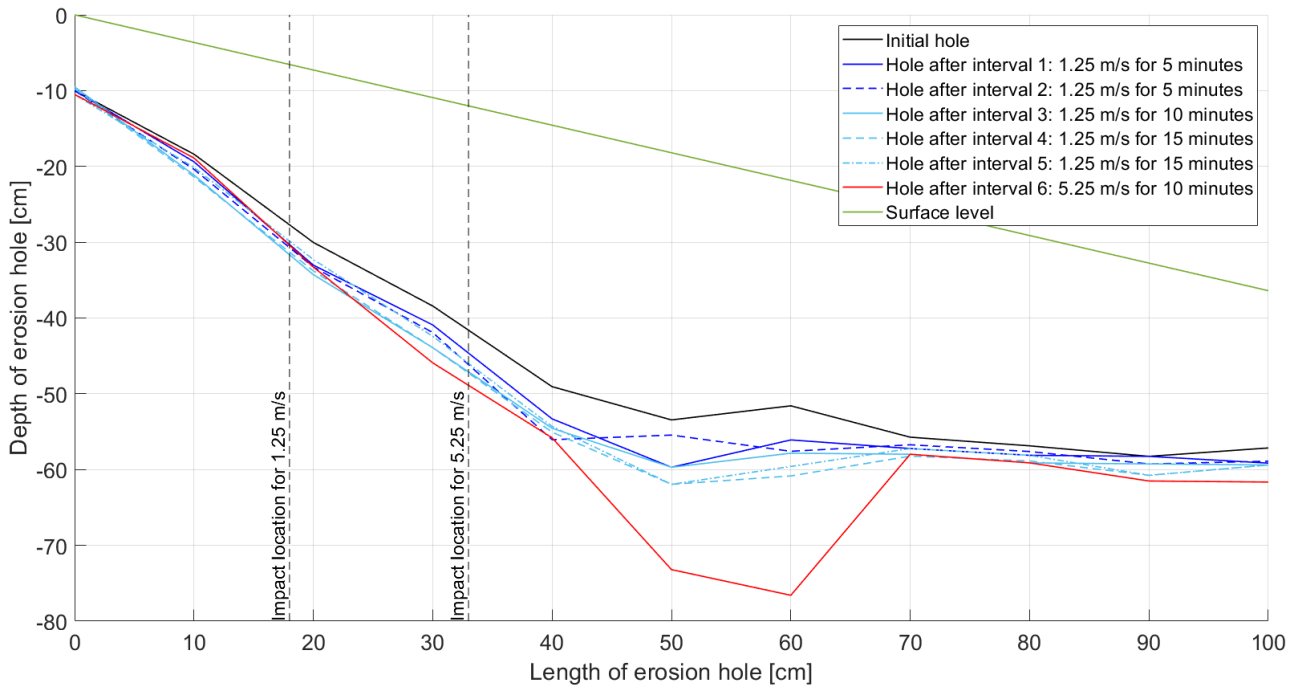


Figure C.10: Development of erosion hole during test D.

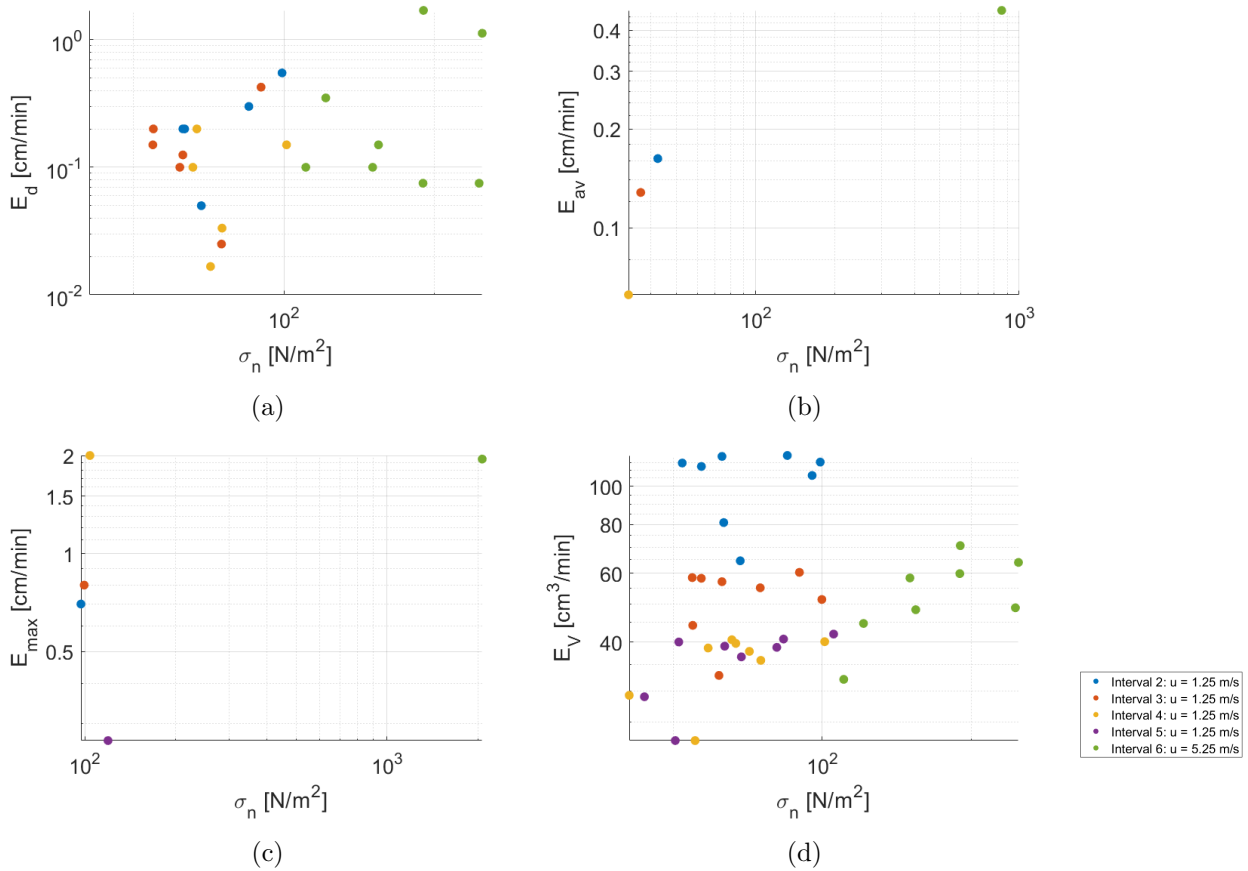


Figure C.11: (a) Erosion rate of depth, (b) average erosion rate, (c) maximum erosion rate, and (d) erosion rate of volume under normal stresses during test D.

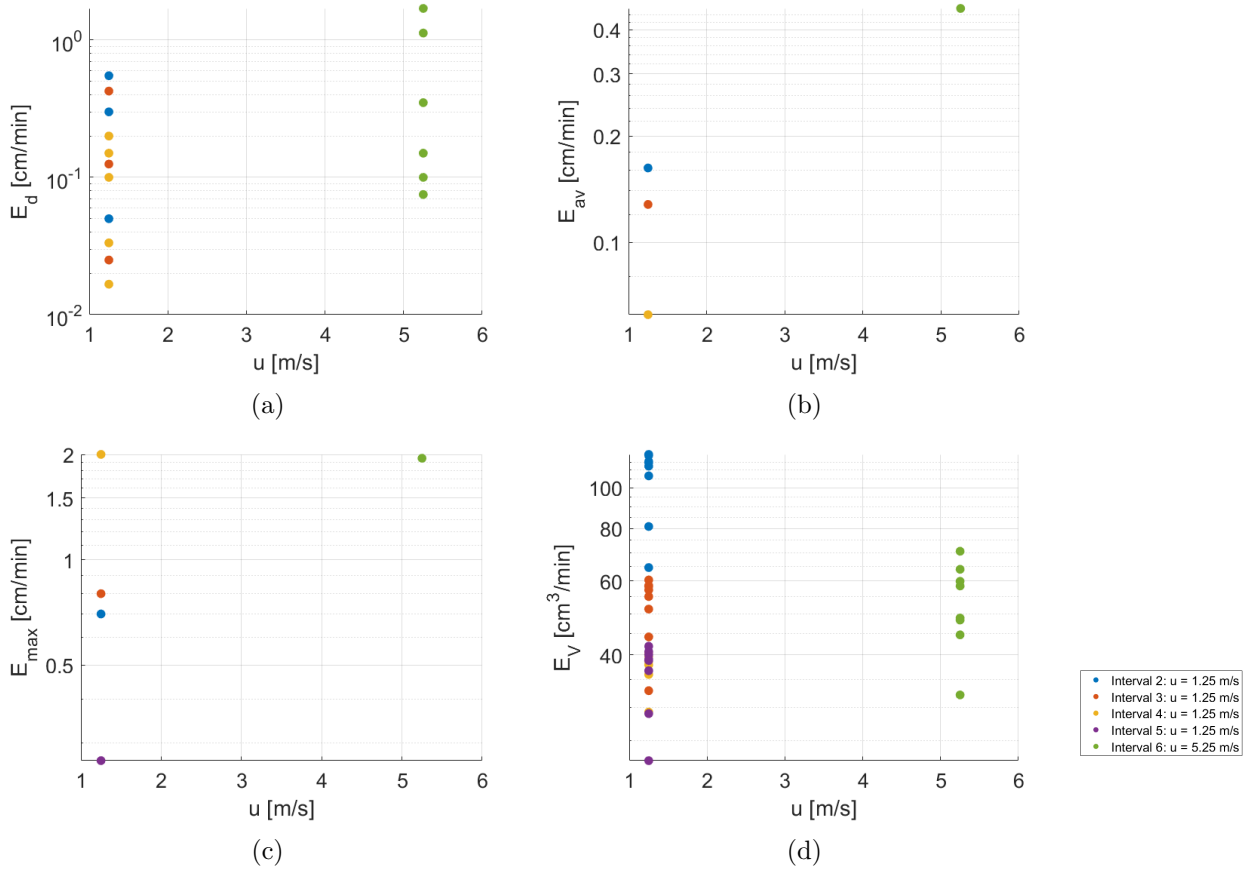


Figure C.12: (a) Erosion rate of depth, (b) average erosion rate, (c) maximum erosion rate, and (d) erosion rate of volume under flow velocities during test D.

C.5 Results Test E

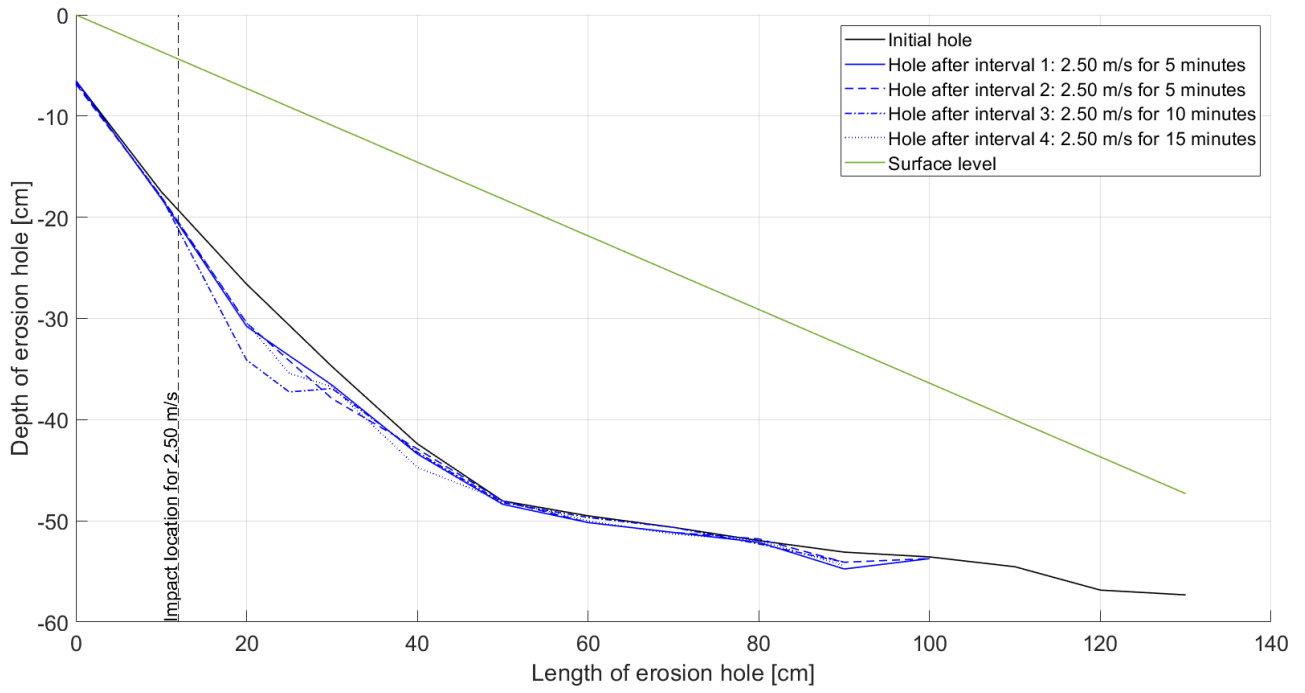


Figure C.13: Development of erosion hole during test E.

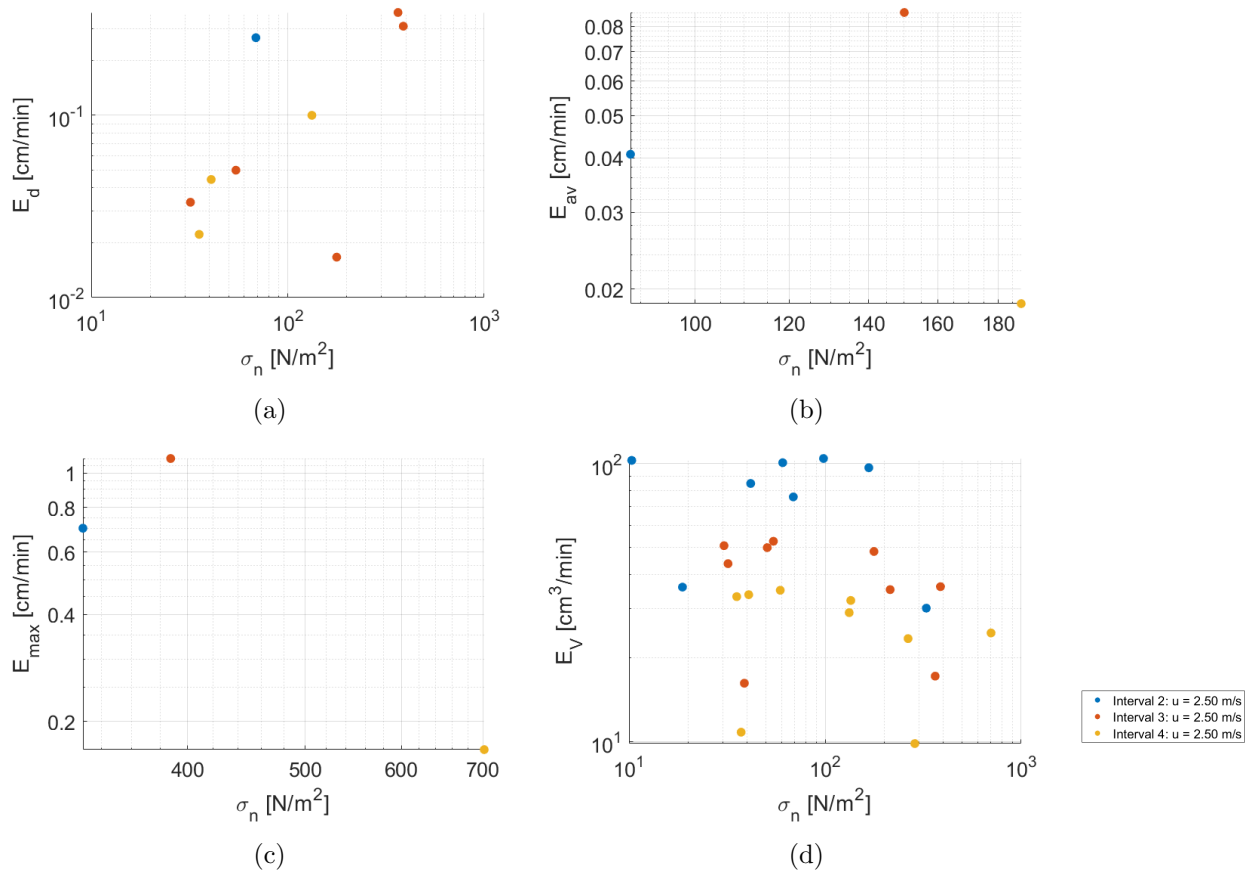


Figure C.14: (a) Erosion rate of depth, (b) average erosion rate, (c) maximum erosion rate, and (d) erosion rate of volume under normal stresses during test E.

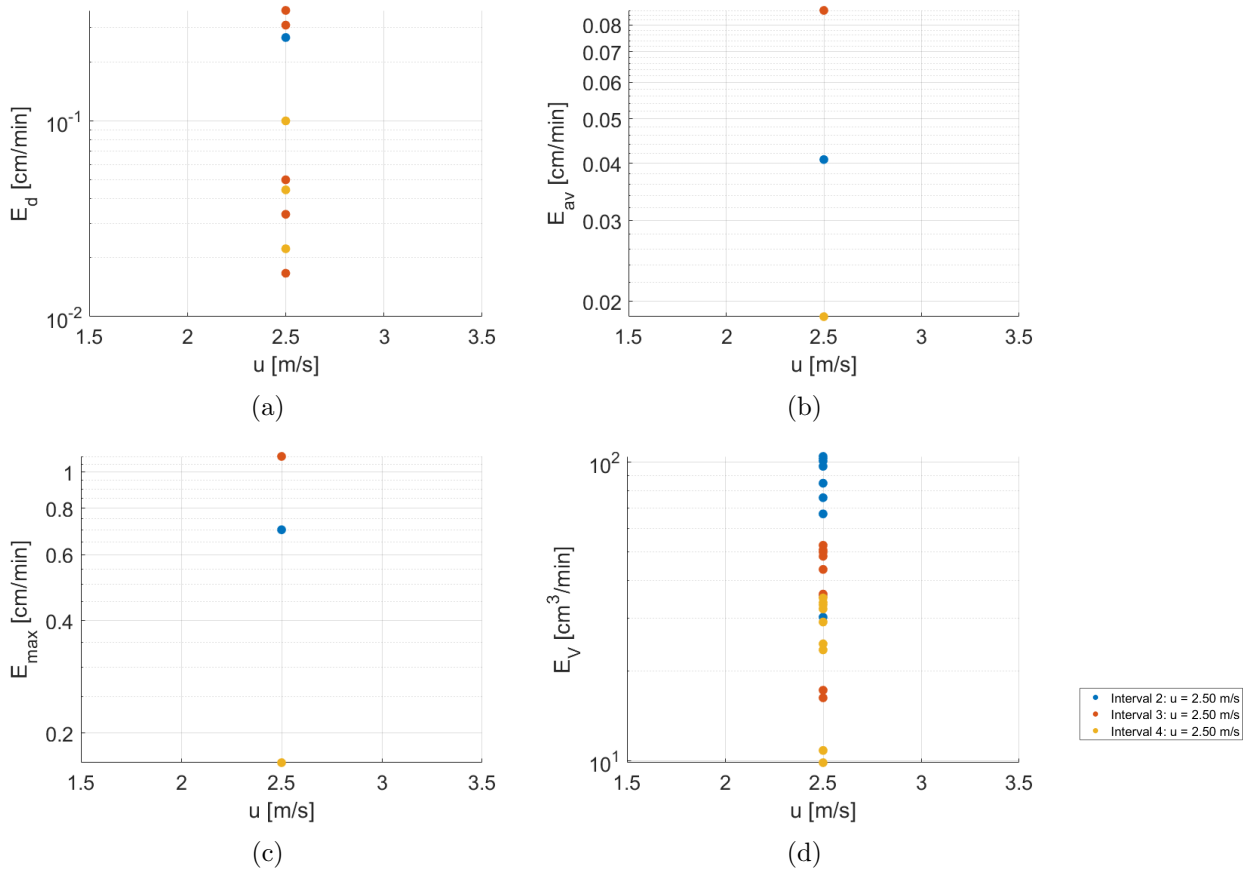


Figure C.15: (a) Erosion rate of depth, (b) average erosion rate, (c) maximum erosion rate, and (d) erosion rate of volume under flow velocities during test E.

C.6 Results Test F

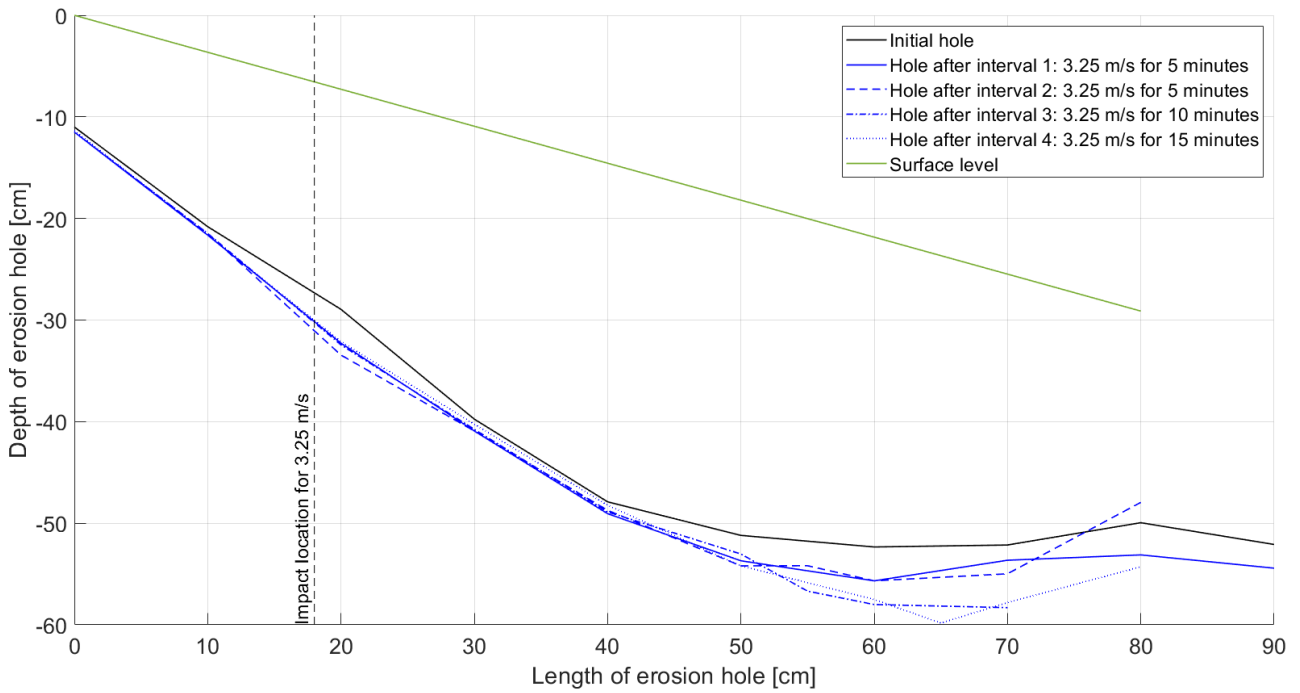


Figure C.16: Development of erosion hole during test F.

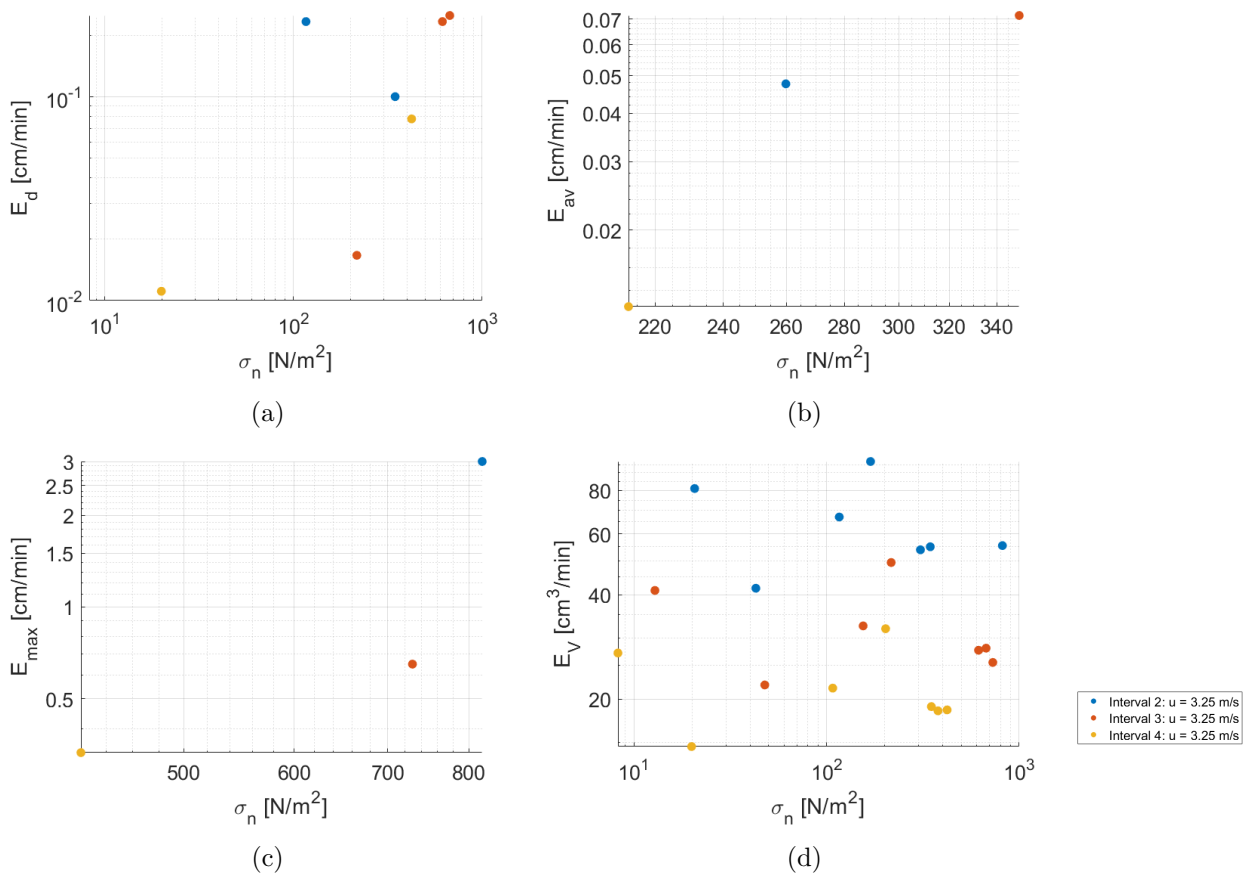


Figure C.17: (a) Erosion rate of depth, (b) average erosion rate, (c) maximum erosion rate, and (d) erosion rate of volume under normal stresses during test F.

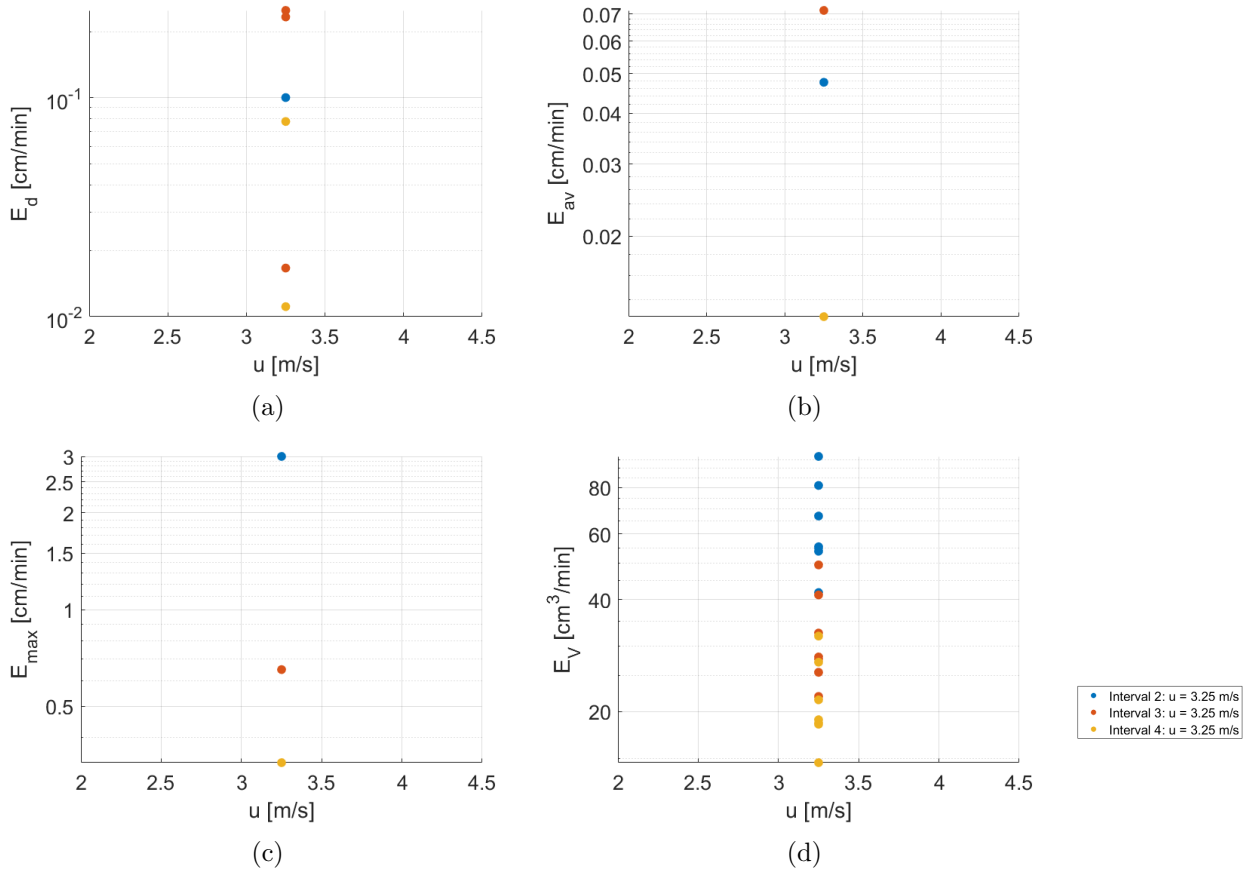


Figure C.18: (a) Erosion rate of depth, (b) average erosion rate, (c) maximum erosion rate, and (d) erosion rate of volume under flow velocities during test F.

Appendix D

Dike Cover Layer at Hedwige-Prosperpolder

The document ‘Test plan wave overtopping reference tests Living Lab HedwigeProserPolder (LLHPP)’ (Koelewijn, 2022) describes the test plan of the wave overtopping experiments performed in the Hedwige-Prosperpolder from February 1st 2022 until February 7th 2022. A description of the cover layer is included in the test plan. Since the structure of the cover layer affects the execution of the experiment and their results, it is important to have insight in this. This section gives a summary of the sections described by Koelewijn informing on the structure of the cover layer of the dike.

D.1 Location of rests

Two exploration pits are excavated at the locations ‘Proefkuil West’ and ‘Proefkuil Oost’ shown in Figure D.1. The wave overtopping experiments and fire hose method tests are performed in between these two locations. According to the design and construction documents of 1982, the thickness of the clay and grass sod should be 80 centimeters. The excavations are performed in November 2021. Each excavation is made vertically downward, and pictures of the back wall and side wall are taken to check the thickness and structure of the different layers over the length of the dike stretch and along the slope of the dike.



Figure D.1: Locations of the exploration pits on the land side slope of the dike (Koelewijn, 2022).

D.2 Description of cover layer

Proefkuil West

Six layers are indicated in the excavation pit at location ‘Proefkuil West’ (Figure D.2). The upper four layers are clay layers containing little to a lot of sand. The lower two layers are sand layers. As can be seen in Figure D.2, the layers are nearly horizontal and parallel to the sloping surface. The details of the layers are described in Table D.1.



Figure D.2: (a) Back wall and (b) side wall of ‘Proefkuil West’ (Koelewijn, 2022). The division between each layer is indicated with a white line.

Table D.1: Description of exploration pit ‘Proefkuil West’ per layer (Koelewijn, 2022).

Layer	Depth [m below surface]	General	Structure	Presence of roots
I	0.00 - 0.10	Clay, slightly sandy. Calcareous.	Loose, fine structure. Sod layer, grass with crumbled soil.	Intensive, underneath damaged closed sod.
II	0.10 - 0.35	Clay, moderately to strongly sandy. Calcareous, stains from iron oxide, with sand pockets.	Loose fine structure with open packing. Chunks of 5-30mm.	Moderate.
III	0.35 - 0.60	Clay, slightly sandy. Calcareous, stains from iron oxide, with sand pockets, som cobbles and debris.	Open coarse structure.	Roots untill 0.80 m below surface.
IV	0.60 - 0.85	Clay, slightly sandy. Calcareous, stains from iron oxide, cemented sand pockets, some cobbles and debris, shell fragments.	Closed coarse structure, wormholes visible, prismatic blocks.	
V	0.85 - 1.00	Moderately fine sand, slightly silty. Calcareous.	Homogeneous sand.	
VI	> 1.00	Moderately fine sand, slightly silty. Calcareous.	Homogeneous sand.	

Proefkuil Oost

In the excavation pit ‘Proefkuil Oost’, seven layers are indicated (Figure D.2). The upper three layers consist of slightly to moderately sandy clay. Layer four is a sand layer, and than again two clay layers are present. Layer seven is the sand core of the dike. The thickness of the layers vary more than at ‘Proefkuil West’. Furthermore, inclusions occur. The thickness of layers E and F quickly decrease at the side walls, whereas the thickness of the upper three layers remain quite constant. The details of the layers is described in Table D.2.

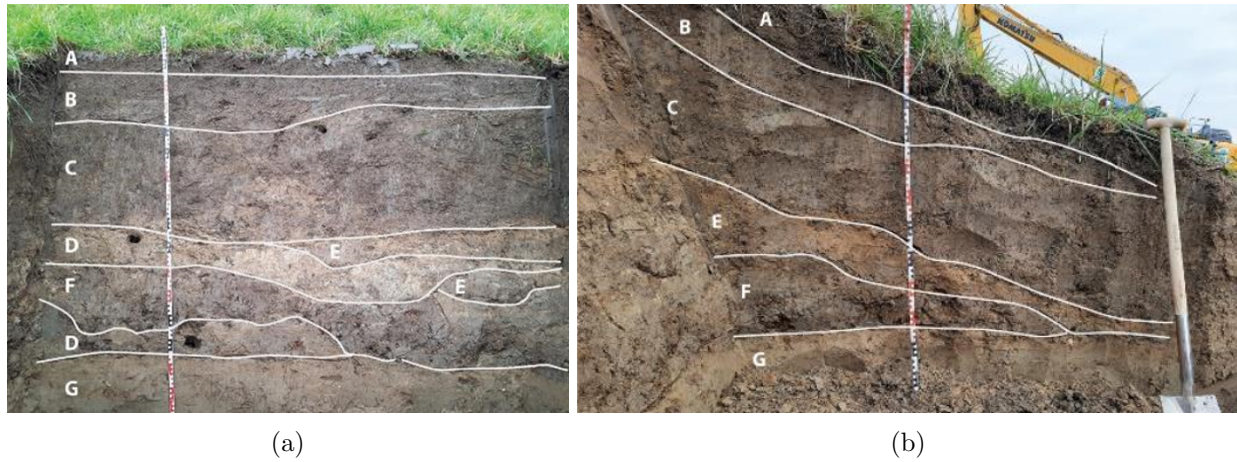


Figure D.3: (a) Back wall and (b) side wall of ‘Proefkuil Oost’ (Koelewijn, 2022). The division between each layer is indicated with a white line.

Table D.2: Description of exploration pit ‘Proefkuil Oost’ per layer (Koelewijn, 2022).

Layer	Depth [m below surface]	General	Structure	Presence of roots
A	0.00 - 0.10	Clay, slightly sandy. Calcareous.	Loose, fine structure. Sod layer, grass with crumbled soil.	Intensive, underneath damaged closed sod.
B	0.10 - 0.40	Clay, moderately sandy. Stains from iron oxide, with wormholes.	Loose fine structure with open packing. Chunks of 10-30mm, 5-10% pores.	Moderate.
C	0.40 - 0.90	Clay, moderately sandy. Stains from iron oxide, with mole burrow and wormholes.	Loose fine structure with open packing. Chunks of 10-40mm, 10-20% pores.	Roots until 1.40 m below surface.
D	0.90 - 1.05 around 1.35	Moderately fine sand, very silty. Calcareous, stains from iron oxide, with pockets of moderately sandy clay, with mole burrow and wormholes.	Homogeneous sand	
E	0.90 - 1.00	Clay, moderately sand with very silty sand. Calcareous, stains from iron oxide, with wormholes	Closed, coarse structure, 3-10% pores.	
F	1.05 - 1.30	Clay, extremely silty. Calcareous, stains from iron oxide, with sand inclusions, with wormholes.	Closed, coarse structure. 3-10% pores	
G	> 1.40	Moderately fine sand, moderately silty. Calcareous, shell fragments.	Homogeneous sand.	

Appendix E

Recommendations for Performing Fire Hose Method Experiments in the Future

The fire hose method still needs to be developed, to find the best setup to determine the critical stress and erodibility coefficient of clay. The maturity level of the design of the experimental setup can be described using the Technology Readiness Level (TRL), which ranges from 1 ‘Basic principles observed’ to 9 ‘Actual system proven in operational environment’ (TWI, 2022). The current level of the fire hose method, when used to determine the erosion resistance of clay, is 4 ‘Technology validated in lab’. By implementing the recommendations described below, the setup may be improved, which results in a higher TRL.

To improve the accuracy of the calculated stresses, the assumptions made to perform the calculations must be similar to what occurs during the experiments. By placing plates at the sides of the excavated hole, the flow can be directed. By placing these plates at maximum 30 centimeters apart, the spread of the flow is reduced. By placing the plates closer together to at minimum 10 centimeters, the assumptions regarding the flow velocity and discharge along the hole is best approximated. However, at the location where the jet impacts, a hole develops. During the experiments performed in the Hedwige-Prosperpolder, the hole became often between 10 and 20 centimeters wide. So placing the plates closer together could reduce the amount and quality of the data.

To improve the accuracy of the calculated normal stress further, the angle of incidence must be 180° , such that the water flows parallel to the wall of the hole, as is also assumed during the calculations. Prior to the tests, the location where the water jet impacts and angle of incidence can be calculated from the predetermined setup and flow velocity. It should be noted that wind or a deviation of the slope of the wall of the hole affect the angle of incidence. The effect of these factors can be reduced by minimizing the distance of the flow through the air by minimizing the height of the nozzle or by guiding the flow to the surface by placing a sheet under the nozzle that guides the flow to the clay. If this sheet has walls on the sides (10 centimeters apart), it prevents the flow to spread out and functions as an extension of the nozzle. This could also reduce the chance that a hole is created at the location of impact.

The current setup, that uses an angle of incidence of 180° , represents the stresses occurring at the bottom of the excavated hole on clay during the large-scale wave overtopping experiments well. However, if one is interested in erosion occurring at the top of the excavated hole where the water impacts after it was separated from the grass cover, the setup of the fire hose method experiments can be altered such that it simulates the conditions during the large-scale experiments. By adjusting the angle of the nozzle, the slope of the wall and the flow velocity, such that it represents the conditions of wave overtopping, it is expected that the fire hose method is capable of representing erosion at the top of the excavated hole for large-scale experiments.

The magnitude of the stresses on the clay is mainly affected by the flow velocity from the nozzle. The magnitude of the stresses determines the dominant erosion mechanism. Smaller hydraulic loads

mainly cause erosion by grains, and larger hydraulic loads cause erosion by clods. Erosion by clods could be the most interesting mechanism to investigate, since this is the mechanism during which significant erosion takes place. Hence, higher flow velocities should be applied to make this the dominant mechanism. The minimum flow velocity can be determined during the experiments, by first determining the critical flow velocity. By setting the pump to the minimum flow velocity initially and increasing the flow velocity when no significant erosion occurs during each interval until significant erosion occurs, the critical flow velocity can be determined. The applied flow velocity for the remaining part of the test, where the flow velocity is kept constant, must be higher than the critical flow velocity to measure significant erosion.

Some adjustments to the initial experiment can be done fairly easy to reduce the time needed to perform the experiments and increase to the accuracy and the amount of data. The first adjustment is to wash out the hole before the start of the experiment for 10 seconds with a low flow velocity. This way, loose particles are washed out and the erosion rate measured during the first interval can be used in the data analysis. Secondly, it is advised to perform an interval for at least 5 minutes. By increasing the duration of the intervals, the inaccuracies in the calculated erosion rate and applied flow velocity are minimised. Lastly, it is advised to reduce the grid size of the measuring system, to for example 5 centimeters, and to measure only at maximum the centre 30 centimeters of the hole and over the length where only significant erosion takes place. This reduces the time needed to measure the hole. If it is possible to prevent remaining water in the hole, it is possible to use an analysing technique such as photogrammetry. This also reduces the time needed to measure the hole and can significantly increase the accuracy of the measured erosion, when water does not remain present in the hole. However, it should be noted that the time needed to analyse the data afterwards increases.

This study has shown that the best relation between the applied stress and observed erosion rate can be described using the erosion rate of the depth or the average erosion rate. It is advised to also use these parameters for data analysis of future experiments. However, for large-scale experiments the erosion rate is often described using the eroded volume. It is advised to also study whether this parameter can be used to define a relation between the stress and erosion rate.

When the setup is adjusted, it is advised to perform new experiments. These can be performed in the field to test the setup on structured clay or performed on homogeneous clay created in the lab. By performing experiments on homogeneous clay, it can be studied whether the new setup is able to generate data with a smaller spread. If this is not the case, it is questionable whether the fire hose method can actually be used to determine the erosion resistance of clay. By performing experiments in the field, it can be studied whether the new setup can be used to determine the erosion resistance of structured clay. Furthermore, if these experiments are performed on a dike section where already large-scale tests have been performed on clay, the outcome of the fire hose method experiments can be correlated to the results of the large-scale experiments and the setup can be validated.